AFML-TR-71-210

Form Approved
Budget Bureau No. 22-R0293

RESEARCH AND DEVELOPMENT OF RARE EARTH-TRANSITION METAL ALLOYS AS PERMANENT-MAGNET MATERIALS

A. E. Ray and K. J. Strnat

Research Institute
University of Dayton

Sponsored by
Advanced Research Projects Agency
ARPA Order No. 1617

TECHNICAL REPORT AFML-TR-71-210
October 1971

Air Force Materials Laboratory
Air Force Systems Command
Wright-Patterson Air Force Base
Dayton, Ohio

MISSING PAGE
NUMBERS ARE BLANK
AND WERE NOT
FILMED

Unclassified
Security Classification

DOCUMENT CONTROL DATA · R&D

(Security classification of title, body of abstract and indexing annotation must be entered when the overall report is classified)

1. ORIGINATING ACTIVITY (Corporate author)
University of Dayton
Research Institute
Dayton, Ohio 45409

2a. REPORT SECURITY CLASSIFICATION
Unclassified

2b. GROUP

3. REPORT TITLE
RESEARCH AND DEVELOPMENT OF RARE EARTH-TRANSITION METAL ALLOYS AS PERMANENT-MAGNET MATERIALS

4. DESCRIPTIVE NOTES (Type of report and inclusive dates)
Semiannual Interim Technical Report: 1 January 1971 - 30 June 1971

5. AUTHOR(S) (Last name, first name, initial)
Ray, Alden E.
Strnat, Karl J.

6. REPORT DATE	7a. TOTAL NO. OF PAGES	7b. NO. OF REFS
October 1971	120	27

8a. CONTRACT OR GRANT NO.	9a. ORIGINATOR'S REPORT NUMBER(S)
F33615-70-C-1625	
b. PROJECT NO. 7371	UDRI-TR-71-32
c. Task No. 737103	9b. OTHER REPORT NO(S) (Any other numbers that may be assigned this report)
d.	AFML-TR-71-210

10. AVAILABILITY/LIMITATION NOTICES
Approval for Public Release - Distribution Unlimited

11. SUPPLEMENTARY NOTES	12. SPONSORING MILITARY ACTIVITY
	Air Force Materials Laboratory Wright-Patterson AFB, Ohio 45433

13. ABSTRACT

Intermetallic phases $R_2(Co,Fe)_{17}$ with R = Ce, Pr, Nd, Sm, Y, and MM (Ce-rich mischmetal) have been prepared and their metallurgical and magnetic properties studied. The melting behavior, phase transformations and Curie temperatures, lattice constants and directions of easy magnetization of the $R_2(Co,Fe)_{17}$ phases were determined and the results are presented. All systems except R = Nd have compositional ranges in which the easy direction of magnetization is the c-axis.

The praseodymium-cobalt phase diagram has been revised and extended. Three previously unreported intermetallic phases were observed, and the structure of one, $Pr_2Co_{1.7}$, is reported.

The design and operation of a thermomagnetic analyzer and of an oscillating specimen magnetometer are described and discussed. Results of thermomagnetic analyses on some of the $R_2(Co,Fe)_{17}$ phases are given and compared with differential thermal analysis measurements.

The results of preliminary sintering experiments with $NdCo_5$ and a 70 w/o Pr + 30 w/o Co sintering aid are given.

DD FORM 1 JAN 64 1473

Unclassified
Security Classification

NOTICE

When Goverment drawings, specifications, or other data are used for any purpose other than in connection with a definitely related Government procurement operation, the United States Government thereby incurs no responsibility nor any obligation whatsoever; and the fact that the Government may have formulated, furnished, or in any way supplied the said drawings, specifications, or other data, is not to be regarded by implication or otherwise as in any manner licensing the holder or any other person or corporation, or conveying any rights or permission to manufacture, use, or sell any patented invention that may in any way be related thereto.

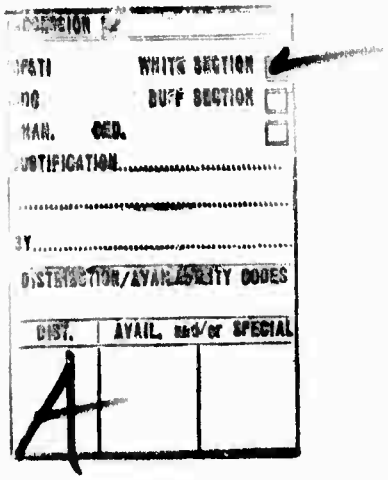

Copies of this report should not be returned unless return is required by security considerations, contractual obligations, or notice on a specific document.

14. KEY WORDS	LINK A		LINK B		LINK C	
	ROLE	WT	ROLE	WT	ROLE	WT
Magnetic Materials Permanent Magnets Rare Earth Alloys Intermetallic Compounds Phase Diagrams Thermomagnetic Analysis						

INSTRUCTIONS

1. ORIGINATING ACTIVITY: Enter the name and address of the contractor, subcontractor, grantee, Department of Defense activity or other organization *(corporate author)* issuing the report.

2*a*. REPORT SECURITY CLASSIFICATION: Enter the overall security classification of the report. Indicate whether "Restricted Data" is included. Marking is to be in accordance with appropriate security regulations.

2*b*. GROUP: Automatic downgrading is specified in DoD Directive 5200.10 and Armed Forces Industrial Manual. Enter the group number. Also, when applicable, show that optional markings have been used for Group 3 and Group 4 as authorized.

3. REPORT TITLE: Enter the complete report title in all capital letters. Titles in all cases should be unclassified. If a meaningful title cannot be selected without classification, show title classification in all capitals in parenthesis immediately following the title.

4. DESCRIPTIVE NOTES: If appropriate, enter the type of report, e.g., interim, progress, summary, annual, or final. Give the inclusive dates when a specific reporting period is covered.

5. AUTHOR(S): Enter the name(s) of author(s) as shown on or in the report. Enter last name, first name, middle initial. If military, show rank and branch of service. The name of the principal author is an absolute minimum requirement.

6. REPORT DATE: Enter the date of the report as day, month, year; or month, year. If more than one date appears on the report, use date of publication.

7*a*. TOTAL NUMBER OF PAGES: The total page count should follow normal pagination procedures, i.e., enter the number of pages containing information.

7*b*. NUMBER OF REFERENCES: Enter the total number of references cited in the report.

8*a*. CONTRACT OR GRANT NUMBER: If appropriate, enter the applicable number of the contract or grant under which the report was written.

8*b*, 8*c*, & 8*d*. PROJECT NUMBER: Enter the appropriate military department identification, such as project number, subproject number, system numbers, task number, etc.

9*a*. ORIGINATOR'S REPORT NUMBER(S): Enter the official report number by which the document will be identified and controlled by the originating activity. This number must be unique to this report.

9*b*. OTHER REPORT NUMBER(S): If the report has been assigned any other report numbers *(either by the originator or by the sponsor)*, also enter this number(s).

10. AVAILABILITY/LIMITATION NOTICES: Enter any limitations on further dissemination of the report, other than those imposed by security classification, using standard statements such as:

(1) "Qualified requesters may obtain copies of this report from DDC."

(2) "Foreign announcement and dissemination of this report by DDC is not authorized."

(3) "U. S. Government agencies may obtain copies of this report directly from DDC. Other qualified DDC users shall request through _____."

(4) "U. S. military agencies may obtain copies of this report directly from DDC. Other qualified users shall request through _____."

(5) "All distribution of this report is controlled. Qualified DDC users shall request through _____."

If the report has been furnished to the Office of Technical Services, Department of Commerce, for sale to the public, indicate this fact and enter the price, if known.

11. SUPPLEMENTARY NOTES: Use for additional explanatory notes.

12. SPONSORING MILITARY ACTIVITY: Enter the name of the departmental project office or laboratory sponsoring *(paying for)* the research and development. Include address.

13. ABSTRACT: Enter an abstract giving a brief and factual summary of the document indicative of the report, even though it may also appear elsewhere in the body of the technical report. If additional space is required, a continuation sheet shall be attached.

It is highly desirable that the abstract of classified reports be unclassified. Each paragraph of the abstract shall end with an indication of the military security classification of the information in the paragraph, represented as *(TS)*, *(S)*, *(C)*, or *(U)*.

There is no limitation on the length of the abstract. However, the suggested length is from 150 to 225 words.

14. KEY WORDS: Key words are technically meaningful terms or short phrases that characterize a report and may be used as index entries for cataloging the report. Key words must be selected so that no security classification is required. Identifiers, such as equipment model designation, trade name, military project code name, geographic location, may be used as key words but will be followed by an indication of technical context. The assignment of links, rules, and weights is optional.

ABSTRACT

Intermetallic phases $R_2(Co, Fe)_{17}$ with R = Ce, Pr, Nd, Sm, Y and MM(Ce-rich mischmetal) have been prepared and their metallurgical and magnetic properties studied. The melting behavior, phase transformations and Curie temperatures, lattice constants and directions of easy magnetization of the $R_2(Co, Fe)_{17}$ phases were determined and the results are presented. All systems except R = Nd have compositional ranges in which the easy direction of magnetization is the c-axis.

The praseodymium-cobalt phase diagram has been revised and extended. Three previously unreported intermetallic phases were observed, and the structure of one, $Pr_2Co_{1.7}$, is reported.

The design and operation of a thermomagnetic analyzer and of an oscillating specimen magnetometer are described and discussed. Results of thermomagnetic analyses on some of the $R_2(Co, Fe)_{17}$ phases are given and compared with differential thermal analysis measurements.

The results of preliminary sintering experiments with $NdCo_5$ and a 70 w/o Pr + 30 w/o Co sintering aid are given.

RESEARCH AND DEVELOPMENT OF RARE EARTH-TRANSITION METAL ALLOYS AS PERMANENT-MAGNET MATERIALS

By:

Dr. Alden E. Ray and Dr. Karl J. Strnat, Principal Investigators
University of Dayton, Research Institute and Electrical Engineering Dept.
300 College Park Ave., Dayton, Ohio 45409
Tel. Numbers: (513) 229-3527 and (513) 229-3611

Sponsored by
Advanced Research Projects Agency
ARPA Order No. 1617

Program Code No. OD10
Contract effective date: 30 June 1970
Expiration date: 30 June 1973
Amount of contract: $525,012

Submitted to:

Air Force Materials Laboratory, AFSC, USAF
Project Scientist: Capt. M. V. Turner, LPE Tel. (513) 255-4474

FOREWORD

The research described in this report is part of the contractual research program of the Materials Physics Division, Air Force Materials Laboratory. It was performed by the authors at the University of Dayton, Research Institute and Electrical Engineering Dept., 300 College Park Ave. Dayton, Ohio 45409, and was sponsored by the Advanced Research Projects Agency, ARPA Order No. 1617, Program Code No. OD10. The contract is administered under Project No. 7371, Task No. 737103, by the Air Force Materials Laboratory, Air Force Systems Command, Wright-Patterson Air Force Base, Ohio. The work was performed under contract F33615-70-C-1625, project scientist, Capt. Michael V. Turner (AFML/LPE/513-255-4474).

The participants in this research were Adolf Biermann, John Geis, Richard Harmer, Michael Hartings, Andrew Kraus, Robert Leasure, Herbert Mildrum, Rolando Bolomay Munez, Alden Ray, Jacques Schweizer, Charles Shanley, Karl Strnat, James Tsui, and David Walsh.

This report covers research conducted between 1 January 1971 and 30 June 1971. The report was submitted by the authors in September 1971.

Publication of this report does not constitute Air Force approval of the report's findings and conclusions. It is published only for the exchange of ideas.

CHARLES E. EHRENFRIED
Major, USAF
Chief, Electromagnetic Materials Branch
Materials Physics Division
Air Force Materials Laboratory

TABLE OF CONTENTS

LIST OF ILLUSTRATIONS

LIST OF TABLES

APPENDIX TABLE

SECTION I

THE METALLURGICAL AND MAGNETIC PROPERTIES OF $R_2(Co, Fe)_{17}$

A. INTRODUCTION

The primary objective of the work described in this section is to learn if mixed phases of the type $R_2(Co, Fe)_{17}$ have useful permanent magnet properties similar to some of the RCo_5 phases which combine high saturation magnetizations and Curie temperatures with large, uniaxial magnetocrystalline anisotropies. The R_2Co_{17} phases have Curie temperatures which are 200°C to 400°C higher than the corresponding RCo_5 phases, as well as slightly larger saturations due to the increased concentration of cobalt. The R_2Fe_{17} phases have saturation magnetizations which are approximately 20 percent larger than the R_2Co_{17} phases. On the negative side, the R_2Fe_{17} phases have Curie temperatures ranging from -180°C to + 200°C, too low to make them of interest, as such, for permanent magnet application. Of all the binary R_2Co_{17} and R_2Fe_{17} phases, only Sm_2Co_{17} is known to have the proper magnetic symmetry of an easy c-axis and a hard basal plane. By preparing ternary phases of the type $R_2(Co, Fe)_{17}$, we hope to achieve a favorable compromise between the high saturation magnetizations of the R_2Fe_{17} and the high Curie temperatures of the R_2Co_{17} phases. The key property for permanent magnet applications, however, is a large, uniaxial magnetocrystalline anisotropy. Alloying combinations of the type $R_2(Co_{1-x}Fe_x)_{17}$ should strongly influence the magnetocrystalline anisotropies of the components, and may be the effect needed to induce a favorable magnetic symmetry in these phases.

B. PREPARATION OF THE ALLOYS*

A total of 123 alloys of the type $R_2(Co_{1-x}Fe_x)_{17}$ with R = Ce, Pr, Nd, Sm, Y, and MM (Ce-rich mischmetal) and x ranging from 0 to 1 have been prepared to date. The 59 nominal compositions for these alloys and the number of each prepared are given in Table I.

All of the alloys were prepared by arc melting of the elemental constituents followed by a high temperature homogenization heat treatment of the arc-melted buttons. The procedures employed for preparing the alloys were described in detail in a previous report[1] and will not be repeated here. The previously mentioned difficulties in obtaining nearly single phase ternary alloys for values of x between 0.6 and 0.7 were not solved completely, especially for R = Sm. In most cases, however, sufficiently large quantities of single phase material were obtained to conduct initial screening tests. Metallographic inspection was employed to determine whether or not single phase alloys were obtained by the homogenization heat treatments. A metallographic etchant developed specifically for the ternary $R_2(Co_{1-x}Fe_x)_{17}$ alloys consisted of 5 gram $FeCl_3$ and 50 ml conc. HCl in 100 ml H_2O. After final polishing, the alloys were immersed in this etchant for 30 to 60 seconds.

The various preparation parameters, heat treatments, and the results of microstructural evaluations are given in Tables II-VII for the phases with R = Ce, Pr, Nd, Sm, Y and MM, respectively.

*A. E. Ray, R. S. Harmer, R. E. Leasure, and A. Kraus

TABLE I

Nominal compositions for $R_2(Co_{1-x}Fe_x)_{17}$ alloys.
The number of alloys of each composition is indicated.

X \ R	Ce	Pr	Nd	Sm	Y	MM
0	9	6	7	5	2	2
.1	2	1	1	1	1	1
.2	2	1	1	1	1	1
.25	1	1	1	-	-	1
.3	2	1	1	1	1	1
.4	3	1	1	1	1	1
.5	6	3	2	2	1	2
.6	1	-	-	2	-	-
.7	1	-	-	2	-	-
.75	1	2	2	-	1	2
.8	1	-	-	1	-	-
.9	1	-	-	1	-	-
1.0	7	10	4	1	2	1

TABLE II

Preparation parameters and microstructural evaluation of the mixed intermetallic phase $Ce_2(Co_{1-x}Fe_x)_{17}$

X	Excess Ce Added[1] %	% Wt. Loss[2] %	Homogenization Treatment Temp.	Time	Microstructural Evaluation
0.0	2.0	1.15	1100°C	8 Hrs.	Little Cobalt on grain boundaries
0.1	2.0	0.09	1100°C	18 Hrs.	Little transition metal on grain boundaries
	2.0	0.09	1000°C	60 Hrs.	Heavily twinned. Single phase
0.2	2.0	0.72	1100°C	18 Hrs.	Little transition metal on grain boundaries
	2.0	0.72	1000°C	18 Hrs.	Heavily twinned. Single phase
0.3	2.0	0.13	1100°C	18 Hrs.	Little transition metal on grain boundaries
	2.0	0.13	1000°C	18 Hrs.	Heavily twinned. Single phase
0.4	3.0	0.73	1100°C	18 Hrs.	Single phase. Untwinned
	3.0	0.73	1000°C	18 Hrs.	Heavily twinned. Single phase
0.5	3.0	1.23	1100°C	18 Hrs.	Single phase. Untwinned
	3.0	1.23	1000°C	18 Hrs.	Heavily twinned. Single phase
0.6	3.0	0.31	1000°C	18 Hrs.	Single phase. Heavily twinned
0.7	3.0	0.18	1000°C	18 Hrs.	Single phase. Heavily twinned
0.8	3.0	0.18	1000°C	18 Hrs.	Single phase. Heavily twinned
0.9	3.0	0.18	1000°C	18 Hrs.	Single phase. Twinned
1.0	2.0	1.24	1100°C	48 Hrs.	Excess iron

1. Wt. % Added based on stoichiometric rare earth required.
2. % Expressed as % of initial rare earth content.

TABLE III

Preparation parameters and microstructural evaluation of the mixed intermetallic phase $Pr_2(Co_{1-x}Fe_x)_{17}$

X	Excess Pr Added[1] %	% Wt. Loss[2] %	Homogenization Treatment Temp.	Time	Microstructure Evaluation
0.0	2.0	0.98	1100°C	8 Hrs.	Single phase
0.1	2.0	0.18	1050°C	6 Hrs.	Little second phase
0.2	2.0	0.40	1050°C	6 Hrs.	Little second phase
0.3	2.0	0.18	1050°C	7 Hrs.	Single phase
0.4	2.5	0.31	1050°C	6 Hrs.	Single phase. Twinned
0.5	2.5	0.22	1050°C	7 Hrs.	Single phase. Twinned
0.6	2.5	0.53	1050°C	65 Hrs.	Twinned 2-17 phase + some 1-5 phase
0.7	2.5	0.19	1050°C	65 Hrs.	Single phase. Twinned
0.8	2.5	1.71	1050°C	65 Hrs.	Twinned 2-17 phase + some 1-5 phase
1.0	2.0	0.84	1100°C	48 Hrs.	Excess iron

1. Wt. % Added based on stoichiometric rare earth required.
2. % Expressed as % of initial rare earth content.

TABLE IV

Preparation parameters and microstructural evaluation of $Nd_2(Co_{1-x}Fe_x)_{17}$ alloys

X	Excess Nd Added[1] %	% Wt. Loss[2] %	Homogenization Treatment Temp.	Time	Microstructure Evaluation
0.0	2.0	2.41	1050°C	7 Hrs.	Single phase
0.1	2.0	1.84	1050°C	50 Hrs.	Single phase
0.2	2.0	0.44	1050°C	50 Hrs.	Single phase
0.3	2.0	0.35	1050°C	50 Hrs.	Single phase
0.4	2.0	0.22	1050°C	50 Hrs.	Single phase
0.5	3.0	0.56	1050°C	50 Hrs.	Single phase
0.7	2.5	0.86	1050°C	65 Hrs.	Single phase. Twinned
0.8	2.5	0.56	1050°C	65 Hrs.	Single phase. Twinned
1.0	2.0	0.78	1100°C	48 Hrs.	Slight second phase on grain boundaries

1. Wt. % Added based on stoichiometric rare earth required.
2. % Expressed as % of initial rare earth content.

TABLE V

Preparation parameters and microstructural evaluation of $Sm_2(Co_{1-x}Fe_x)_{17}$

X	Excess Sm Added[1] %	% Wt. Loss[2] %	Homogenization Treatment Temp.	Time	Microstructure Evaluation
0.0	12.0	17.18	1200°C	6 Hrs.	Single phase. Twinned
0.1	12.0	16.30	1200°C	6 Hrs.	Excess transition metal on grain boundaries
0.2	12.0	16.31	1200°C	18 Hrs.	Excess transition metal on grain boundaries
0.3	12.0	18.33	1200°C	18 Hrs.	Excess transition metal on grain boundaries
0.4	13.0	21.34	1200°C	20 Hrs.	Excess transition metal on grain boundaries
0.5	13.0	22.98	1200°C	20 Hrs.	Excess transition metal on grain boundaries
0.6	12.0	10.66	1100°C	90 Hrs.	Excess transition metal on grain boundaries
0.7	12.0	16.96	1100°C	90 Hrs.	Excess transition metal on grain boundaries
0.8	12.0	27.26	1150°C	30 Hrs.	Excess transition metal on grain boundaries
0.9	12.0	25.77	1150°C	30 Hrs.	Excess transition metal on grain boundaries
1.0	2.0	38.51	1100°C	48 Hrs.	Excess iron

1. Wt. % Added based on stoichiometric rare earth required.
2. % Expressed as % of initial rare earth content.

TABLE VI

Preparation parameters and microstructural evaluation of $Y_2(Co_{1-x}Fe_x)_{17}$ alloys

X	Excess Y Added[1] %	% Wt. Loss[2] %	Homogenization Treatment Temp.	Time	Microstructure Evaluation
0.0	2.0	6.70*	1100°C	48 Hrs.	Two phase. Segregation at grain boundaries
0.1	2.0	11.52*	1050°C	6 Hrs.	Excess transition metal
0.2	2.0	4.93*	1050°C	6 Hrs.	Single phase
0.3	2.0	60.42*	1050°C	7 Hrs.	Single phase. Heavily twinned
0.4	2.5	7.97*	1200°C	6 Hrs.	Single phase. Heavily twinned
0.5	2.5	5.65*	1200°C	6 Hrs.	Single phase. Heavily twinned
0.6	2.5	1.54*	1150°C	70 Hrs.	Single phase. Heavily twinned
0.7	2.5	2.56*	1150°C	70 Hrs.	Single phase. Heavily twinned
0.8	2.5	3.84*	1150°C	70 Hrs.	Single phase. Heavily twinned
1.0	2.0	12.29*	1100°C	48 Hrs.	Trace of Y_6Fe_{23}

1. Wt. % Added based on stoichiometric rare earth required.
2. % Expressed as % of initial rare earth content.

* Wt. Loss data erroneous due to fragmentation of alloy on cooling.

TABLE VII

Preparation parameters and microstructural evaluation of $MM_2(Co_{1-x}Fe_x)_{17}$ alloys

X	Excess MM Added[1] %	% Wt. Loss[2] %	Homogenization Treatment Temp.	Time	Microstructure Evaluation
0.0	---	0.65	1100°C	48 Hrs.	Nearly single phase
0.1	2.0	2.08	1050°C	6 Hrs.	Nearly single phase
0.2	2.0	4.09	1050°C	6 Hrs.	Nearly single phase
0.3	2.0	3.05	1050°C	7 Hrs.	Nearly single phase
0.4	3.0	1.88	1050°C	6 Hrs.	Single phase. Twinned
0.5	3.0	1.48	1050°C	7 Hrs.	Single phase. Twinned
0.75	2.0	1.11	1000°C	18 Hrs.	Excess transition metal
	2.0	1.11	1050°C	65 Hrs.	Excess transition metal
1.0	2.0	3.65	1100°C	48 Hrs.	Two phase. Excess iron

1. Wt. % Added based on stoichiometric rare earth required.
2. % Expressed as % of initial rare earth content.

C. LATTICE CONSTANTS DETERMINATIONS FOR THE $R_2(Co, Fe)_{17}$ ALLOYS*

Hexagonal lattice constants for the rhombohedral Th_2Zn_{17} - type phases, $R_2(Co_{1-x}Fe_x)_{17}$, with R = Ce, Pr, Nd, Sm, Y and MM (Ce-rich mischmetal) and x having values from 0.0 to 1.0 were determined by standard powder X-ray diffraction techniques. A G.E. XRD-6 diffractometer and Type 700 detector with vanadium-filtered CrK_α radiation was employed. Resultant diffraction patterns were indexed and lattice constants were computed. Computer refinements of lattice constant data were obtained using the methods of Vogel and Kempter.[2] Zero degree 2θ errors were corrected through the use of Ni as an internal standard.

Results of the lattice constant determinations and standard deviations are summarized in Table VIII.

A more detailed discussion of the lattice constant study and its results is presented in the Appendix.

*R. S. Harmer, J. Geis, C. Shanley, and A. E. Ray

TABLE VIII

Hexagonal lattice parameters for the rhombohedral Th_2Zn_{17}-type phases $R_2(Co_{1-x}Fe_x)_{17}$

R	Ce		Pr		Nd	
X	a_o, Å	c_o, Å	a_o, Å	c_o, Å	a_o, Å	c_o, Å
0.0	8.381 ± .001	12.207 ± .001	8.432 ± .002	12.274 ± .002	8.429 ± .001	12.246 ± .001
0.1	8.3947 ± .0006	12.225 ± .002	8.457 ± .001	12.302 ± .002	8.447 ± .002	12.287 ± .004
0.2	8.412 ± .001	12.300 ± .006	8.4739 ± .0006	12.322 ± .002	8.463 ± .001	12.325 ± .002
0.3	8.4299 ± .0009	12.356 ± .002	8.484 ± .001	12.387 ± .003	8.482 ± .001	12.366 ± .002
0.4	8.4353 ± .0008	12.391 ± .001	8.502 ± .001	12.390 ± .004	8.4999 ± .0008	12.407 ± .001
0.5	8.446 ± .002	12.433 ± .002	8.520 ± .001	12.478 ± .006	8.512 ± .002	12.435 ± .004
0.6	8.4645 ± .0009	12.473 ± .002	8.5408 ± .0007	12.493 ± .003		
0.7	8.480 ± .001	12.495 ± .002	8.556 ± .002	12.514 ± .003	8. 5540 ± . 0006	12. 501 ± . 001
0.75			8.563 ± .001	12.520 ± .002	8.561 ± .002	12.512 ± .003
0.8	8.487 ± .001	12.489 ± .002	8.567 ± .002	12.515 ± .005	8.566 ± .001	12.507 ± .001
0.9	8.492 ± .001	12.460 ± .002				
1.0	8.487 ± .002	12.404 ± .001	8.698 ± .007	11.950 ± .003	8.597 ± .003	12.460 ± .004

TABLE VIII (Continued)

Hexagonal lattice parameters for the rhombohedral Th_2Zn_{17}-type phases $R_2(Co_{1-x}Fe_x)_{17}$

R	Sm		Y		MM	
X	a_o, Å	c_o, Å	a_o, Å	c_o, Å	a_o, Å	c_o, Å
0.0	8.405 ± .003	12.226 ± .007	8.361 ± .001	12.12 ± .010	8.4062 ± .0007	12.233 ± .001
0.1	8.414 ± .001	12.256 ± .002	8.3664 ± .0009	12.232 ± .002	8.424 ± .002	12.262 ± .009
0.2	8.4298 ± .0009	12.297 ± .001	8.3847 ± .0009	12.259 ± .009	8.446 ± .004	12.364 ± .003
0.3	8.452 ± .002	12.361 ± .006	8.401 ± .002	12.315 ± .002	8.4514 ± .0007	12.372 ± .005
0.4	8.4667 ± .0009	12.408 ± .009	8.424 ± .001	12.347 ± .001	8.471 ± .001	12.407 ± .001
0.5	8.471 ± .001	12.387 ± .001	8.445 ± .001	12.381 ± .002	8.487 ± .001	12.448 ± .002
0.6	8.501 ± .002	12.432 ± .004	8.4635 ± .0009	12.416 ± .002		
0.7	8.516 ± .002	12.469 ± .003	8.476 ± .001	12.429 ± .002		
0.75			8.482 ± .001	12.437 ± .002	8.520 ± .002	12.518 ± .003
0.8	8.524 ± .002	12.484 ± .003	8.492 ± .001	12.438 ± .002		
0.9	8.537 ± .002	12.472 ± .003				
1.0	8.552	12.444	8.501 ± .003	12.398 ± .005	8.526 ± .002	12.451 ± .005

D. DIFFERENTIAL THERMAL ANALYSIS*

The description and use of the Differential Thermal Analysis (DTA) apparatus in the study of binary phase equilibria in the mixed intermetallic systems $R_2(Co, Fe)_{17}$ has been presented previously.[1] Complete results of these studies are presented in Tables IX through XIV and are summarized in Figure 1.

*A. Biermann and A. E. Ray

TABLE IX

Thermal events observed for the mixed intermetallic phase $Ce_2(Co_{1-x}Fe_x)_{17}$

X	Temperature in °C Observed for						Heat Treatment	
	Curie Event	Ordering in Fe-Co Lattice	Rhomb. Hex. Transformation	Peritectic	Monotectic(?)	Liquidus	Temp.	Time
0.0	801	---	----	1206	----	1289	1100°C	50 Hrs.
0.1	787	---	----	1186	----	1273	1100°C	18 Hrs.
0.1	783	---	----	1192	----	1278	1050°C	6 Hrs.
0.1	790	---	1045	1188	----	1268	1000°C	60 Hrs.
0.2	772	---	1032	1173	----	1283	1100°C	18 Hrs.
0.2	759	---	1035	1182	----	1287	1050°C	6 Hrs.
0.2	766	---	1050	1178	----	1279	1000°C	18 Hrs.
0.3	742	---	1048	1156	----	1292	1100°C	18 Hrs.
0.3	722	---	1045	1156	----	1293	1050°C	7 Hrs.
0.3	735	---	1050	1156	----	1285	1000°C	18 Hrs.
0.4	688	851	1063	1139	----	1304	1100°C	18 Hrs.
0.4	672	861	1066	1137	----	1266	1050°C	6 Hrs.
0.4	673	847	1065	1140	----	1289	1000°C	18 Hrs.
0.5	693	876	1085	1116	----	1311	1100°C	18 Hrs.
0.5	647	879	1080	1115	----	1292	1050°C	7 Hrs.
0.5	608	876	1081	1119	----	1289	1000°C	18 Hrs.
0.6	522	870	1005	1091	----	1290	1000°C	18 Hrs.
0.7	433	822	985	1075	1320	1334	1000°C	18 Hrs.
0.8	303	---	956	1060	1318	1356	1000°C	18 Hrs.
0.9	132	---	940	1054	1332	1413	1000°C	18 Hrs.
1.0	(-180)*	---	----	1065	1284	1397	1100°C	48 Hrs.

* See Ref. 11.

TABLE X

Thermal events observed for the mixed intermetallic phase $Pr_2(Co_{1-x}Fe_x)_{17}$

X	Temperature in °C Observed for			Heat Treatment	
	Curie Event	Peritectic	Liquidus	Temp.	Time
0.0	890	1265	1327		
0.1	876	1259	1315	1050°C	6 Hrs.
0.2	850	1245	1309	1050°C	6 Hrs.
0.3	817	1230	1309	1050°C	7 Hrs.
0.4	760	1214	1320	1050°C	6 Hrs.
0.5	698	1198	1326	1050°C	7 Hrs.
0.75	466	1050	1372	1050°C	18 Hrs.
1.0	(14)*	1106	1436	1100°C	48 Hrs.

*See Ref. 11.

TABLE XI

Thermal events observed for the mixed intermetallic phase $Nd_2(Co_{1-x}Fe_x)_{17}$

	Temperature in °C Observed for			Heat Treatment	
X	Curie Event	Peritectic	Liquidus	Temp.	Time
0.0	906	1290	1309	1050°C	7 Hrs.
0.1	884	1277	1306	1050°C	50 Hrs.
0.2	871	1264	1304	1050°C	50 Hrs.
0.3	817	1256	1312	1050°C	50 Hrs.
0.4	773	1250	1325	1050°C	50 Hrs.
0.5	710	1238	1331	1050°C	50 Hrs.
0.75	481	1218	1383	1050°C	65 Hrs.
1.0	(54)*	1208	1399	1100°C	48 Hrs.

*See Ref. 11.

TABLE XII

Thermal events observed for the mixed intermetallic phase $Sm_2(Co_{1-x}Fe_x)_{17}$

	Temperature in °C Observed for			Heat Treatment	
X	Curie Event	Peritectic	Liquidus	Temp.	Time
0.0	926	1310	1355	1200 °C	6 Hrs.
0.1	916	1304	1342	1200 °C	6 Hrs.
0.2	886	1296	1331	1200 °C	18 Hrs.
0.3	856	1286	1341	1200 °C	18 Hrs.
0.4	806	1283	1348	1200 °C	20 Hrs.
0.5	747	1280	1360	1200 °C	20 Hrs.
0.6	675	1278	1394	1150 °C	30 Hrs.
0.7	580	1275	1423	1150 °C	30 Hrs.
0.8	468	1276	1433	1150 °C	30 Hrs.
0.9	311	1278	1458	1150 °C	30 Hrs.
1.0	121	1279	1483	1100 °C	48 Hrs.

TABLE XIII

Thermal events observed for the mixed intermetallic phase $Y_2(Co_{1-x}Fe_x)_{17}$

X	Temperature in °C Observed for			Heat Treatment	
	Curie Event	Rhomb. to Hex. Transformation	Liquidus	Temp.	Time
0.0	916	1321	1359	1100°C	48 Hrs.
0.1	909	1333	1352	1050°C	6 Hrs.
0.2	881	1326	1349	1050°C	6 Hrs.
0.3	847	1332	1340	1050°C	7 Hrs.
0.4	793	1320	1334	1200°C	6 Hrs.
0.5	741	1314	1333	1200°C	6 Hrs.
0.6	642	1264	1339	1150°C	70 Hrs.
0.7	535	1291	1334	1150°C	70 Hrs.
0.8	423	1309	1347	1150°C	70 Hrs.
1.0	31	1337	1359	1100°C	48 Hrs.

TABLE XIV

Thermal events observed for the mixed intermetallic phase $MM_2(Co_{1-x}Fe_x)_{17}$

X	Temperature in °C Observed for			Heat Treatment	
	Curie Event	Peritectic	Liquidus	Temp.	Time
0.0	836	1218	1279	1100°C	48 Hrs.
0.1	830	1216	1287	1050°C	6 Hrs.
0.2	803	1198	1300	1050°C	6 Hrs.
0.3	763	1177	1303	1050°C	7 Hrs.
0.4	708	1162	1309	1050°C	6 Hrs.
0.5	647	1141	1331	1050°C	7 Hrs.
0.75	534	1093	1356	1000°C	18 Hrs.
1.0	nd*	1106	1430	1100°C	48 Hrs.

* not yet determined

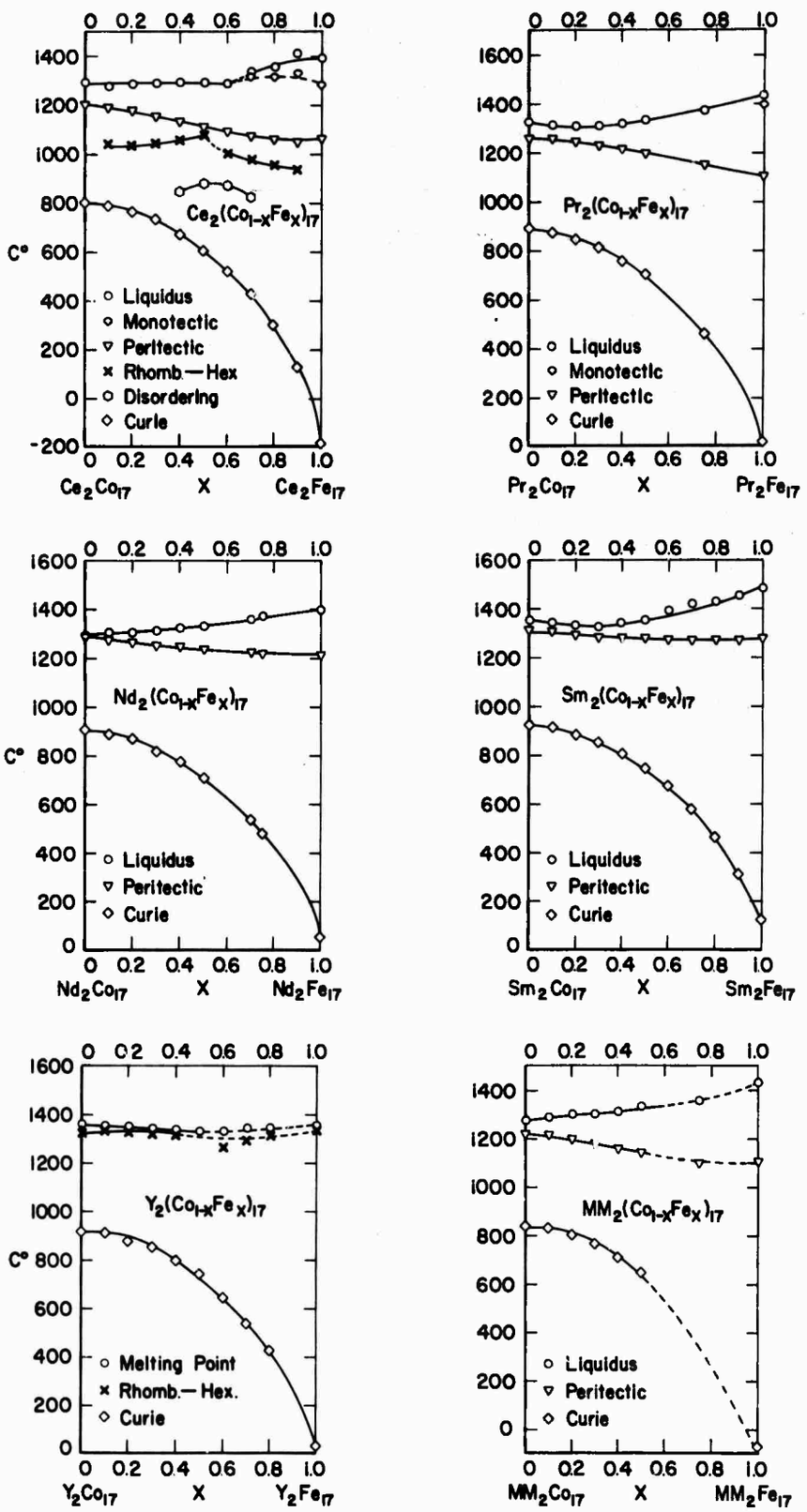

Figure 1. Melting behavior and Curie temperatures for $R_2(Co_{1-x}Fe_x)_{17}$ phases obtained by DTA.

E. THERMOMAGNETIC ANALYSES OF $R_2(Co, Fe)_{17}$ ALLOYS*

Initial thermomagnetic analyses have been conducted on several of the mixed ternary phases with R = Ce. These results are reported in Section III.B.4 d. The TMA and DTA results are in essential agreement concerning the Curie temperatures of the $R_2(Co, Fe)_{17}$ phases. Furthermore, the TMA measurements show that the intense thermal events observed between 850 and 900°C for $Ce(Co_{1-x}Fe_x)_{17}$ alloys with x = 0.4 to 0.7 also involve strong magnetic transitions.

*H. Mildrum and M. Hartings

F. DETERMINATION OF THE EASY AXIS OF MAGNETIZATION BY MEANS OF X-RAY DIFFRACTION*

1. Discussion of the Method

The determination of the easy axis of magnetization of a ferromagnetic or ferrimagnetic compound generally requires either magnetic measurements on an oriented single crystal or the use of neutron diffraction. When the magnetic anisotropy of the substance is high, however, a simpler method may be employed. This method involves X-ray diffraction measurements on powders pre-aligned in a magnetic field. The crystallographic direction of the easy axis is deduced from the study of the orientation texture of the diffraction pattern. Strong anomalies are observed in diffraction patterns of pre-aligned powders obtained by the rotating crystal method as well as the Debye-Scherrer method. We shall briefly discuss these as an aid to a better understanding of the method used here.

If the sample is a powder without preferential orientation, the Bragg X-ray maxima are diffracted in cones, whose angles are at discrete values of $2\theta_{hk\ell}$. The recorded X-ray diffraction patterns have the general appearance of Figure 2.

If the sample is a single crystal rotating around an axis $[u, v, w]$, the points $(hk\ell)$ of the reciprocal lattice lie in a set of planes that are perpendicular to the vector $[u, v, w]$. As a consequence, during the rotation of the crystal, these planes cut the Ewald sphere along a discrete number of circles and the rotating crystal diffraction patterns

*J. Schweizer and C. Shanley

appear as shown in Figure 3. The Bragg reflections are located on discrete horizontal lines. In particular, a reflection (hkℓ), lies on the n^{th} line, where uh + vk + wℓ = n.

2. Diffraction by a Powder Aligned in a Magnetic Field

The sample is a needle formed from a powder of the ferromagnetic compound consisting, ideally, of single-crystal particles which have been aligned and bonded with a cement in a magnetic field. The sample is mounted on the goniometer of a rotating crystal camera with the long axis of the needle parallel to the rotation axis. Each grain is now supposed to be oriented with its easy axis of magnetization parallel to the axis of the needle and therefore parallel to the axis of rotation. If the orientation were perfect, the X-ray pattern obtained would be equivalent to that of a single crystal rotating around its easy axis of magnetization. This is not exactly the case; the magnetic alignment is not perfect and the X-ray pattern is intermediate between a powder pattern and a rotating crystal pattern. Debye-Scherrer lines are present, but they are very inhomogeneous with strong intensity maxima occurring where the reflections would be if the sample were a single crystal rotating around the same axis, as illustrated in Figure 4. The stronger the magnetic anisotropy and the stronger the magnetic field applied during the alignment process, the stronger is the orientation texture of these lines. The analysis of the texture indicates which crystalline axis of the grains are aligned on the average with the long axis of the needle, which is the easy axis of magnetization at the temperature at which the needle has been bonded.

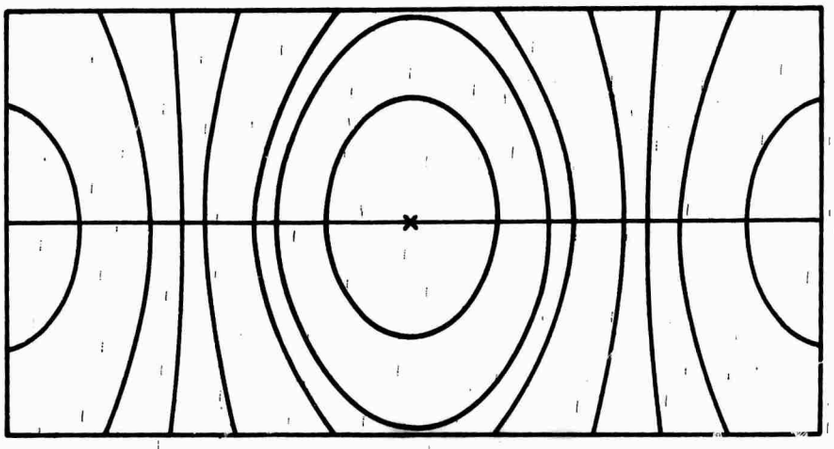

Figure 2. Rotating crystal method X-ray diffraction pattern of a crystalline powder without preferential orientation.

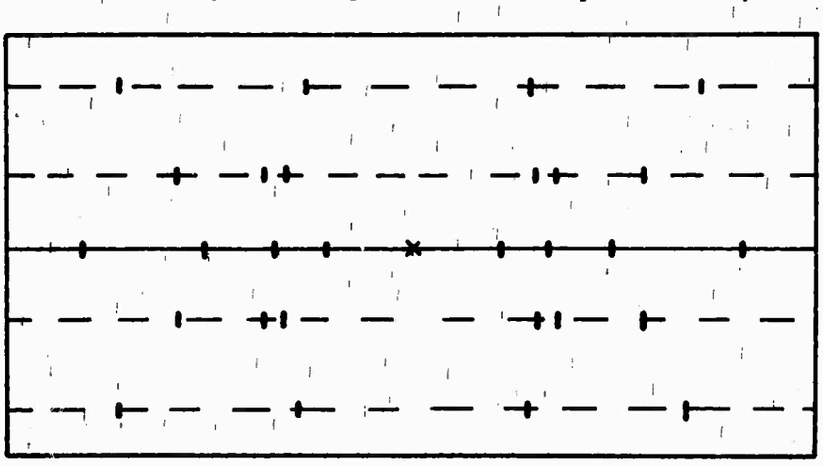

Figure 3. Rotating crystal method X-ray diffraction pattern of a single crystal aligned around a major axis.

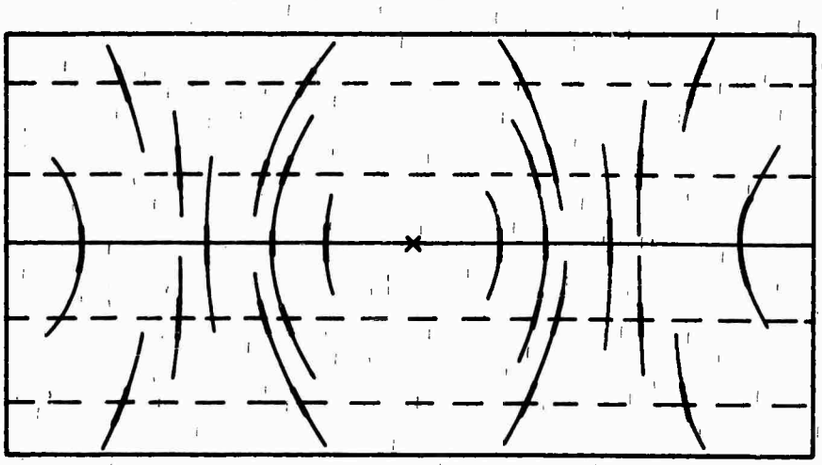

Figure 4. Rotating crystal method X-ray diffraction pattern of a crystalline powder with a strong preferential orientation around a major axis.

3. Conclusions

a. This method is very convenient for determining the easy axis of magnetization at room temperature.

b. The magnetic field must be large enough to saturate the sample, i.e., to remove all magnetic domains except one in each grain. An insufficient field may align even single-crystal grains parallel to an axis different from the easy axis if two or more easy directions exist in the crystal. Even in a single-crystal grain with a unique easy axis, however, to which the total magnetic moment can only be parallel, the orienting mechanical torque moment exerted by the field may be too small unless the grain is nearly saturated.

c. This method works well only for materials with a strong magnetic crystal anisotropy. If the crystal anisotropy is not high, the shape anisotropy of the grains will also play a role in the alignment and may lead to wrong conclusions. The method is therefore very suitable for studying rare earth-cobalt-iron compounds because they are in general quite strongly anisotropic.

4. Experimental Procedures

Freshly powdered, -200 mesh (<78μm), $R_2(Co, Fe)_{17}$ alloys were premagnetized in a field of 26 KOe, mixed with an epoxy to form a thick paste and placed in a 6 KOe field to grow thin needles of oriented alloy particles. After the epoxy cured, needles were placed in a Weissenberg camera and rotating crystal diffraction patterns were obtained.

Vanadium-filtered CrK_α radiation was employed. The direction of easy magnetization was determined by qualitative evaluation of the texture exhibited in the diffraction patterns.

5. Results

The results of the magnetic easy axis determination are presented in Table XV. It should be noted that, with the exception of R = Nd, there exists a range of composition in the mixed intermetallic $R_2(Co, Fe)_{17}$ alloys over which the easy direction of magnetization corresponds to the crystallographic c-axis.

TABLE XV

Magnetic easy axis determination

in the mixed intermetallic phases $R_2(Co_{1-x}Fe_x)_{17}$

R / X	Ce	Pr	Nd	Sm	Y	MM
0.0	basal	basal	basal	c-axis	basal	basal
0.1	c-axis	basal	basal	nd	c-axis	c-axis
0.2	c-axis	c-axis	basal	nd	nd	c-axis
0.25	nd	c-axis	nd	nd	nd	c-axis
0.3	c-axis	c-axis	basal	nd	c-axis	c-axis
0.4	c-axis	c-axis	basal	c-axis	c-axis	c-axis
0.5	basal	c-axis	basal	c-axis	c-axis	basal
0.6	basal	c-axis	nd	basal	basal	nd
0.7	basal	basal	basal	basal	basal	nd
0.75	nd	basal	basal	nd	basal	basal
0.8	nd	basal	basal	basal	basal	nd
0.9	basal	-	-	basal	-	-
1.0	basal	basal	basal	basal	basal	basal

nd - not yet determined

G. CONCLUSIONS

The mixed intermetallic phases of the type $R_2(Co_{1-x}Fe_x)_{17}$ were studied with view toward their possible utility as permanent magnet materials. Three basic magnetic properties must be favorable if a material is to qualify for this application: the saturation magnetization, the Curie temperature and the magnetocrystalline anisotropy. We know that the saturation is high enough to qualify virtually all the phases under consideration, namely those with R = Ce, Pr, Nd, Sm, Y and MM (Ce-rich mischmetal), so that we concentrated on the Curie temperature and crystal anisotropy as the principal selection criteria.

The investigation had the hoped-for result: It showed that a number of the phases have indeed properties which promise magnets far superior even to the ones made from RCo_5 compounds.

The Curie temperatures of the cobalt compounds are all over 800°C, but those of the iron compounds are uncomfortably low: all below 180°C and some even below room temperature. If the Curie point fell linearly from the R_2Co_{17} value as iron was introduced, only very limited Fe substitutions would be tolerable. But our experiments show that the Curie points remain very high, namely above 600°C, even for large substitutions of iron, up to 50% or more.

With respect to crystal anisotropy, the prospects looked bleak on the basis of earlier measurements on the "pure" iron and cobalt compounds.

All of the compounds of Fe and most of those of Co were found to have a magnetic symmetry featuring an easy basal plane, rather than the desirable easy axis. But, somewhat surprisingly, the recent extension of these studies to the mixed compounds revealed that in every quasibinary system except that with R = Nd, a composition range exists in which the ternary phase has an easy direction of the magnetization coinciding with the crystallographic c-axis.

Future work will concentrate on these ranges and on the quantitative determination of the anisotropy field strengths. For the permanent-magnet application, the existence of an easy axis is not enough; the anisotropy field must also be quite high. We shall also begin measurements of the magnetic saturation moments and the temperature dependence of the magnetization. There is some likelihood that the saturation may also be higher for some of the ternary alloys than for the terminal binary compounds; at least it should rise faster than linearly from the R_2Co_{17} values as iron is substituted for cobalt.

SECTION II

METALLURGICAL AND STRUCTURAL STUDIES OF PRASEODYMIUM-COBALT ALLOYS

A. INTRODUCTION

Sintering experiments on $PrCo_5$ with Pr-rich Pr-Co alloys as sintering aids have shown that the coercivities and energy products of the resulting magnets are very sensitive to the sintering temperatures.[3] The sensitive sintering temperatures correlate closely with thermal events in the Pr-Co phase diagram.[4] Models have been proposed to account for the observed correlations and the mechanisms by which the coercivities of the magnets are increased.[5] In view of the importance of reliable phase diagrams, not only for determining methods for alloy preparation and heat treatment but also as guides to understanding and controlling the magnetic behavior of the rare earth alloys, a further investigation of the praseodymium-cobalt alloy system was undertaken. Although alloys across the entire range of compositions between the pure components have been examined, this investigation has been concentrated on the region between 0 and 50 at. % Co, which had been neglected in the earlier study, and on the region between the intermetallic phases Pr_2Co_7 (77.8 at. %Co) and $PrCo_5$ (83.3 at. %Co). The features of the Pr-Co phase diagram which have been established are given in part B of this section. In part C, the crystal structure of a previously unreported phase, $Pr_2Co_{1.7}$, is described.

B. THE PRASEODYMIUM-COBALT PHASE DIAGRAM*

1. Materials and Alloy Preparation

Analyses of the cobalt and praseodymium metals employed for the preparation of the alloy are given in Table XVI. Two different shipments of praseodymium supplied by the Lunex Company have been used. Differential thermal analyses showed the first shipment to melt at 928°C and undergo the $\alpha \rightleftharpoons \beta$ transformation at 788°C. For the second shipment, these thermal events were observed at 932°C and 792°C, respectively. Both measurements are within experimental error of each other and agree closely with the accepted values of 935 ±5°C and 792 ±5°C.[6]

The alloys were prepared by arc melting the pure components in a purified argon-helium atmosphere, the arc passing from a thoriated tungsten electrode to a water-cooled copper hearth. The buttons were inverted and remelted several times to enhance mixing. Weight losses on melting were minimal, seldom exceeding 0.1%. However, to correct for impurity pickup during processing, the praseodymium content of each alloy was increased by 1.0 wt. % of the amount nominally required. The arc melted alloys were wrapped in tantalum foil and annealed in vacuum for 1 to 7 days. Alloys containing from 5 to 65 at. %Co were homogenized at 500°C, from 66 to 75 at. %Co at 800°C, from 76 to 78 at. %Co at 1000°C, from 78 to 83 at. %Co at 1075°C and 83 to 95 at. %Co at 1100°C. Thus, metallography, X-ray diffraction, and differential thermal analyses were performed on alloys near equilibrium conditions.

*A. E. Ray, A. Biermann, and R. S. Harmer

TABLE XVI

Analyses of metals used for the preparation of praseodymium-cobalt alloys

	Impurities in ppm			
	Pr_I	Pr_{II}	Cobalt (99.93%)	
Ta	10*	10*	Ni	4300
Pb	-	10*	C	700
Ca	200**	200**	Fe	300
Be	10*	10*	Zn	300
B	50*	50*	Pb	40
Zn	50*	50*	Cu	200
Zr	-	20*	S	300
La	10*	-	Si	200
Ce	50*	50*	Mn	50
Nd	50*	50*	P	30
Tb	50*	50*		
Ho	50*	50*		
Er	100*	100*		
Yb	-	50		
Leco O_2	515	<800		
Kjeldahl N_2	12	<5		
Total all other elements	<50	<50		

*No persistent line was found. Value reported is the detection limit for the element.

**Value for calcium is high since the electrode case is made of a calcium containing compound.

(Sources: Praseodymium - The Lunex Company
Pleasant Valley, Iowa
Cobalt - African Metals Corporation
New York, New York)

2. Results

Previous work on the Pr-Co alloy system has established a eutectic reaction near 34 at. %Co. It was further established that an intermetallic phase exists at 25 at. %Co (Pr_3Co) and peritectic phases exist at 66.7 ($PrCo_2$), 75 ($PrCo_3$), 77.8 (Pr_2Co_7), 83.3 ($PrCo_5$), and 89.5 (Pr_2Co_{17}) at. %Co. It was suspected, on the basis of thermal events observed by DTA, that at least one peritectic phase existed in the vicinity of 50 at. %Co. Subsequent X-ray diffraction and metallographic examinations of nearly equiatomic Pr-Co alloys used in sintering experiments established the existence of $Pr_2Co_{1.7}$ (See section II.C). It was assumed that the lower of two closely spaced thermal events at 1119 ±5 and 1127 ± 4°C in alloys between 75 and 83 at. %Co was associated with a phase transformation in Pr_2Co_7 although another peritectic phase existing between Pr_2Co_7 and $PrCo_5$ was also possible. In the present study, initial sets of alloys were prepared, one set corresponding to each of the known or suspected invariant reactions in the alloy system and another corresponding to compositions halfway between each of the invariant points. Results obtained from the initial alloys indicated additional compositions were necessary to outline features not previously known concerning the alloy system. Some of the latter group of alloys have not yet been examined.

The invariant reactions observed in the praseodymium-cobalt alloy system are given below. Since several details remain to be established, the phase diagram, Figure 5, must still be regarded as tentative.

Eutectic I - A eutectic reaction occurs between praseodymium metal and Pr_3Co at 570± 2°C and 19.5± 0.5 at. % Co.

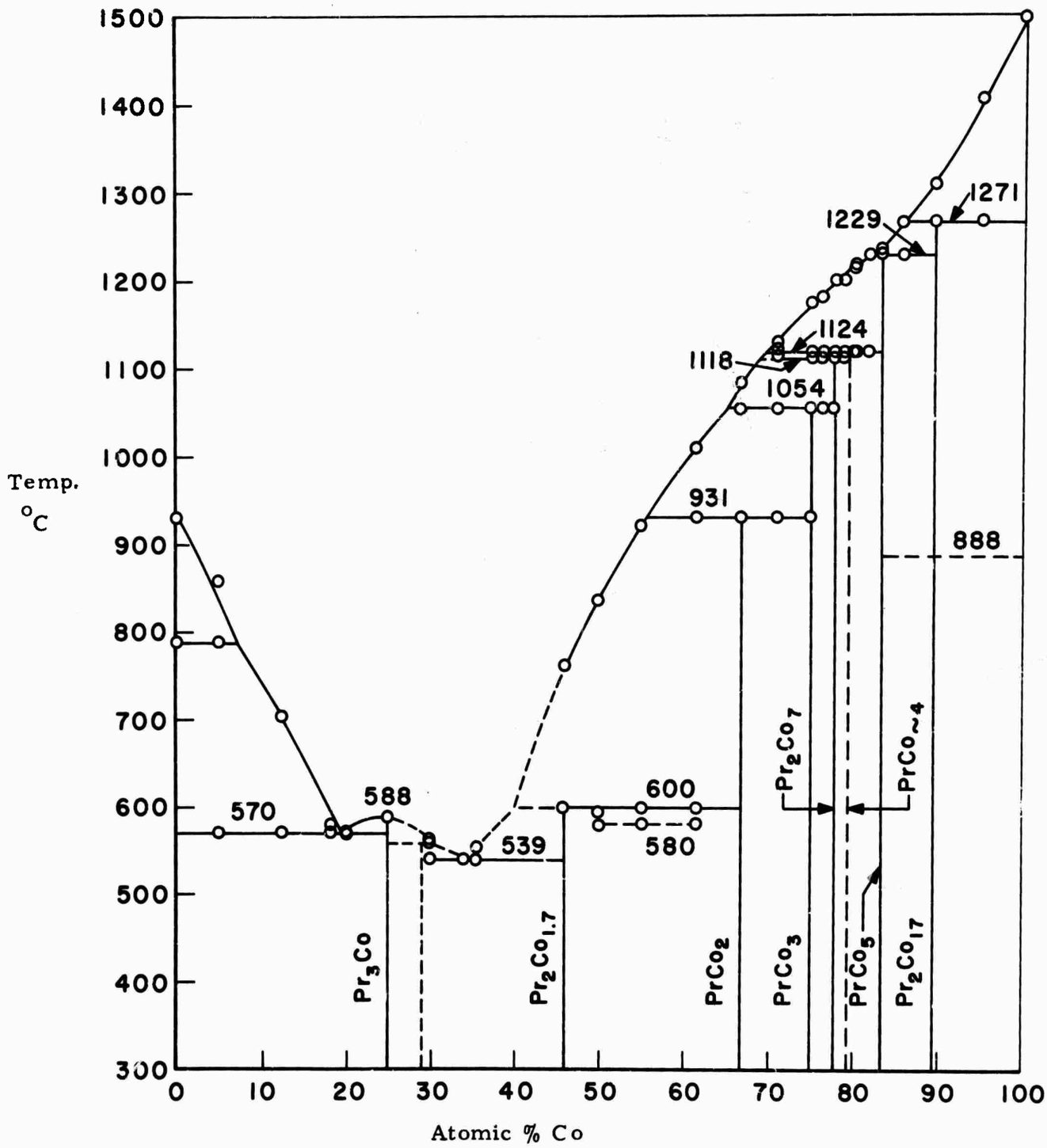

Figure 5. Proposed phase diagram for the praseodymium-cobalt alloy system.

Pr_3Co - The intermetallic phase Pr_3Co melts congruently at 588 ± 2°C. The lattice constants observed for orthorhombic Pr_3Co at 25 at. %Co were a = 7.13 ± .01Å, b = 9.82 ± .02Å, and c = 6.42 ± .01Å. Buschow and van der Goot[7] report Pr_3Co, which is isomorphous with Fe_3C, with lattice constants a = 7.143Å, b = 9.780Å, and c = 6.410Å. A slight range of solubility on either side of stoichiometric Pr_3Co is indicated. The lattice constants for Pr_3Co in the Pr + Pr_3Co phase field were 7.14 ± .01Å, 9.90 ± .02 Å, and 6.44 ± .01Å. In the Pr_3Co + $Pr_{\sim 7}Co_{\sim 3}$ phase field, the observed lattice constants were a = 7.09 ± .01Å, b = 9.76 ± .02Å, and c = 6.41 ± .01Å.

$Pr_{\sim 7}Co_{\sim 3}$ - A previously unreported phase was observed to form by peritectic reaction at 558°C. This existence of this phase has been established metallographically, by DTA and by XRD. No attempt has been made to index the powder X-ray diffraction pattern for this phase, Table XVII, and its exact composition will probably have to await crystal structure analysis. Micrographs for 29.5 and 30 at. %Co alloys are compared in Figure 6. It appears that the 29.5 at. %Co is very close to the single phase composition, but slightly cobalt-rich.

Eutectic II - A eutectic reaction between $Pr_{\sim 7}Co_{\sim 3}$ and $Pr_2Co_{1.7}$ occurs at 541 ± 2°C and 34 at. %Co.

$Pr_2Co_{1.7}$ - The intermetallic phase $Pr_2Co_{1.7}$ forms by peritectic reaction at 598 ± 5°C and 46 at. %Co. The details of the crystal structure of this phase are discussed in part C of this Section.

Unidentified Thermal Event - Thermal analyses of alloys containing 50, 55, and 61.5 at. %Co show an event at 580 ± 4°C. The nature of

TABLE XVII

X-ray diffraction pattern for Pr-30 at. %Co

d	I/Io
3.483	W
3.255	W
3.180	W
3.110	M
2.993	W
2.944	S
2.820	S
2.741	M
2.622	M
2.596	M
2.548	M
2.453	W
2.398	VW
2.345	VW
2.291	W
2.253	W
2.224	M
2.160	W
1.960	W
1.919	W
1.781	W
1.760	W
1.729	W
1.714	W

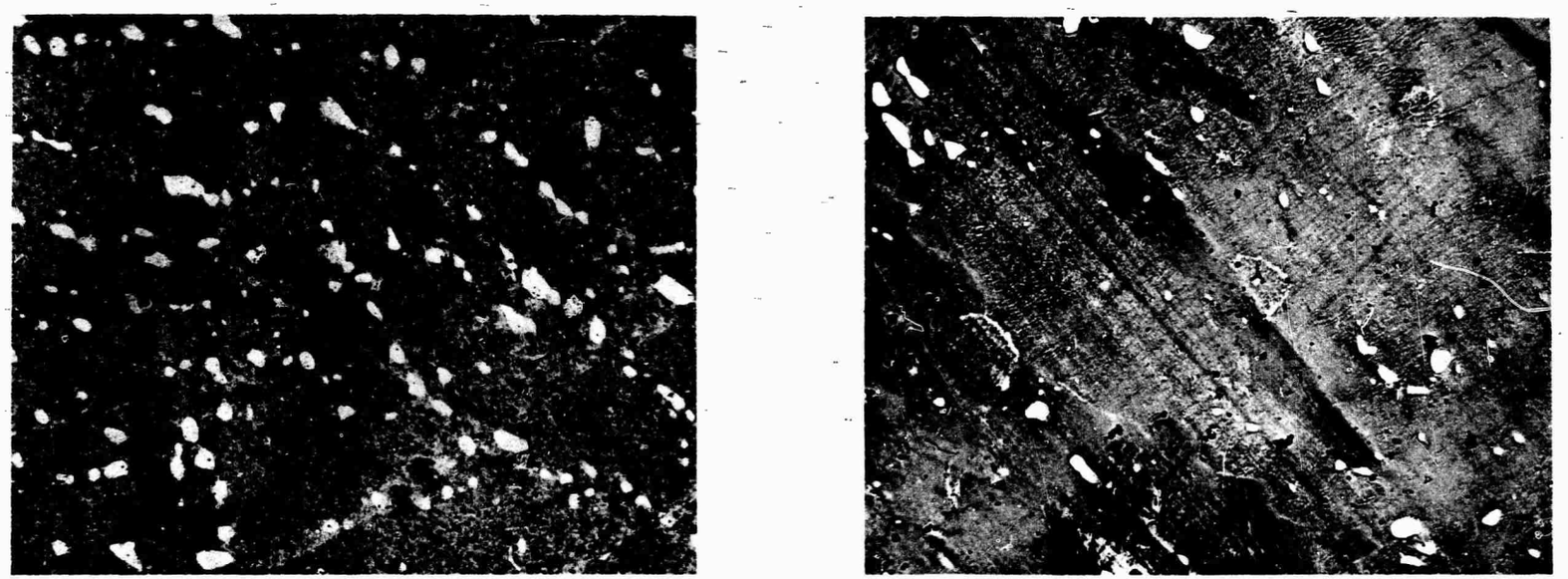

(a) Pr-30 at. %Co
Magnification: 250x

(b) Pr-29. 5 at. %Co
Magnification: 250x

Figure 6. Microstructures of (a) 30. 0 and (b) 29. 5 at. %Co alloys annealed 168 hours at 500C. In each case, the light, isolated phase is $Pr_2Co_{1.7}$ and the matrix is the unidentified peritectic phase $Pr_{\sim 7}Co_{\sim 3}$. The 29. 5 at. %Co alloy is close to the single phase composition.

this event is not known. X-Ray diffraction patterns of these alloys, annealed at 500°C, show only $Pr_2Co_{1.7}$ and $PrCo_2$ to be present. Furthermore, the event is not observed in DTA traces of either of the single phase alloys.

$PrCo_2$ - The intermetallic phase $PrCo_2$ forms by peritectic reaction at 931 ± 5°C. The lattice constant obtained for $PrCo_2$, which has a cubic $MgCu_2$-type structure, was 7.306 ± .001Å. No significant change in the lattice constant of $PrCo_2$ with composition was noted.

$PrCo_3$ - The intermetallic phase $PrCo_3$ forms by peritectic reaction at 1057 ± 5°C. Lattice constant measurements indicate a small range of solubility for this rhombohedral, $PuNi_3$-type structure. In the $PrCo_2$ + $PrCo_3$ phase field that we observed a = 5.071 ± .001Å and c = 24.80 ± .02Å. For single phase $PrCo_3$ at 75 at. %Co, we found a = 5.066 ± .001Å and c = 24.77 ± .01Å. In the $PrCo_3$ + Pr_2Co_7 phase field we measured a = 5.049 ± .006Å and 24.48 ± .02Å.

Pr_2Co_7 - The intermetallic phase Pr_2Co_7 forms by peritectic reaction at 1118 ± 5°C. It was previously suggested[4] that this reaction was probably the rhombohedral to hexagonal transformation in Pr_2Co_7 and that thermal event at 1124°C was the peritectic reaction for Pr_2Co_7. We now propose that this latter event is the peritectic reaction temperature for a previously unreported phase existing between Pr_2Co_7 and $PrCo_5$ as discussed below. As with $PrCo_3$, lattice constant measurements indicate a small range of solid solubility for Pr_2Co_7. We observed the lattice constants for this hexagonal Ce_2Ni_7-type structure to decrease from a = 5.072 ± .003Å and

c = 24.51 ± .01Å for single phase Pr_2Co_7 at 77.8 at. %Co to a = 5.055 ± .005Å and c = 24.38 ± .01Å in the Pr_2Co_7 + $PrCo_{\sim 4}$ phase field.

$PrCo_{\sim 4}$ - An intermetallic phase forms by peritectic reaction at 1125 ± 5°C between 79 and 80 at. %Co. The evidence for this phase is based primarily on XRD, DTA, and TMA measurements since metallographic results obtained to date are inconclusive. Homogenized alloys containing 71, 75, 76.4, 77.8, 78.9, and 79.0 at. %Co. show thermal arrests at both 1118°C and 1124°C while alloys containing 80.0, 80.2, and 81.9 at. %Co show only the arrest at 1124°C on heating. Moreover, for the alloys showing both events, the arrest at 1118°C becomes progressively weaker with increasing cobalt content. TMA measurements of the alloy containing 78.9 at. %Co showed two Curie temperatures, one at 311°C and another at 417°C. Salmans, et al.[10,11] report the Curie temperatures for Pr_2Co_7 and $PrCo_5$ at 301°C and 612°C, respectively. The Curie temperatures of praseodymium cobalt intermetallic phases increase in a regular manner with cobalt content, Figure 7, and 415°C (688°K) is precisely where one would expect to find the Curie temperature of a Pr-Co intermetallic phase containing 79-80 at. %Co.

$PrCo_5$ - The intermetallic phase $PrCo_5$ forms by peritectic reaction at 1229 ± 5°C. Lattice constants for this hexagonal $CaZn_5$-type structure homogenized at 1100°C indicate a range of solubility extending toward Pr_2Co_{17}. We determined a = 5.032 ± .002Å and c = 3.992 ± .002Å in both the $PrCo_{\sim 4}$ + $PrCo_5$ phase field and at the stoichiometric $PrCo_5$ composition, 83.3 at. %Co. In the $PrCo_5$ + Pr_2Co_{17} phase field, however, we observed a = 5.021 ± .005Å

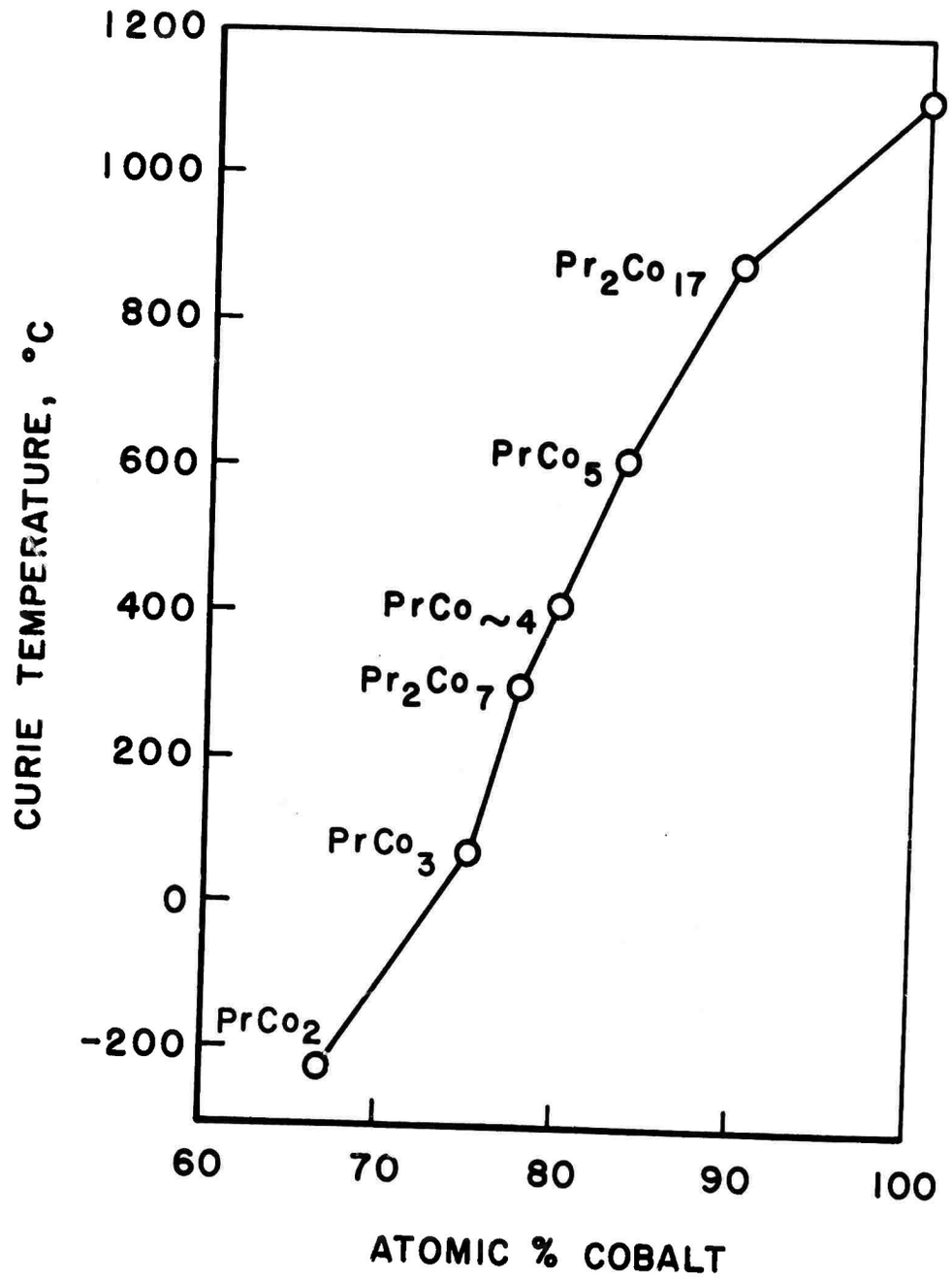

Figure 7. Curie temperatures vs atomic % cobalt for Pr-Co intermetallic phases $PrCo_2$,[6] $PrCo_3$,[7] Pr_2Co_7,[8] $PrCo_{\sim 4}$, $PrCo_5$,[8] and Pr_2Co_{17}.[9]

and c = 4.028 ± .007 Å. The relatively large increase in the c-axis accompanied by a smaller decrease in the a-axis is characteristic of a random substitution of some Pr atoms by pairs of Co atoms aligned parallel to the c-axis.

Pr_2Co_{17} - The intermetallic phase Pr_2Co_{17} forms by peritectic reaction at 1271 ± 5°C. The lattice constants of this rhombohedral Th_2Zn_{17}-type phase were both observed to decrease slightly with increasing at.% Co for alloys homogenized at 1100°C. At 87.5 at.% Co, in the $PrCo_5$ + Pr_2Co_{17} phase field, we obtained a = 8.451 ± .009 Å and c = 12.276 ± .010 Å, at stoichiometric Pr_2Co_{17} (89.5 at.% Co) a = 8.436 ± .002 and c = 12.276 ± .002 and, at 95 at.% Co in the Pr_2Co_{17} + Co phase field, a = 8.429 ± .006 Å and c = 12.238 ± .014 Å.

3. Discussion

The praseodymium-cobalt phase diagram is now well established except for the following features:

a. The exact composition of the previously unreported intermetallic phase near 29 at. % Co will probably have to await crystal structure analysis. We have prepared alloys at 27.5 and 29 at.% Co for additional details concerning the liquidus and the composition of this phase.

b. An alloy containing 40 at.% Co has been prepared to define the liquidus in the composition range between 35 and 45 at.% Co.

c. The thermal event observed at 581°C for alloys containing from 50 to 60 at.% Co remains a puzzle. Since it is not observed by DTA on heating the single phase alloys, the event can not be associated with a phase transformation in either $Pr_2Co_{1.7}$ or $PrCo_2$. A peritectoid reaction between $Pr_2Co_{1.7}$ and $PrCo_2$ is also unlikely since no unidentifiable lines were observed in XRD patterns of homogenized alloys in this composition range.

d. The composition and crystal structure of the previously unreported phase between 79 and 80 at.% Co must probably await single crystal structure analysis. All attempts to isolate a single crystal of this phase to date have been unsuccessful. X-Ray powder patterns of alloys containing this phase indicate its structure is closely related to the $PrCo_5$ and Pr_2Co_7 structures since all but a few of the observed lines coincide with d-spacings for one or the other of these phases. Lemaire[27] suggests that the RCo_2, RCo_3, and R_2Co_7 phases are derived from the RCo_5 structure as follows:

$$RCo_5 - Co + R = 2\,RCo_2$$

$$2RCo_5 - Co + R = 3RCo_3$$

$$3RCo_5 - Co + R = 2R_2Co_7$$

From its known composition range between 79 and 80 at. % Co and relationship to the RCo_5 structure, one is tempted to propose that $PrCo_4$ might be Pr_5Co_{19} (79.2 at.%Co) derived from $PrCo_5$ by substituting one Pr atom for one Co atom in every four $PrCo_5$ units.

$$4PrCo_5 - Co + Pr = Pr_5Co_{19}.$$

e. Each of the phases $PrCo_2$, $PrCo_3$, Pr_2Co_7 and $PrCo_5$ have been observed to exist over limited compositional ranges near their peritectic reaction temperatures. The extent of these ranges of solid solubility were not determined.

C. THE CRYSTAL STRUCTURE OF THE INTERMETALLIC COMPOUNDS $Pr_2Co_{1.7}$ AND $Nd_2Co_{1.7}$*

1. Introduction

The phase diagrams of cobalt with any of the rare earth metals are characterized by a great number of intermetallic compounds, each of them existing over a very narrow homogeneity range. This alloying behavior is attributable to the large difference in the atomic radii of the two component metals. An intermediate phase of a given stoichiometric composition usually exists with all or most of the rare earth elements, thus forming a family of isostructural compounds. However, some exceptions from this rule occur, and they are primarily found in the rare earth-rich portions of the phase diagrams and with the light rare earths. As a case in point, the compound R_4Co_3 has been reported to exist with the elements from gadolinium through thulium.[12] This crystal structure does not appear to be stable with the lighter rare earth, though, and in fact no compound near the equiatomic composition was found in investigations of the cerium-cobalt[13, 14] and the samarium-cobalt[7] phase diagrams. The published diagrams for praseodymium and neodymium with cobalt as the partner[4] each show an unexplained thermal arrest in the composition range near 50 atomic %.

Studies of the liquid-phase sintering of $PrCo_5$-based permanent magnets using a praseodymium-rich Pr-Co alloy as the sintering additive[15] caused us to investigate more closely the alloys near the equiatomic

*J. Schweizer and J. Y. Tsui

composition in the Pr-Co system. This work resulted in the identification of a previously unreported compound which also exists with neodymium. The structure of this compound has been studied and is reported here.

2. Results and Interpretation

Alloy samples of various compositions were prepared by both arc and crucible melting of the component metals. The arc melted buttons were studied in the as-cast condition and after annealing in vacuum at 500°C. The samples containing 74 weight % Pr showed almost single phase structures in either condition. This single-phase composition corresponds to 54 atomic % praseodymium and 46% cobalt.

X-Ray powder patterns were indexed in a hexagonal cell. The lattice constants are a = 4.81 Å and c = 4.09 Å. At first glance, the very small dimensions of the unit cell seem irreconcilable with the composition, since the number of atoms per cell cannot exceed four and mutual substitutions between praseodymium and cobalt are not expected.

Rotating-crystal diffraction patterns, generated by rotating the sample around the a-axis and the c-axis, showed that the reflections ($hk\ell$) were absent when $2h + k = 3n$ and ℓ was odd. A very striking feature was noticed in the patterns that were produced by rotating the crystal around the c-axis: besides the regular layers of reflections corresponding to c = 4.09 Å, weak diffuse layers exist which are also perpendicular to the c-axis and correspond to a distance in the direct lattice of 2.37 Å. Incommensurable with the c value, these diffuse planes are the diffraction

pattern of one-dimensional crystals extending parallel to the c-axis. Such an arrangement was first observed by Huml[16]. These linear crystals consist of cobalt atoms which are arranged in regular chains parallel to the c-axis with x = y = 0, and the distance between the nearest neighbors along the chain is 2.37 Å. There is no correlation with respect to z from one chain to the other, and no correlation exists between the z-values of these cobalt atoms and the z-values of the praseodymium atoms which are located in the positions (1/3, 2/3, 3/4; 2/3, 1/3, 1/4) and form the skeleton of the described cell. The observed X-ray intensities fit well with this model. For the (hkℓ) reflections, both the praseodymium and the cobalt atoms contribute to the structure factors because they are independent of the z values; for the (hkℓ) reflections with $\ell \neq 0$, only the praseodymium atoms contribute to the structure factor because of the lack of correlation between the z coordinates of the cobalt atoms. The composition and cell content deduced from these crystallographic data is $Pr_2Co_{1.7}$. This is in good agreement with the composition for which single-phase microstructures were observed.

A closer examination of the diffuse layers shows the existence of weak reflections indicating some correlation between the z values of the different rows of cobalt. This is probably due to some small shift of the praseodymium atoms away from their theoretical positions.

The praseodymium positions are the same as those of the atoms in a single hexagonal close packed structure. But because of the presence

of the rows of cobalt, the praseodymium stacking in this case is indeed not close packed, and the c/a-ratio has the low value 0.85. The distance of closest approach between two praseodymium atoms is 3.45 Å, the distance between a Pr and Co atom can vary between 2.78 Å and 3.02 Å.

$Nd_2Co_{1.7}$ has the same crystal structure as $Pr_2Co_{1.7}$, but with the parameters a = 4.79 Å and c = 4.07 Å.

In the discussion of the hexagonal R_4Co_3 compounds which exist with the heavy rare earths[12] the observed intensities were also explained by assuming that the cobalt atoms located in x = y = 0 were not well correlated in z with the other atoms of the cell. Because of the large number of atoms in that cell, however, the actual observation of diffused planes was impossible there. (The cell dimensions are a≈11.4 Å and c≈4.0Å.)

3. Acknowledgment

The authors want to thank Dr. K. Toman of Wright State University in Dayton, Ohio for very helpful discussions.

SECTION III

INSTRUMENTATION FOR MAGNETIC MEASUREMENTS

A. THERMOMAGNETIC ANALYSIS

In previous work on magnetic intermetallic compounds[10,17,18] we had found it very beneficial to measure the temperature dependence of a property which is proportional to the initial permeability of the material. Upon heating, the initial permeability rises to a peak just below the Curie temperature and then drops precipitously to the low value for the paramagnetic state. The Curie temperature can be determined rather precisely by measuring the temperature at which this permeability peak, the so-called Hopkinson maximum, or the subsequent steep drop occurs. But such "initial permeability spectra" can reveal much more than the Curie point. Another, generally smaller, peak occurs at the disordering temperature of an antiferromagnetic spin arrangement, the Neel point. When the magnetocrystalline anisotropy changes drastically with temperature, this is reflected as a similarily drastic change in the initial permeability. Especially, a minimum of the anisotropy - - as it occurs for instance in the compound $NdCo_5$ near the ice point - - is reflected as a high and broad peak in the permeability spectrum. Changes in the crystal morphology can also be seen provided they have an associated change in one of the basic magnetic properties: saturation magnetization, Curie point, or crystal anisotropy.

If a sample is a physical mixture of two or more ferro- or ferrimagnetic substances, the initial permeability spectrum is a direct superposition of the permeability plots for the components. Thus, if the "spectra", or just some crucial basic properties such as the Curie temperature or other transition points of the likely components are known, a measurement of the initial permeability spectrum can be used as a tool for identifying the phases present. This kind of measurement can thus be used as a qualitative method of phase analysis. Of course, the method only reveals impurities which exhibit magnetic order in some temperature range. For this reason, we are calling the method "thermomagnetic analysis", abbreviated in the following as TMA.

One of the authors of this report, in previous work at the Air Force Materials Laboratory, had helped develop a variation of this TMA method which is particularly simple and convenient to use and requires very small sample quantities. In this version, the powdered sample is made the core of a transformer which is excited with a low level field at an audio frequency, and the mutual inductance of this transformer is measured and recorded while the temperature of the sample is varied over a wide range. This kind of thermomagnetic analysis has been used from room temperature up to about 1150°C, in which case the sample is in a vacuum jacket inside a furnace.[10,17] It has also been used below room temperature with the sample transformer cooled by a cold gas or liquid nitrogen.[10,18] Based upon the experiences just mentioned, we have built a new version

of such a TMA apparatus for the work under this contract, while keeping close contact with Captain M.V. Turner at the Air Force Materials Laboratory who has developed still another version along somewhat different lines.[19]

Our thermomagnetic analyzer in its present form is useful for work above room temperature to approximately 1000°C. The instrument has been described and used rather extensively for the work described in Section III. B, which is also a master's thesis to be submitted at the University of Dayton. Thermomagnetic analysis of this kind is especially valuable when used in a combination with differential thermal analysis, and when it is followed up by high temperature X-ray or neutron diffraction studies and by measurements of the d. c. magnetization as a function of temperature and applied magnetic field. Such magnetometric measurements and diffraction studies can be much more to the point, and a great deal of time can be saved, if they are preceded by the quick and more qualitative study of the sample by TMA.

B. DESCRIPTION OF THE THERMOMAGNETIC ANALYZER*

1. Introduction

a. Background

There have been important developments in the field of permanent magnets during the last decade. These will not only bring many improvements in established devices now using permanent magnets, but they have also opened the door for dramatic new applications of magnets. Most important among these may be new concepts in the field of transportation, such as magnetic levitation and the use of linear electric motors for propulsion.

The discovery of new magnetic materials may thus render a solution towards one of the problems of the modern world - - air pollution by the exhaust of internal combustion engines. The research on permanent magnet materials of which this thesis is a part can be seen as a contribution toward this goal.

The utility of materials for permanent magnets depends principally on the following characteristics:

(1) Curie temperature T_c

(2) Magnetic saturation I_s

(3) Crystal anisotropy constant K

(4) Coercive force H_c

*Part B of this Section is essentially identical with an M. S. thesis of Mr. Rolando Bolomay Munez submitted in September 1971 to the Electrical Engineering Department at the University of Dayton. It also incorporates experimental results by Mr. Michael Hartings.

b. Objectives

The objective of the work described in this thesis was to design a thermomagnetic analyzer with which the Curie temperature and other magnetic transition points can be determined in a precise and rapid way and at low cost.

2. Determination of Magnetic Transitions

The properties of magnetic materials depend on chemical composition, fabrication, and heat treatment. Properties may be divided into structure-sensitive and structure-insensitive groups.

Some properties, such as saturation magnetization, change only slowly with chemical composition and are usually unaffected by fabrication or heat treatment. They are structure-insensitive.

However, permeability μ, coercive force H_c, and hysteresis loss W_h are highly structure-sensitive and often show rather extreme changes when changes are made in impurities or heat treatment.

TABLE XVIII

Properties commonly sensitive or insensitive to small changes in structure, and some of the factors which affect such changes.

Structure-Insensitive Properties	Structure-Sensitive Properties	Factors Affecting the Properties
Saturation mag.	Permeability	Composition
Curie Point	Coercive Force	Impurities
Magnetostriction	Hysteresis Loss	Strain
Crystal Anisotropy Constant		Temperature
		Crystal Structure
		Crystal Orientation

Together with magnetic field and stress, temperature is one of the important factors in causing change in magnetization. The greatest influence of temperature is rarely near room temperature but rather just below Curie point or near the temperature of a phase transformation. Taking as our example a familiar and much studied substance, namely, iron, magnetization curves at different temperatures can be obtained as shown in Figure 8.

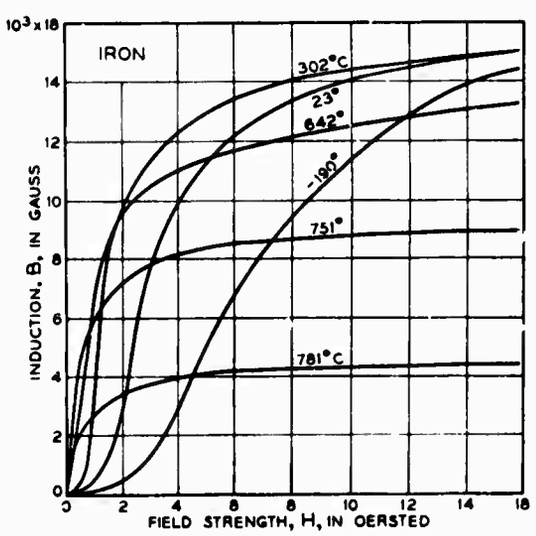

Figure 8. Magnetization curves of iron measured at different temperatures, after annealing at 800°C. (From Ferromagnetism by Richard M. Bozorth, Ph. D. Copyright © 1951 by Litton Educational Publishing Inc. Reprinted by permission of Van Nostrand Reinhold Company and the author.)

At higher temperature, the curves rise more quickly at lower values of H, and then flatten out and saturate at lower inductions. As the temperature increases, the technical saturation continues to decrease and

approaches zero at some temperature called Curie point. (C. P., symbol T_c.) Cobalt has the highest C. P., $T_c = 1120^{\circ}C$. For iron $T_c = 770^{\circ}C$.

When a magnetic material is subjected to a high constant field, an increase in temperature normally brings about a continuously accelerating decrease in the intrinsic induction of the material, the intrinsic induction comes down abruptly, almost to zero at the Curie point.

The intrinsic induction, B_i, is related to the normal induction, B, the field strength, H, and the magnetization intensity, I (all in the electromagnetic CGS system) by the following equation:

$$B_i = B - H = 4\pi I$$

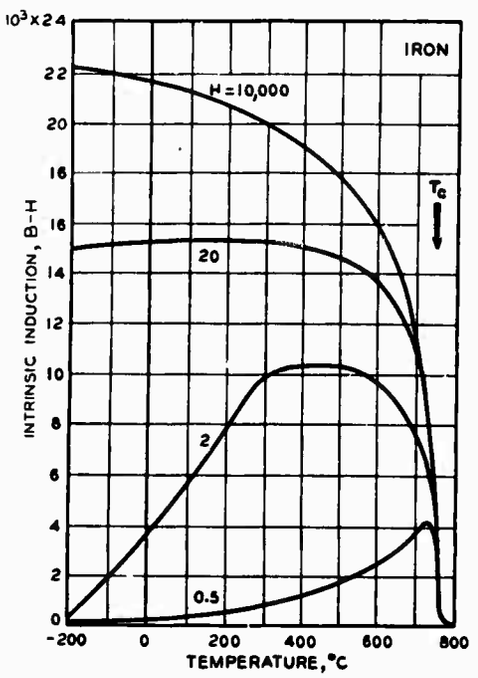

Figure 9. Dependence of spontaneous induction at constant field upon the temperature. (From Ferromagnetism by Richard M. Bozorth, Ph. D. Copyright © 1951 by Litton Educational Publishing Inc. Reprinted by permission of Van Nostrand Reinhold Company and the author.)

When the magnetic material is subjected to a weak field, the induction will first increase with temperature and, after passing through a maximum, will drop rather abruptly to a low value at the Curie point.[10, 20-24]

a. Magnetization Near the Curie Point

The change from the ferromagnetic (F. M.) to the paramagnetic state (P. M.) is not perfectly sharp, and it is difficult to define and determine the Curie point exactly. Careful work on this subject has been carried out by Weiss and his colleagues.

According to the modified Weiss theory the curve relating the saturation magnetization I_s to the absolute temperature T is given by:

$$\frac{I_s}{I_o} = \tanh \frac{I_s/I_o}{T/T_c}$$

This is true when the field strength is negligibly small.

In high fields, especially when the temperature is near the Curie point, the more complete Weiss equation is:

$$\frac{I_s}{I_o} = \tanh \frac{I_s/I_o + H/NI_o}{T/T_c}$$

because the H/NI_o is not negligibly small. In these equations, I_o is the absolute saturation magnetization (= spontaneous magnetization at 0^oK), and N is the molecular field constant.[20]

At any temperature the magnetization I of the specimen as a whole is equal to the local magnetization within a domain, I_s, when, and only

when, the domains are oriented in a parallel manner. This state can be attained only by the application of a high field, which at the same time will produce a slight increase in the domain magnetization over its spontaneous value at a weak field.

b. Permeability

Curves of permeability vs temperature, for various fixed values of field strength, derived from data like those of Figure 9, have the characteristic shapes given by Figure 10 .

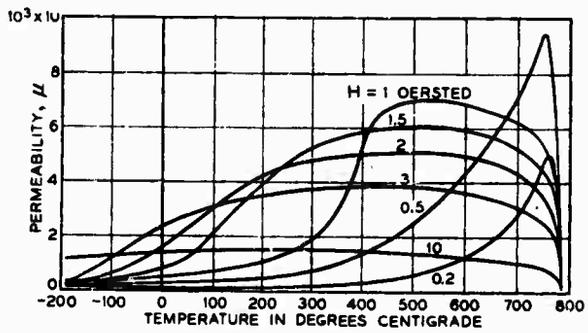

Figure 10 . Dependence of the permeability of Fe on temperature, the field being constant for each curve. (From Ferromagnetism by Richard M. Bozorth, Ph. D. Copyright © 1951 by Litton Educational Publishing Inc. Reprinted by permission of Van Nostrand Reinhold Company and the author.)

The initial permeability increases with an increase of temperature, having a sharp maximum just below the Curie point, and then drops off to a very small value (Hopkinson effect).

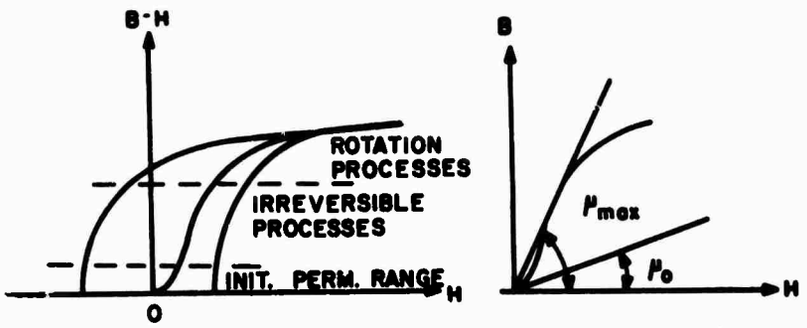

Figure 11. The initial permeability.

The initial permeability is the limit approached by the normal permeability, $\mu = B/H$, as B and H are decreased toward zero.

The hysteresis loss continually decreases with increasing temperature. The way in which the size and shape of the hysteresis loop of iron changes as the temperature approaches the Curie point is shown in Figure 12.[20, 21]

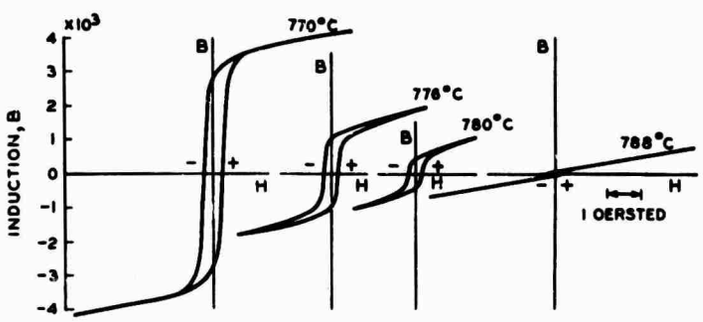

Figure 12. Hysteresis loops of iron at temperature near the Curie point. (From Ferromagnetism by Richard M. Bozorth, Ph. D. Copyright © 1951 by Litton Educational Publishing Inc. Reprinted by permission of Van Nostrand Reinhold Company and the author.)

c. Effect of Phase Changes

Iron and Ni are normal as to their magnetic behavior with change of temperature. No changes in their crystal structure occur between room temperature and the Curie point. On the contrary, such changes in structure do occur in many alloys, among which are the so-called irreversible alloys of iron and nickel (5-30% Ni) investigated by Hopkinson, and some of the iron-cobalt alloys may also be considered as examples.

In the 20-70% cobalt-iron alloys, a change in phase due to a rearrangement of the atoms in the crystal from a body-centered cubic (α) to a face-centered cubic (γ) form takes place on heating at temperatures between 920° and 980°C. (see Figure 13.)

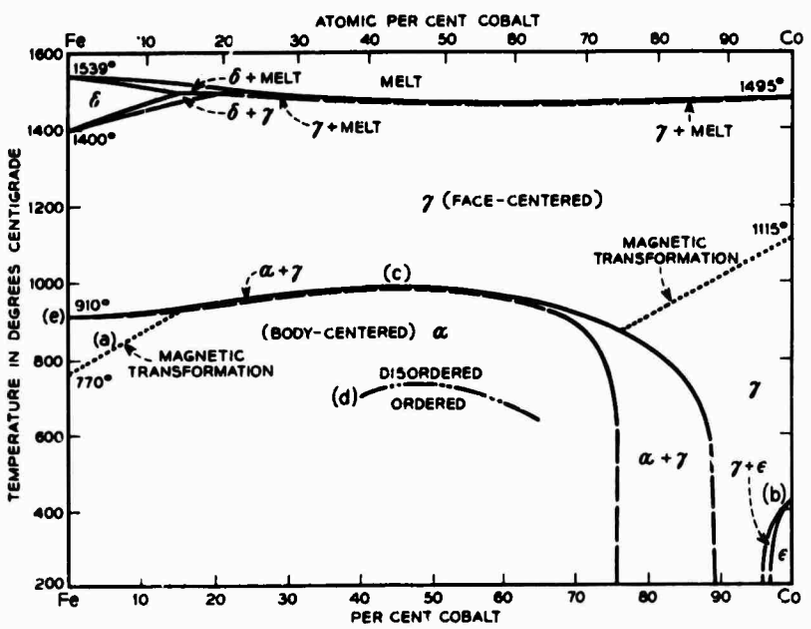

Figure 13. Phase diagram for iron-cobalt alloy system. (From Ferromagnetism by Richard M. Bozorth, Ph. D. Copyright © 1951 by Litton Educational Publishing Inc. Reprinted by permission of Van Nostrand Reinhold Company and the author.)

The α phase is ferromagnetic, the γ phas is nonmagnetic (P. M.). Consequently the material loses its ferromagnetism when heated through the temperature of change of phase, 920°C to 980°C, and the magnetization drops toward zero precipitously instead of in the normal fashion. When the temperature is lowered, this material recovers its magnetization without appreciable temperature hysteresis and the same B vs. T curve is retraced.

This is not always the case, however, when a phase change occurs. In the iron-nickel alloys just mentioned, there is a considerable difference between the temperature at which magnetization disappears on heating and that at which it reappears on cooling, sometimes as much as 500°C. (see Figure 14)

Such a temperature lag in B vs. T curve, when observed in any material, indicates that some change has occurred in the metallurgical state of the material, such as a change in phase or in the state of order of the atoms, or a change in the solid solubility of some component. When no such lag occurs, the effect of temperature on the loss or recovery of magnetization is immediate.[20]

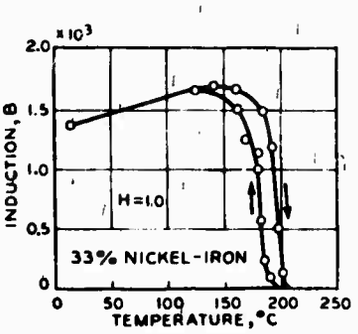

Figure 14. Effect of phase change on induction vs. temperature curves. (From Ferromagnetism by Richard M. Bozorth, Ph. D. Copyright © 1951 by Litton Educational Publishing Inc. Reprinted by permission of Van Nostrand Reinhold Company and the author.)

d. High Field D C Measurements

Determination of magnetic transitions: The most common method of determining the Curie temperature uses a large D C field (often up to 30 kOe, and recently 100 kOe) to measure the intensity of magnetization as a function of the field while maintaining a controlled temperature. This is done for several temperature values in the ferromagnetic range. A plot is then made of the intensity of magnetization squared versus the temperature, and the intensity of magnetization is extrapolated to the value it would have if the field were zero. This value of magnetization is defined as the spontaneous magnetization. The temperature where the spontaneous magnetization becomes zero is then defined as the Curie temperature.[20]

e. Low Field A C Measurements

Another method is to measure the magnetization in a very small magnetic field as a function of the temperature. In most materials this low field magnetization gradually increases with increasing temperature and drops off to near zero at Curie temperature.

In the presence of a constant field the magnetization is proportional to the permeability of the material. Curves of permeability versus temperature for various fixed values of field strength, derived from the same data as those for Figure 9, have the characteristic shapes shown in Figure 10. For most materials the permeability first increases and then decreases with increasing temperature, dropping to near zero at the Curie point.

We define inductance as the relationship between the terminal voltages and currents of, say, a transformer with two windings, 1 and 2,

$$V_1 = L_1 \frac{d\,J_1}{dt} \quad ,$$

$$V_2 = L_2 \frac{d\,J_2}{dt} \quad .$$

We know that the physical basis for such a current-voltage characteristic rests upon the production of a magnetic flux by a current, the flux being proportional to the current in linear inductors; and the production of voltage by the time-varying magnetic field, the voltage being proportional to the time rate of change of the magnetic field.

Mutual inductances are defined by a slight extension of this argument. A current flowing in one coil establishes a magnetic flux about that coil and a flux linkage with a second coil which is in its vicinity. The time-varying flux through the turns of the second coil produces a voltage across the terminals of this second coil; this voltage is proportional to the time rate of change of the current flowing through the first coil.

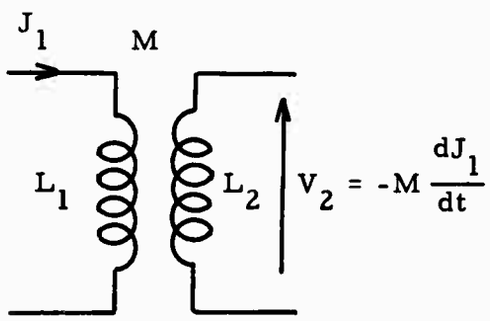

where $$M = k \sqrt{L_1 L_2}$$

and k is the factor of coupling, $k \leq 1$. Large values of the coefficient of coupling k are obtained with coils which are physically close and which are wound and oriented to provide a large common magnetic flux.

f. Inductance of a Coil Containing a Magnetic Core

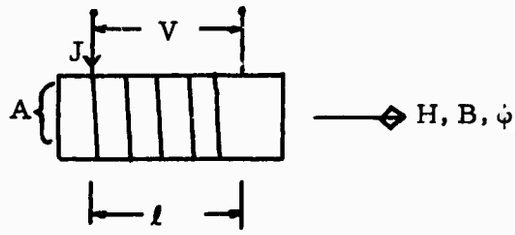

n = turns/meter, $N = n\ell$ = total number of turns

The B-flux is: $$\phi = B A = \mu H A = \mu A n J$$

The induced voltage is:

$$V = - N \frac{d\phi}{dt} = - n\ell (\mu n A) \frac{dJ}{dt}$$

$$V = - \mu \ell A n^2 \frac{dJ}{dt}$$

$$V = - L \frac{dJ}{dt}$$

And thus the inductance: $L = \mu \ell A n^2$ Henry.

Now if the voltage induced in a secondary coil, V_2, by the time rate of change in the primary, $\frac{dJ_1}{dt}$, is: $$V_2 = M \frac{d J_1}{dt}$$

and

$$M = k \sqrt{L_1 L_2} \quad ,$$

we can say V_2 is proportional to the permeability μ of the core material. Thus, if we produce a small A C field (H) with the primary coil and measure the resultant induction voltage V_2 as the core is heated, the relative magnitude of the permeability can be plotted as a function of the temperature.

If the initial permeability is defined as the limit of B/H as H approaches zero for a small field, the behavior of ferromagnetic material is similar to that of a paramagnetic material in the sense that the magnetization is reversible. Under these conditions, the permeability has a unique value called the initial permeability (μ_o). The permeability measured with a finite but small field can be considered to be essentially the initial permeability.

In a magnetic material the initial permeability is proportional to the square of the saturation magnetization and inversely proportional to the magnetic anisotropy energy. Both of these quantities vary with the temperature. The characteristic maximum in the initial permeability below the Curie point is associated with the low magnetic anisotropy at this temperature.

The anisotropy constant is the difference in energy per unit volume between the states in which a single crystal is magnetized in the hardest and in the easiest direction. It usually decreases as a high power of the intrinsic magnetization as the temperature increases.

The Curie temperature can be defined empirically as the temperature at which the point of inflection of an induction versus temperature plot occurs provided the measurement was made at a low field strength. Therefore, since the induction is proportional to the permeability for

constant fields, the point of inflection will fall at the same temperature on the initial permeability versus temperature graph.[23]

3. Thermomagnetic Analyzer

a. Principle of Operation

The apparatus built as this thesis project makes use of the relationships just discussed. It permits measurement of a low-field A C permeability as a function of temperature between room temperature and approximately 1150°C.

What is actually measured is the voltage induced in the secondary winding of a transformer when a magnetic material sample is made the core of the transformer and the primary is excited with a constant, low-level current of, usually, 1000 Hz frequency. The measurement can also be seen as one of mutual inductance, and thus, as said before, as an approximate measurement of the temperature dependence of the permeability of the sample material. The exciting current is kept so low that we can assume to operate in the initial permeability region.

b. Parts of the System

The principal parts of the thermomagnetic analyzer are: an audio frequency generator, a current amplifier, a "sample transformer," a sample holder, a nulling transformer, a signal preamplifier and synchronous rectifier (lock-in amplifier), a furnace, a furnace programmer, a thermocouple, an x-y recorder, and a vacuum pump.

The audio frequency generator and the preamplifier are contained within the lock-in amplifier. This is an extremely versatile

tool for the recovery of low-level signals in the presence of noise. It features plug-in low-noise preamplifiers (capable of remote operation) a calibrated 360^{o} phase control, and a high degree of sensitivity, stability, linearity and overall accuracy. The above features are coupled with the unit's internal oscillator.

The lock-in amplifier is used to produce a frequency of 1 kHz to feed the primary coil of the sample transformer and to produce a low A C field in the sample.

The resultant emf induced in the secondary coil is fed back into the voltage audio amplifier portion of the lock-in amplifier, where it is synchronously rectified. Then the output goes to the y axis of the x-y recorder. The current amplifier is fed by the audio frequency generator of the lock-in amplifier; it is used to adjust current values in the primary coil of the transformer ranging from 40 mA to 250 mA. This current produces peak fields in the primary coil which vary from approximately 0.26 Oe to 1.66 Oe.

The nulling transformer, a variable mutual inductance, is connected in series with the coils of the transformer, both on the primary and the secondary sides. This mutual inductance was built so that it has approximately the same geometry and the same dimensions as the sample transformer, except with more turns. The primary has 24 turns and the secondary has 20 turns; both coils are mounted on threaded phenolic tubes with 14 grooves per inch. The secondary slides inside the primary coil thus changing the mutual inductance. Adjusting this mutual inductance, it is

possible to change the emf in the secondary. As this emf is in opposition with the emf induced in the secondary coil of the sample transformer, the emf produced by the air flux in the latter can be cancelled out. When this is done first in absence of a magnetic sample, the output of the sample transformer during the thermomagnetic analysis of a material is then due entirely to the presence of the sample core. (The nulling transformer is shown in Figure 19.)

The thermomagnetic analyzer in the narrower sense therefore consists of the sample transformer (ratio 1:1), a sample holder, and the thermocouple in a quartz tube which fits inside the transformer and can be evacuated.

The primary and secondary coils of the transformer were made by winding 15-mil Pt-13% Rh wire on 1-1/2 inch-long concentric cylinders of boron nitride. Boron nitride was selected because it is a nonmagnetic material, a good conductor of heat capable of withstanding temperatures above 1200°C, and an excellent electrical insulator (10^{13} ohm-cm at room temperature, 10^{2} ohm-cm at 2000°C).[22] The cylinders were threaded on the outside surface with 14 threads per inch and wound with 20 turns of wire. The primary and secondary fit into another cylinder of boron nitride (Figure 15). This entire unit is suspended by three tubes of alumina ceramic. These "spaghetti" of alumina are used to insulate the wires for feeding the primary and picking up the secondary signal.

All of this is placed inside a quartz tube, two inches in diameter by 19 inches long. The head of the tube, sealed to it with a vacuum-tight flange, contains the transformer's connections and serves to hold

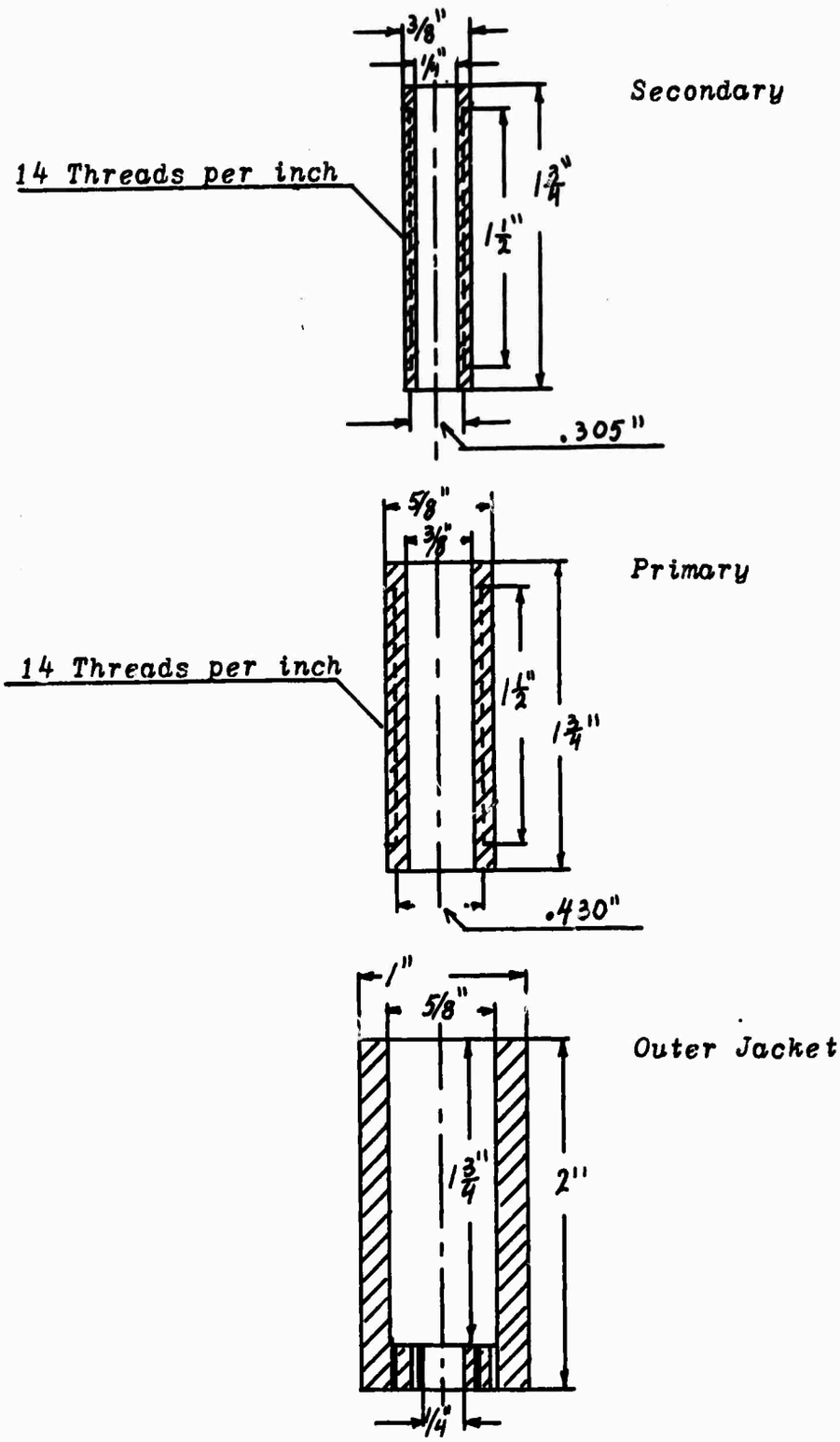

Figure 15. Sample transformer - boron nitride parts.

the small quartz tube which contains the sample to be analyzed (Figure 16).

A quarter inch hole was drilled longitudinally through the secondary BN cylinder to admit the sample holder. The sample is placed into a quartz tube. This sample holder has a thin, drawn-out end part 6 mm in diameter and 2 inches long at the bottom. This end is placed into the quarter inch hole of the transformer.

The thermocouple head is directly buried in the powder sample, and the output signal of the thermocouple is corrected to $0^{\circ}C$ reference by means of an electronic cold junction and fed into the x-axis of the x-y recorder.

A vertical, single-phase A C, 110 V furnace capable of reaching $1200^{\circ}C$ was used to heat the thermo-analyzer. This furnace is connected to a programmable power supply with which one can control temperature variations at will. Linear heating and cooling rates in the range from 0. 6 to $8.8^{\circ}C$/minute are possible.

This furnace has a bore that is 18 inches long by two inches in diameter. It has a property of maintaining a constant temperature over a length of 3. 5 inches in the middle of the bore. The sample transformer is positioned in this zone, thus avoiding problems of temperature gradients (See Figure 17). Figure 18 shows the head portion of the outer quartz envelope with transformer suspension, electrical feedthroughs and pumping ports.

A mechanical vacuum pump and an oil-diffusion pump are used to create a vacuum inside of the tube which contains the ferromagnetic sample, and all of this is placed inside the tube which contains the thermomagnetic

Figure 16. Disassembled view of thermomagnetic analyzer.
Left: Outer vacuum envelope (quartz)
Center: Sample holder-quartz tube with provision for evacuation, thermocouple feed-through, and sample loading.
Right: Sample transformer assembly with head part showing electric feed-throughs and center access port for sample holder.

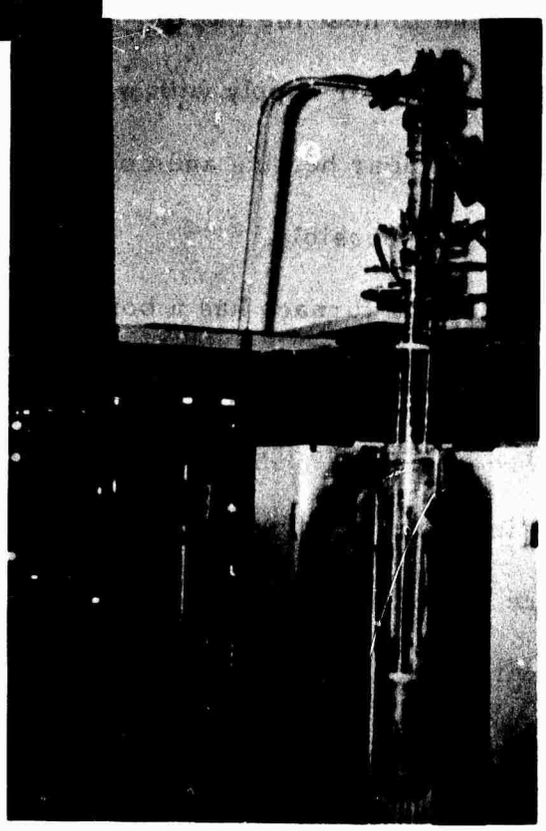

Figure 17. Thermomagnetic analyzer in position inside the split-barrel furnace. Vacuum control valves visible on the left side.

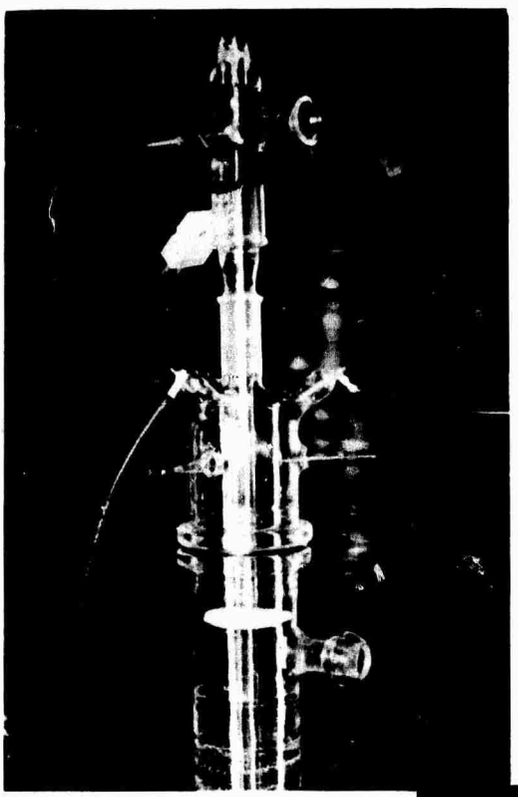

Figure 18. Closeup view of the head portion of the thermomagnetic analyzer, showing electrical feed-throughs, thermocouple connector, sample holder port, pumping port and sample transformer suspension.

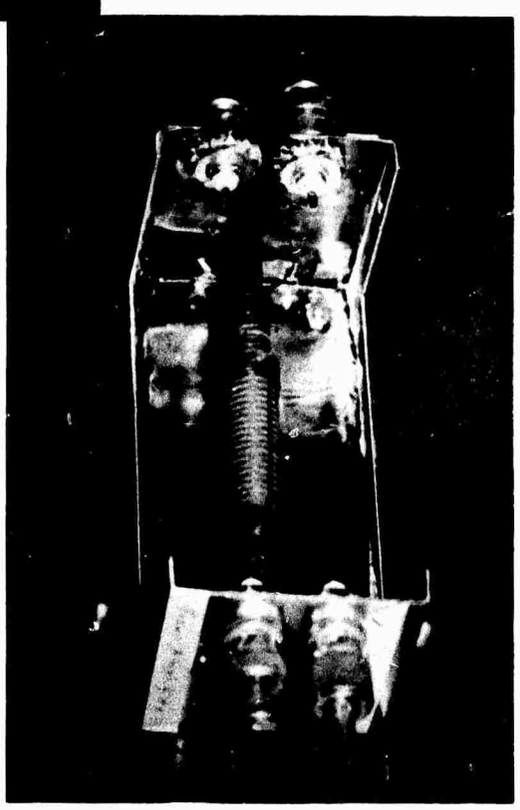

Figure 19. Variable mutual inductance for compensating the output signal of the sample transformer in the absence of a sample.

analyzer. The latter can also be evacuated. This vacuum protects the sample and the boron nitride from possible oxidation.

The x-y recorder is used to trace the voltage-temperature curves, using the lock in amplifier voltage and the thermocouple voltage, respectively.

The electric circuit of the entire thermomagnetic analysis apparatus is shown in the circuit diagram, Figure 20. The block diagram, Figure 21, shows all the parts associated with the furnace, the temperature control mechanism, and the vacuum system. Finally, Figure 22 is a photograph of the entire TMA apparatus and its auxiliary equipment. It should be noted that the large horizontal tube furnace visible in the background to the left is not a part of the TMA apparatus. However, this furnace shares with the thermomagnetic analyzer the temperature control console (not shown in the picture) and a part of the vacuum system.

Electric Circuit

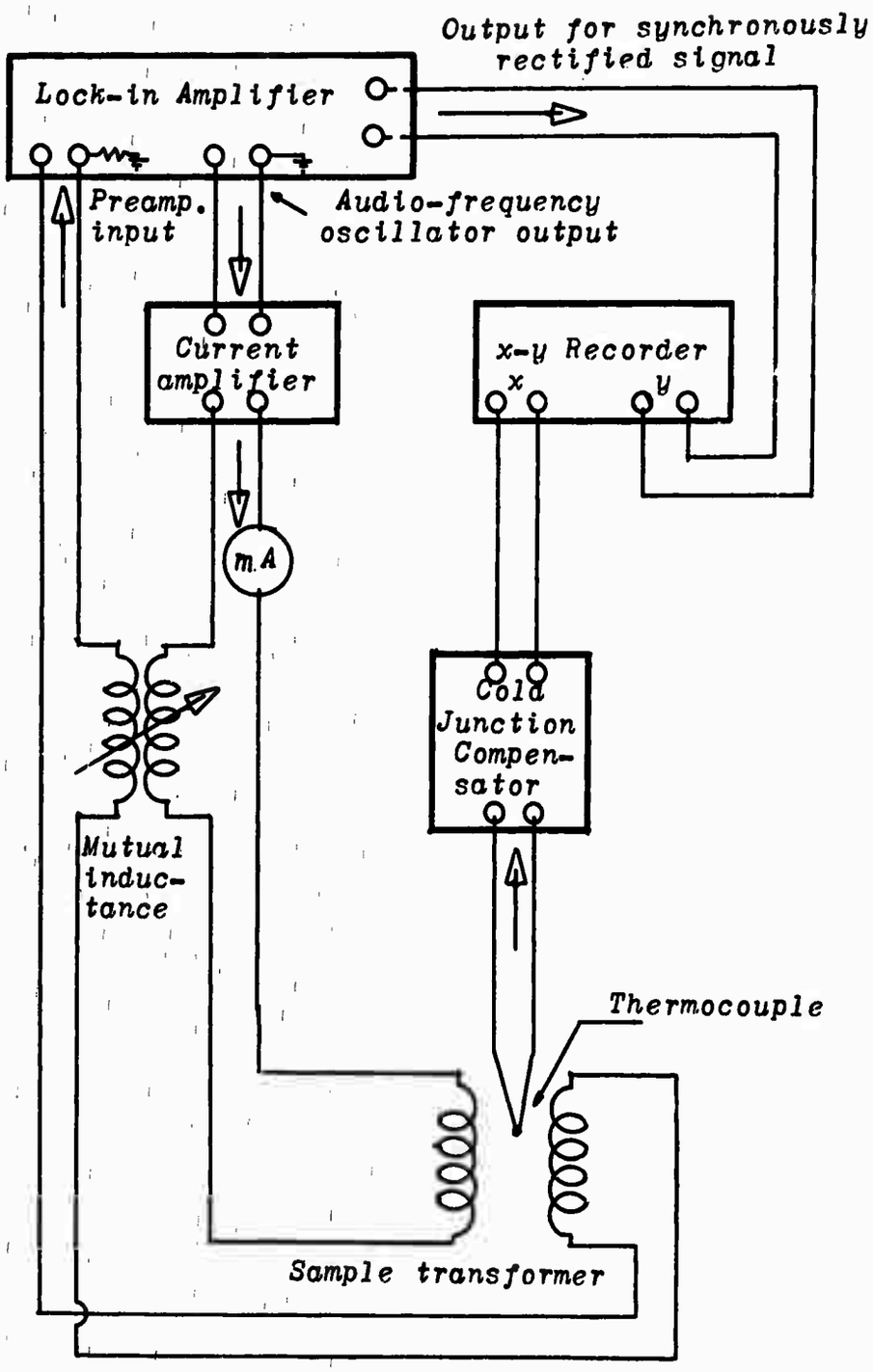

Figure 20. Electric circuit diagram of the TMA apparatus.

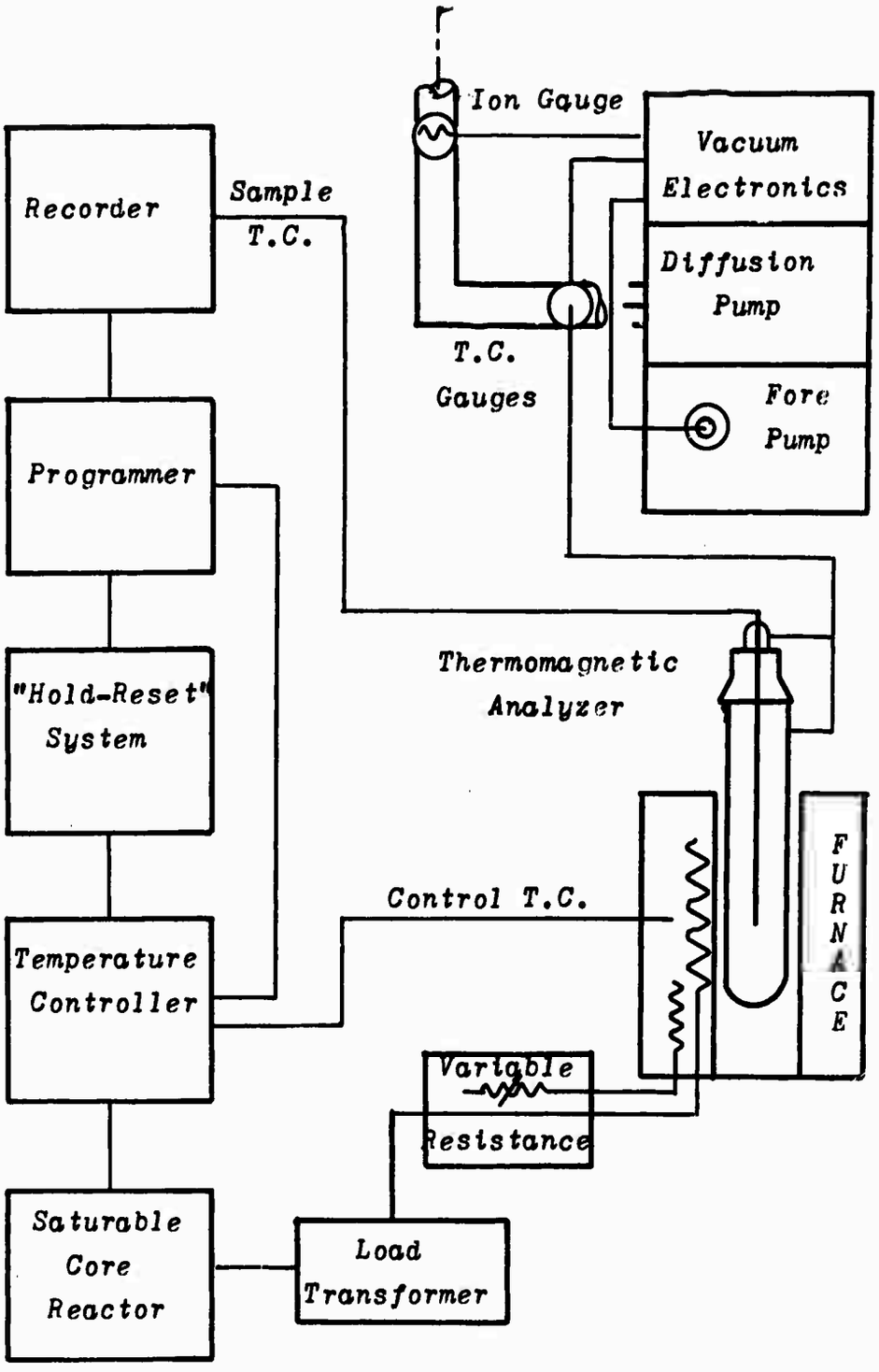

Figure 21. Block diagram of furnace, high vacuum system, and controller.

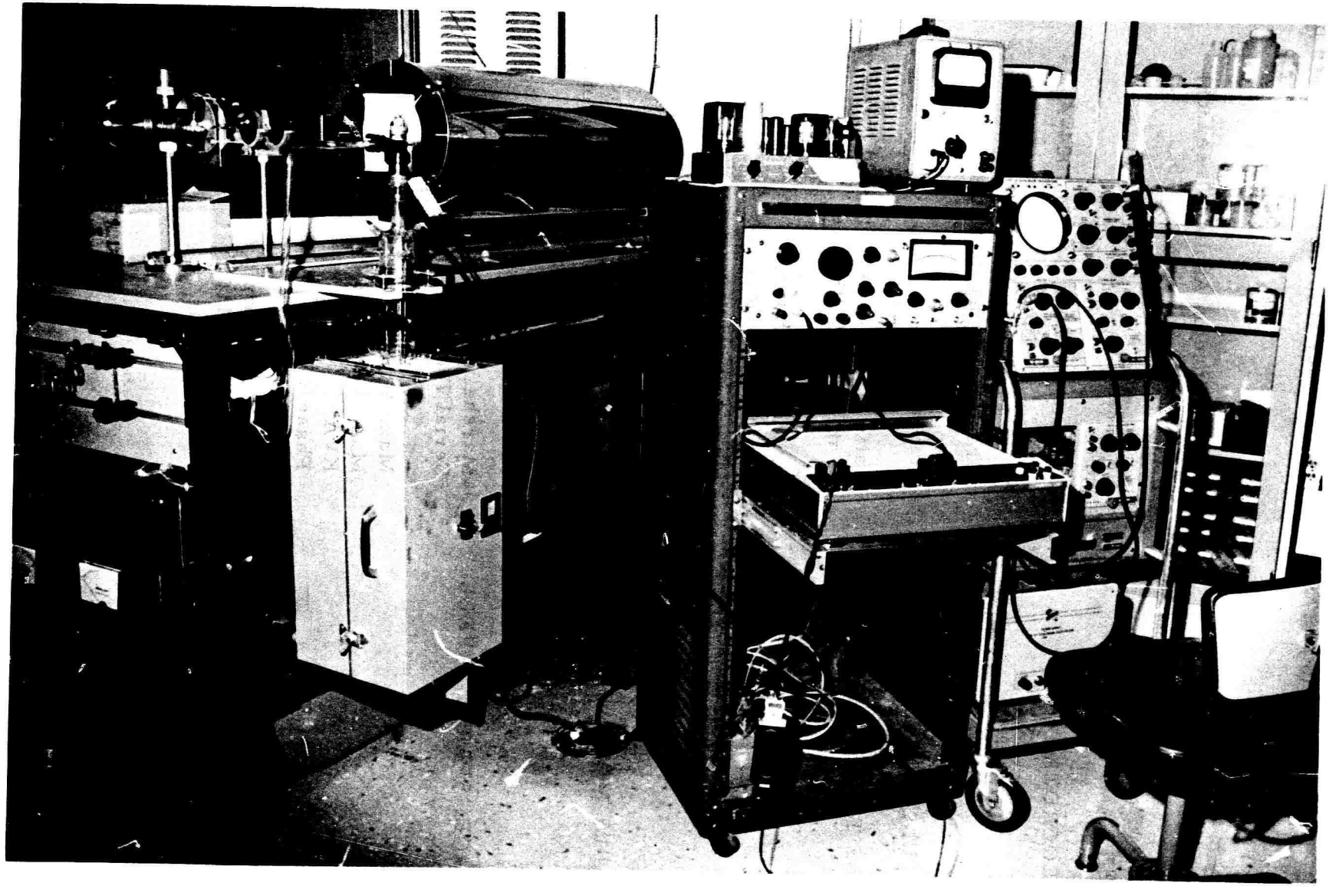

Figure 22. Overall view of the thermomagnetic analysis apparatus.

The types and technical characteristics of the instruments used in the experiments are:

LOCK-IN AMPLIFIER:	PAR (Princeton Applied Research) Model HR-8 Serial No. 2732	
CURRENT AMPLIFIER:	Heathkit, Model A-7E	
X-Y RECORDER:	Hewlett-Packard, Model 7004-A	
THERMOCOUPLE:	Pt vs Pt + 13% Rh, 8 mil diam. bare wires in alumina insulators	
COLD JUNCTION COMPENSATOR:	Omega CJ	
SAMPLE TRANSFORMER:	Ratio 1:1 - Each coil has 20 turns of 15 mil Pt 13% Rh wire	
	Primary Inductance	3.16 mH
	Secondary Inductance	2.2 mH
	Mutual Inductance	2.636 mH
	Primary Resistance	3.598 ohms
	Secondary Resistance	3.013 ohms
VARIABLE MUTUAL INDUCTANCE:	Primary	24 turns of copper wire
	Secondary	20 turns of copper wire
	Mutual Inductance (Maximum)	2.73 mH
FURNACE, SPLIT-BARRELL TYPE:	Marshall Co., Model No. 2223, Serial 7004107	
	Max. Volts:	110
	Max. Temp:	2200°F = 1200°C
	KVA:	620/550
	Phase/Cycle:	1/60
PROGRAMMER:	Data-Trak Corp., R-I Controls, Model FGE 5110	

c. Setup and Checkout Procedure

The thermomagnetic analyzer is set up for use in the following way:

(1) Steps to be taken before initial use and repeated occasionally.

(a) Calibrate the x-y recorder following the instructions in the service manual.

(b) Calibrate the lock-in amplifier following the instructions in the service manual.

(c) Set up and energize the thermomagnetic analyzer as described below, but without a ferromagnetic sample. Set the primary current to the frequency and level to be used in the measurement.

Then adjust the variable mutual inductance until the input signal of the preamplifier is closest to zero. This is done by putting the METER/MONITOR switch in SIGNAL position, and adjusting the sensitivity switch for a full-scale setting consistent with the expected maximum signal value. Then increase the sensitivity of the lock-in amplifier and repeat the procedure until the sensitivity dial is in the 500 or 200 nV position. For this position, the scale-meter indication must be near zero.

(2) The following steps must be taken before each thermomagnetic analysis of a new sample ("TMA run").

(a) Introduce the sample to be analyzed into the core tube of the thermomagnetic analyzer.

(b) Connect the vacuum pump to both tubes, producing a vacuum of 10^{-5} or 10^{-6} Torr.

(c) Check out the electrical connections.

(d) Turn on the lock-in amplifier and adjust the frequency to 1000 Hz. Set the reference mode switch to INTERNAL and the Reference Attenuator and Vernier to the maximum positions.

(e) Turn on the current amplifier. It is fed from the Reference IN/OUT jack of the oscillator section of the lock-in amplifier. Feed the primary of the sample transformer with a current of 200 mA.

(f) Adjust the electronic cold junction compensator for a correct $0^{o}C$ reference temperature.

(g) Put the METER/MONITOR switch in the MIXER position and the TIME CONSTANT switch at 30 ms. Adjust the PHASE dial for zero meter indication, signifying that the input signal and reference signal are in quadrature.

Rotate the QUADRANT SELECTOR one step either clockwise or counter-clockwise and allow the meter indicator to stabilize. The meter now directly indicates the rms amplitude of the fundamental component of the input signal. Adjust the SENSITIVITY switch so as to get a meter indication as close as possible to the full scale valve.

(h) Rotate the SENSITIVITY switch one step clockwise, adjust the primary input current for some value between 40 mA and 250 mA, for one quarter scale meter indication.

(i) Put the METER/MONITOR switch in the OUT position and choose the scale for the x-y recorder. (Typically 1 V/cm for the y-axis and 0.25 or 0.5 mV/cm for the x-axis.)

(j) Connect the furnace, programming for a temperature change of no more than 5°C per minute for heating and cooling.

4. Experimental Procedure

a. Sample Preparation

The samples were prepared in the Metallurgical Laboratory of the University of Dayton Research Institute using different techniques; one of these methods was arc melting in a nonconsumable electrode arc-melting furnace in an atmosphere of argon-helium. To assure adequate mixing, the ingots were inverted and remelted several times. They were then annealed in a vacuum at temperatures between 800°C to 1200°C for different periods of time.

Approximately one-half gram of the sample was used for a thermomagnetic analysis. The samples were ground in a mortar and pestle and then sieved to provide a powder with particle size varying from 420 to 210 microns. With these particles it is possible to assure adequate field penetration in spite of the eddy currents and yet avoid undesirable plastic deformation during grinding, or oxidation on heating. Very fine powders are easily oxidized, especially the rare earth-iron, or rare earth-cobalt compounds, at temperatures as high as their Curie temperatures. Oxidation of the moderately finely powdered sample is effectively prevented by maintaining

a very high vacuum within the sample holder or by backfilling the system with a purified gas such as argon or helium.

b. Operation of the Thermomagnetic Analysis Apparatus

Several mutual inductance vs temperature plots were made to determine what effects the changing of the field intensity would produce on the apparent Curie point of the sample, using field intensities between 0.4 to 2 Oe. It was found that the inflection point of the drop after the Hopkinson maximum does not depend on the field strength in this range.

For samples of simple ferromagnets such as pure iron, nickel or Ce_2Co_{17}, the position of this inflection point (Curie point) agrees to within a few tenths of a degree on heating and cooling for the slow rates of temperature change used. However, in some sample powders there exists a difference in the inflection points between the heating and cooling curves, even at rates as low as $1^{\circ}C$/minute. These curves were similar to that of Figure 27b. In these samples, there is a true physical reason for this thermal hysteresis. It cannot be attributed to the instrument.

Another possible source of error was the effect produced by a frequency variation. Changes of 10 percent below and above 1000 Hz did not cause a change in value of the Curie temperature of Ni or Fe indicated by the inflection points.

c. Calibration

Several Curie temperature measurements were made on combined samples of high-purity nickel powder and iron lathe shavings. The latter were ground in the mortar to reduce them to finer particles of 250 microns

or less. Both powders were mixed and put into the sample holder, using a peak field intensity of 0.9 Oe (130 mA) and a rate of change of 1.9°C/minute. The x-y recorder drew two inflection points, one for nickel at 358.4°C, and another for iron at 751°C.

The Curie point given by Bozorth is 358°C for nickel and 770°C for iron. The difference of 19°C for the Fe is probably due to the fact that the iron used in these experiments was not very pure. In previous TMA work of the kind described here, the accepted value of Tc = 770°C could be very closely reproduced when a pure iron sample was used.

d. Determination of the Curie Points of Alloys

Several experiments were performed to find the Curie temperature in alloys of the type $R_2(Co_{1-x}Fe_x)_{17}$. All of these alloys were prepared by the Metallurgical Laboratory of the University of Dayton.

Thermomagnetic analysis was performed on the following alloys.

Alloy I. D. No.	Composition	Prior Heat Treatment
AR - 755	$Ce_2(Co_{.9}Fe_{.1})_{17}$	6 hrs. 1050°C
AR - 764	$Ce_2(Co_{.8}Fe_{.2})_{17}$ + 2 w/o Ce	6 hrs. 1050°C
AR - 771	$Ce_2(Co_{.7}Fe_{.3})_{17}$ + 2 w/o Ce	7 hrs. 1050°C
AR - 775	$Ce_2(Co_{.6}Fe_{.4})_{17}$ + 3 w/o Ce	6 hrs. 1050°C
AR - 785	$Ce_2(Co_{.5}Fe_{.5})_{17}$ + 3 w/o Ce	7 hrs. 1050°C

For the sample AR - 755, 1 gram of material was used. It was ground to 250 microns and 1/2 gram was put into the sample holder. A 1.02 Oe-peak-intensity field (150 mA current) was applied, with a temperature variation of 3.4°C/minute. The temperature reached a maximum of 870°C, giving one curve for heating and another for cooling. These curves

show very definite sharp peaks before the inflection point. There is a hysteresis of 4°C between the position of the latter on the heating curve(780°C) and the cooling curve (784°C). The inflection points appear to indicate a normal Curie temperature. The Hopkinson maxima occurred at 777°C on heating and at 779°C on cooling (Figure 23a).

Due to the fact that in the first part of the curve (near 380°C) something similar to the inflection point appeared which was not seen on cooling, a second run was made with the same sample. The low temperature "event" had now disappeared and so had the hysteresis of the Curie point. The maxima occurred at 780°C on heating and cooling, and the inflection point at 782°C was also identical on heating and cooling (Figure 23b).

In the sample AR - 764, the same field intensity was used. A maximum temperature of 918°C was reached. The rate of temperature change was 3.4°C/minute. This time, two peaks appeared during the heating process, at 754°C and 879°C. During the cooling process a rather noticeable hysteresis appeared at the second peak. The inflection points occurred at 755°C during the heating, and at 757°C during cooling. The positions of the peaks on the left of the graph are at 754°C on heating and at 756°C on cooling (Figure 24).

The mutual inductance vs. temperature curves of AR - 771, $Ce_2(Co_{.7}Fe_{.3})_{17}$ + 2 w/o Ce, show peaks at 720.5°C on heating and 722°C on cooling. The inflection points in both runs come at 724°C. There was no hysteresis for this alloy (Figure 25).

The sample AR - 775, $Ce_2(Co_{.6}Fe_{.4})_{17}$ + 3 w/o Ce, was analyzed three times: once as a powder sample of less than 250 microns, and twice using larger pieces of approximately 2 mm size.

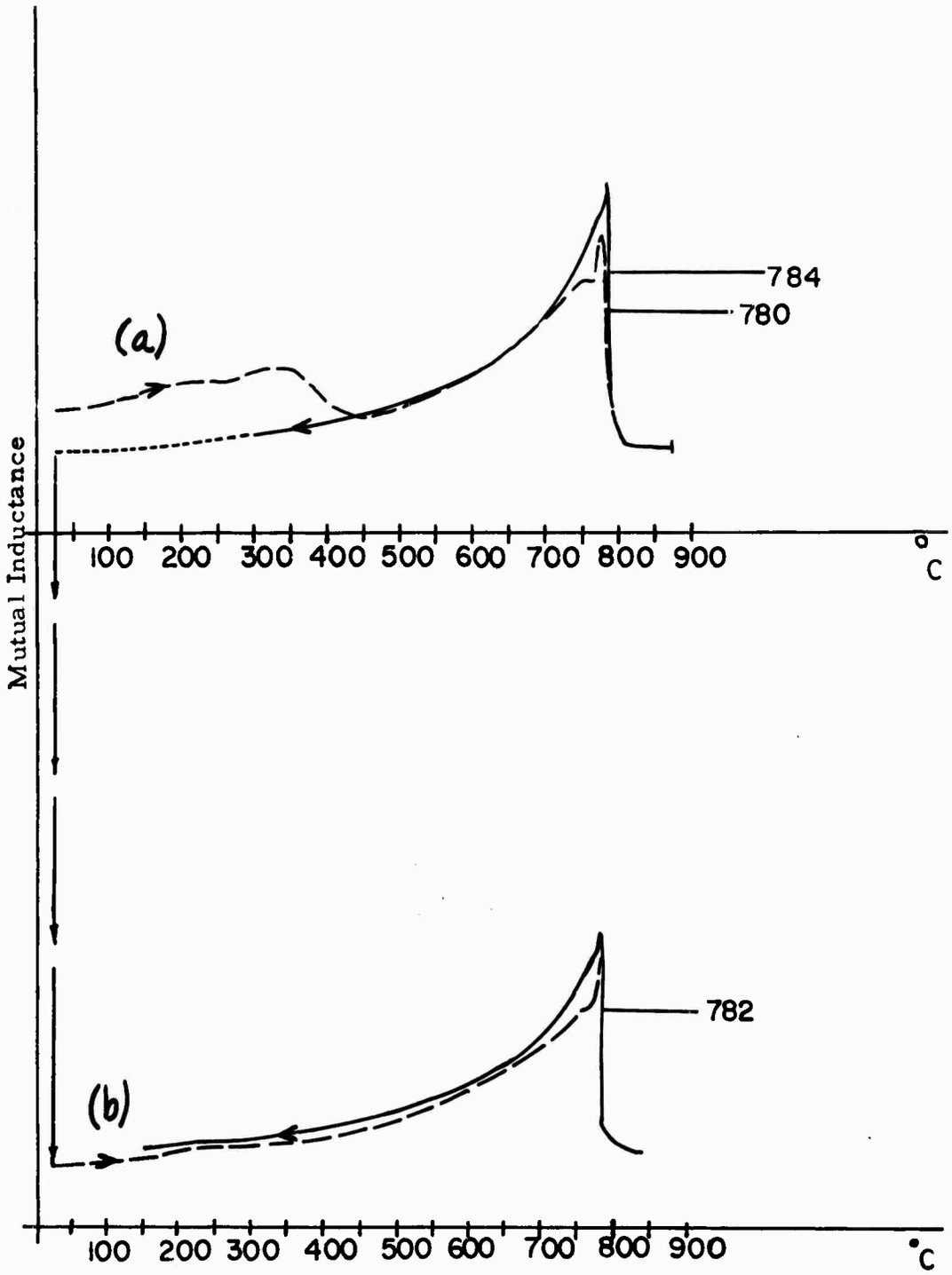

Figure 23. TMA Spectra of $Ce_2(Co_{.9}Fe_{.1})_{17}$ Alloy AR-755, annealed 6 hrs. at 1050°C.
(a) Initial heating and cooling curves
(b) Second TMA run on the same powder sample

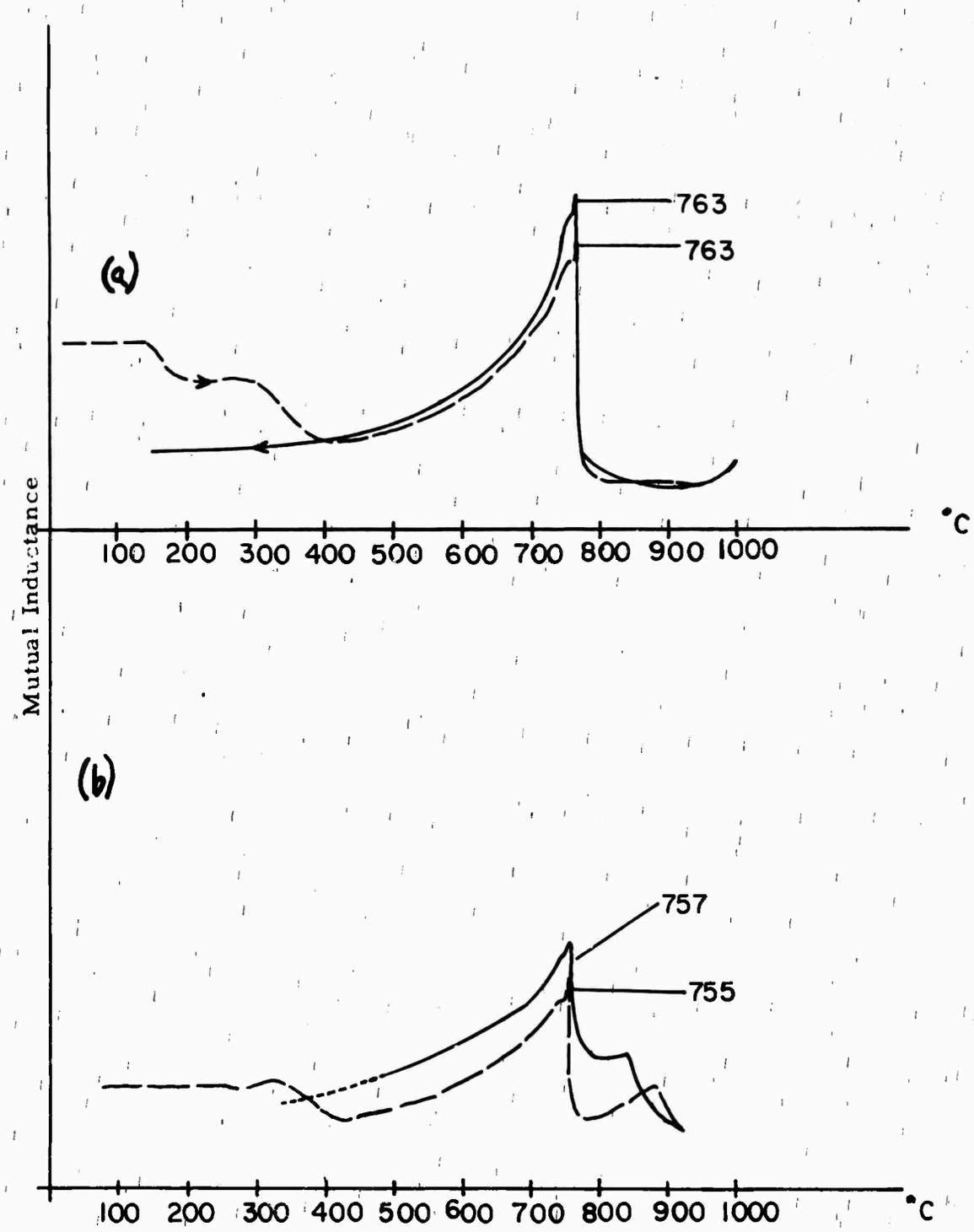

Figure 24. TMA Spectra of $Ce_2(Co_{.8}Fe_{.2})_{17}$; initial heating and cooling curves
(a) Alloy AR-834, annealed 18 hrs. at 1000°C
(b) Alloy AR-764, annealed 6 hrs. at 1050°C

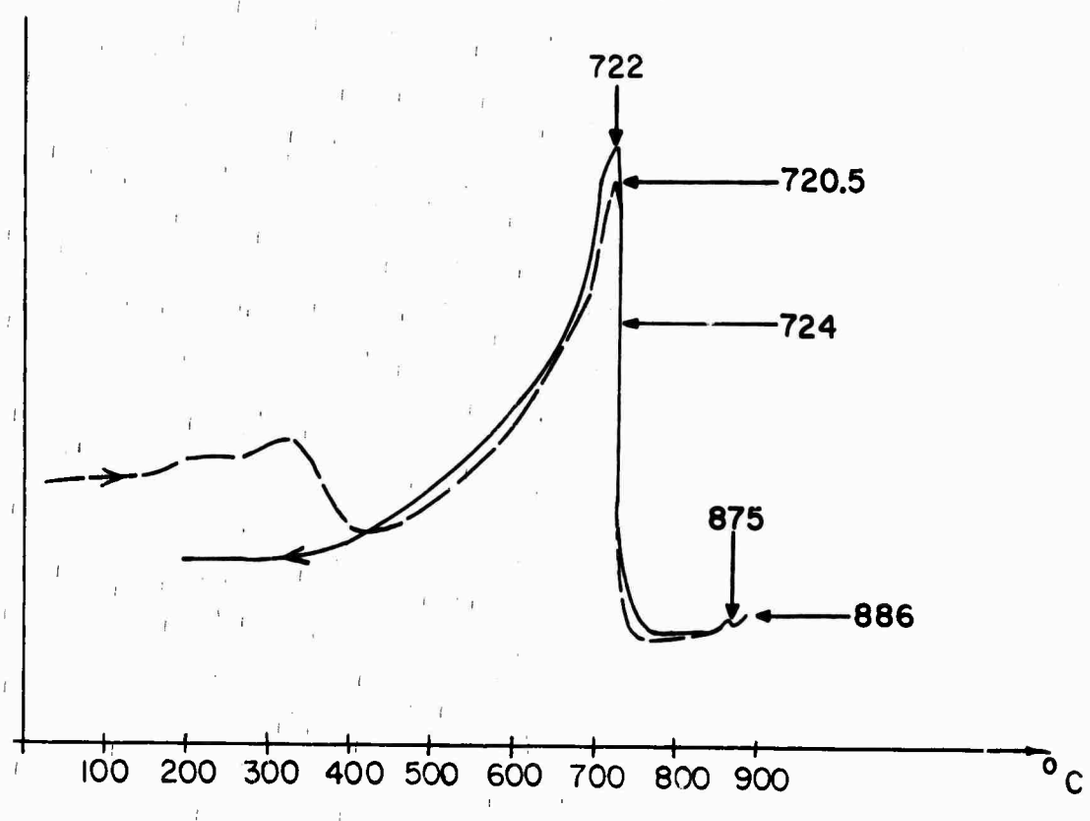

Figure 25. TMA Spectra of $Ce_2(Co_{.7}Fe_{.3})_{17}$; initial heating and cooling curves. Alloy AR-771, annealed 7 hrs. at 1050°C.

The curves obtained the first time show two inflection points during the heating process, at 669°C and at 852°C, with a definite sharp peak at 835°C. During the cooling process, the upper inflection point completely disappears, the curve showing only the first one at 674°C with a peak at 669°C. This hysteresis, which was hinted at in the previous case (AR - 771) and which now appears so noticeably, forced us to make an X-ray analysis to determine if during the heating process the physical and chemical properties of the sample had changed. It was surmised that the fine powder might have oxidized and the $Ce_2(Co,Fe)_{17}$ completely transformed to an Fe-Co alloy and an oxide rich in cerium (See Figure 26a).

As a precaution against such excessive oxidation, two further TMA runs were made with the larger sample pieces. The first of these (Figure 26b) reached a maximum temperature of 705°C, and the second (Figure 26c) 911°C. The inflection points of the first case showed up at 671°C during heating and 666°C cooling. The mutual inductance vs. temperature curves are similar during both the heating and cooling processes. Notice that this sample was not heated to the temperature of the previously observed upper peak.

In the third run (maximum temperature of 911°C), one inflection point shows up at 671°C on heating and cooling; and at approximately 851°C another inflection point weakly shows up but again only during the heating process. On cooling the sample, the hysteresis cycle of the first TMA run on fine powder shows up again, and we have only one inflection point at 672°C. The X-ray analysis showed no chemical change in the samples of the large

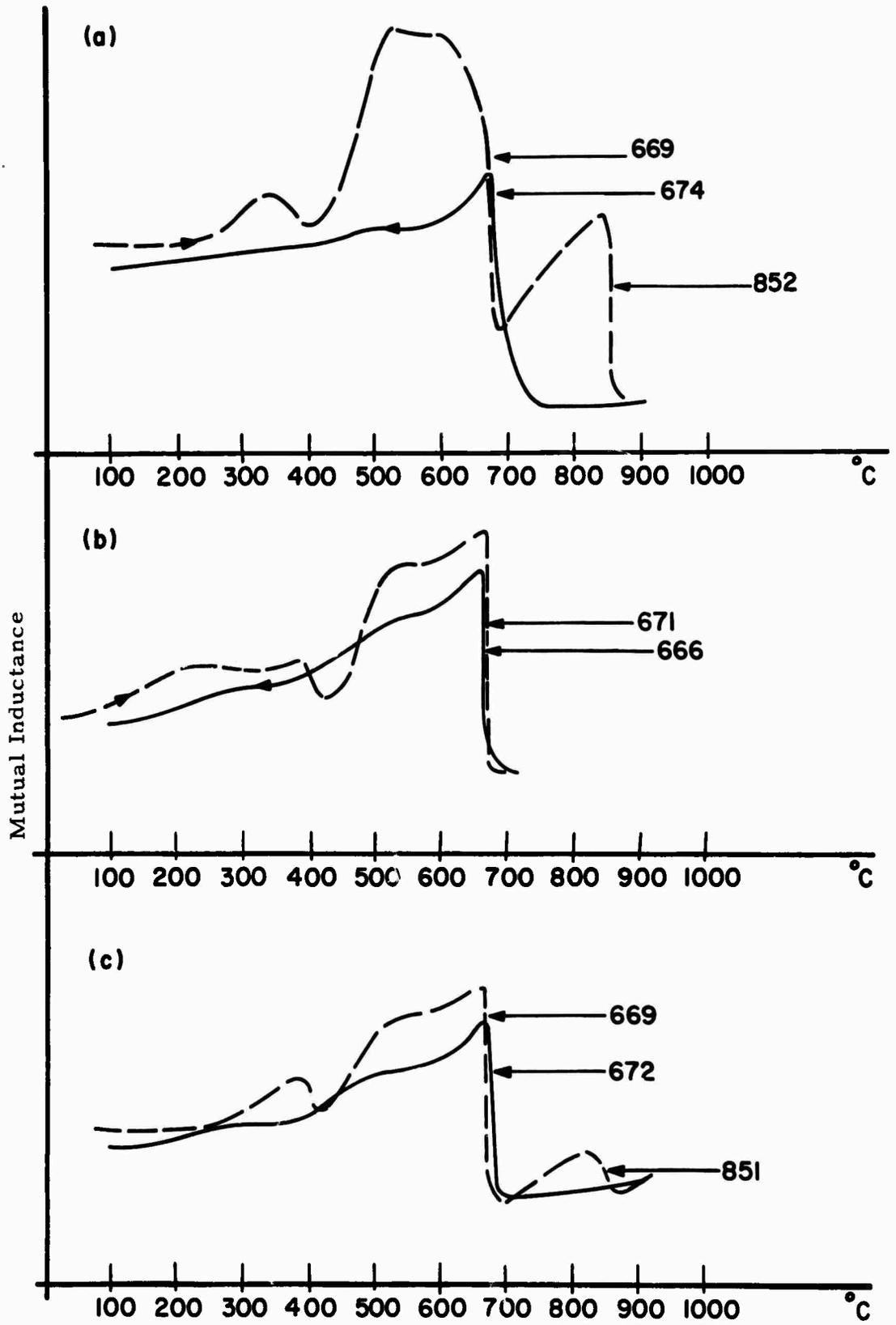

Figure 26. TMA Spectra of $Ce_2(Co_{.6}Fe_{.4})_{17}$ Alloy AR-775, annealed 6 hrs. at 1050°C.
(a) Initial heating and cooling of powder sample.
(b) Initial heating and cooling of a sample consisting of coarse pieces.
(c) Second heating and cooling of another coarse sample.

pieces. The X-ray patterns of the fine powder showed some changes which have not yet been interpreted.

In the last analysis of the series, two runs were made on the sample AR-785, $Ce_2(Co_{.5}Fe_{.5})_{17}$ + 3 w/o Ce. The first run was only up to 50°C above the first observed inflection point, and the second up to 911°C. During the first run, one inflection point showed up during the heating process at 601°C and another one at 869°C. On cooling, only one point, at 771°C was observed. During the second run, we have only one Curie point at 868°C on heating, and again only one at 769°C on cooling (Figure 27). Once we arrive at the highest mutual inductance value below this transition, this value remains constant during the whole ensuing cooling period. Here again a strong hysteresis appears.

This phenomenon, which clearly shows up in the thermomagnetic analyzer, had been hinted at in the differential thermal analysis of these same materials. From the DTA curves it is difficult to tell precisely where the transitions occur or that they are indeed magnetic in nature.

With the thermomagnetic analyzer one gets very pronounced signals at the same transition points. Since one can easily regulate the temperature variation and the field intensity, it is possible to determine the critical temperatures with great precision.

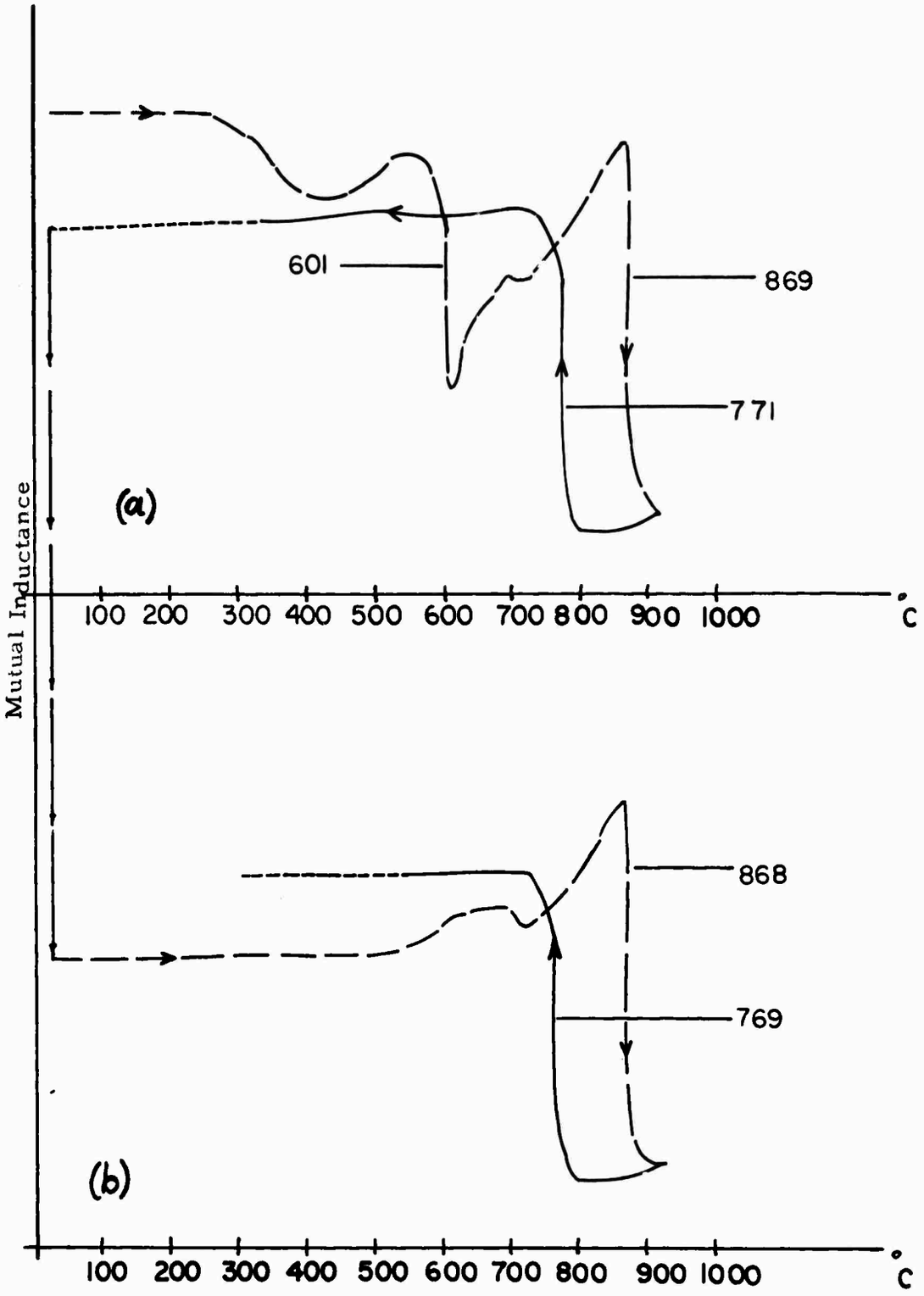

Figure 27. TMA Spectra of $Ce_2(Co_{.5}Fe_{.5})_{17}$ Alloy AR-785, annealed 7 hrs. at 1050°C.
(a) Initial heating and cooling curves
(b) Second TMA run of the same powder sample

C. DESCRIPTION OF THE OSCILLATING SPECIMEN MAGNETOMETER*

The temperature dependence of the spontaneous magnetization, and the magnetocrystalline anisotropy and its temperature dependence are some of the basic magnetic properties of the various substances to be studied under this contract. The practical significance of these quantities for the possible permanent magnet application of the alloys lies in the fact that the spontaneous magnetization, M_s, at any given temperature constitutes an absolute upper limit on the possible remanence, and it also determines the highest energy product one might expect from a given compound under the most favorable circumstances i. e., $4\pi^2 M_s^2$. The crystal anisotropy constant is one of the principal factors determining whether a high intrinsic coercive force can be expected when the substance is converted to a fine powder or its structure disrupted by a finely dispersed nonmagnetic precipitate.

As the tool for determining these properties, we built a magnetometer which is a further development of an instrument previously designed by one of the authors at the Air Force Materials Laboratory.[25] Two versions of this magnetometer have been built by us. They have the sample drive and the electrical signal detection and recording system in common,

* H. Mildrum and K. Strnat

but differ in the device used to produce the magnetic field and also with regard to the temperature range and the measuring tasks for which they can be most conveniently used.

One version of the system is built around a superconducting solenoid system which can provide very high field strengths up to 65 kOe and incorporates a sample cooling system which allows one to reach and closely control cryogenic temperatures down to 1.5°K. This version is especially well suited for measurements of the absolute saturation magnetization which require extrapolations of measured magnetic moment values to infinite field strength and absolute zero temperature. High fields which only the superconducting solenoid can provide are also very necessary for the accurate measurement of the magnetocrystalline anisotropy constants in the case of materials which have a very high anisotropy. Since these materials are the ones which are best for fine-particle permanent magnet use, this form of the instrument would obviously be most useful in the present investigation. The disadvantage of the system is that it is awkward to operate, since it requires the use of large quantities of liquid helium to bring the coil into the superconducting state. We have completed the construction of this version (to which we shall refer as the SCS-OSM), but we have encountered serious experimental difficulties with the commercial Dewar vessel and the liquid helium transfer mechanisms associated with the solenoid.

We have also designed and almost completed the construction of another version of the OSM which uses as the source of the magnetic field a 9" pole diameter Varian laboratory electromagnet. In this version, the sample motion is perpendicular to the field direction, while in the SCS-OSM the direction of the sample motion and the field axis coincide. The version of the OSM using this electromagnet (referred to for short as the(EM-OSM) is much more restricted in its maximum field capability than the SCS-OSM. The highest field strength that can be used for room temperature measurements is approximately 15 kOe, and the field is restricted to about 10 kOe if a liquid helium sample dewar is used. The advantages of this low field version are that the magnet is always ready for use without the requirement for cryogenic liquids, and that the magnetometry with the field perpendicular to the sample motion is more convenient for anisotropy studies in cases where relatively low fields are sufficient. In fact, the instrument in this form can be used like a torque magnetometer, provided an appropriate arrangement of four signal pickup coils is used.[26]

The magnetometer employs a slow sinusoidal motion of the sample over a relatively large distance. The magnetometer head built to produce this sample motion, which both versions of the instrument have in common, is shown in Figure 28. It consists of a synchronous motor and a speed reducer which incorporates a pair of interchangeable gears, an eccentric drive which permits adjustment of the throw between 0 and 30 mm, and a crosshead translating the rotary into a vertical linear motion. The motion

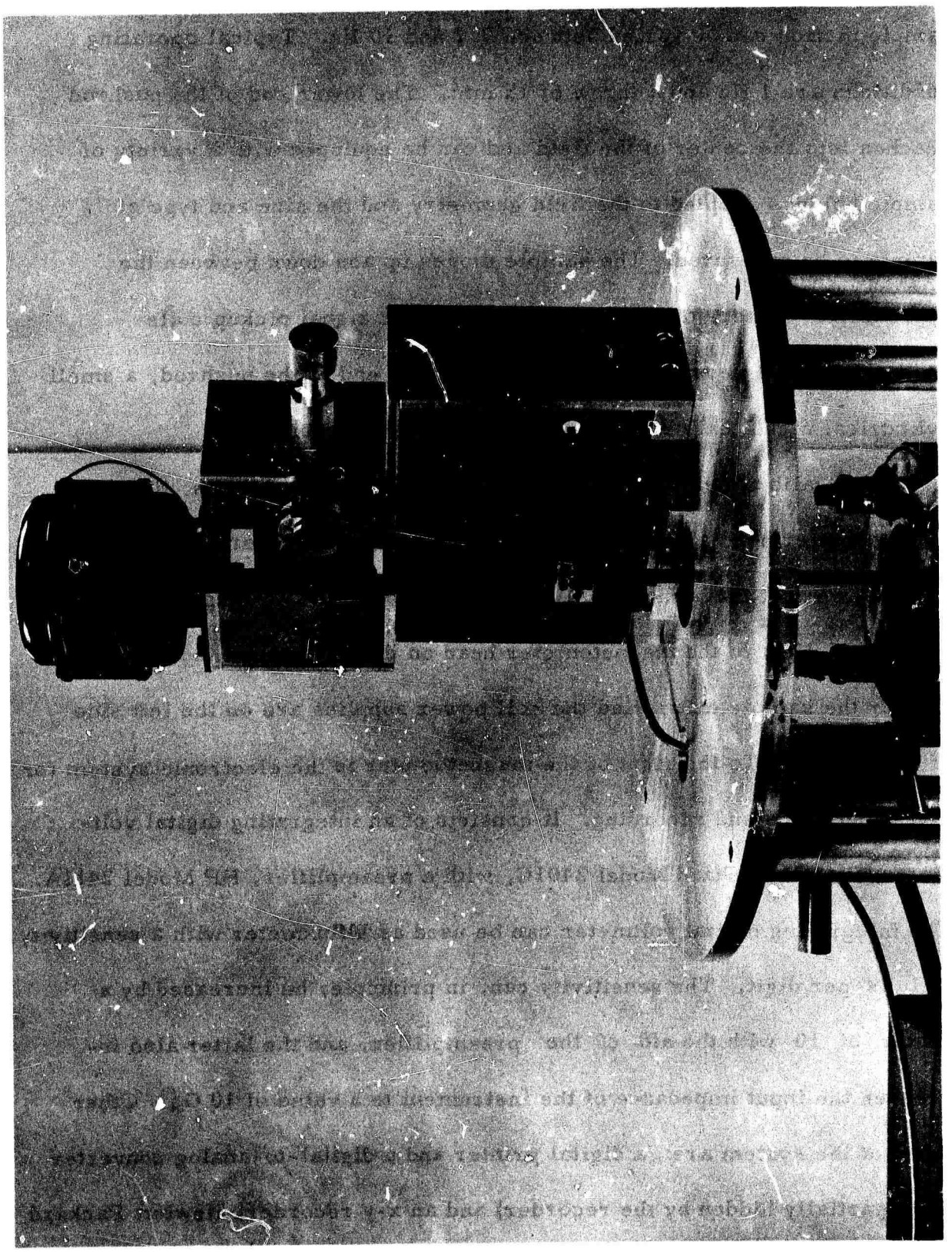

Figure 28. Magnetometer head with a low-field solenoid magnet.

is transmitted to the sample by a long pushrod. The frequency of the sample motion can be varied between 0.1 and 10 Hz. Typical operating conditions are 1 Hz and a throw of 15 mm. The lower end of the pushrod reaches into the center of the field and can be equipped with a variety of sample holders adapted to the field geometry and the size and type of sample to be measured. The sample moves up and down between the approximate centers of two identical concentric signal pickup coils (in the SCS-OSM version). Figure 29 shows the end of the pushrod, a small cylindrical nickel calibration sample and the signal coils.

For calibration purposes and for low field measurements, this magnetometer head and coil set were combined with a water-cooled solenoid magnet that can produce approximately 2500 Oe. Figure 30 shows this setup. Next to the magnetometer head on the left we see the control box for the sample drive, and the coil power supplies are on the left side of the picture. To the right of the magnetometer is the electronic system for signal detection and recording. It consists of an integrating digital voltmeter, Hewlett-Packard Model 2401C, with a preamplifier, HP Model 2411A. The integrating digital voltmeter can be used as a fluxmeter with a sensitivity of 1μVs per digit. The sensitivity can, in principle, be increased by a factor of 10 with the aid of the preamplifier, and the latter also increases the input impedance of the instrument to a value of 10 GΩ. Other parts of the system are: a digital printer and a digital-to-analog converter (both partially hidden by the recorder) and an x-y recorder, Hewlett Packard

Figure 29. Pickup coil configuration for use with the setup of Figure 30 and the SCS-OSM version. The end of the pushrod with a sample holder and a nickel calibration sample are also shown.

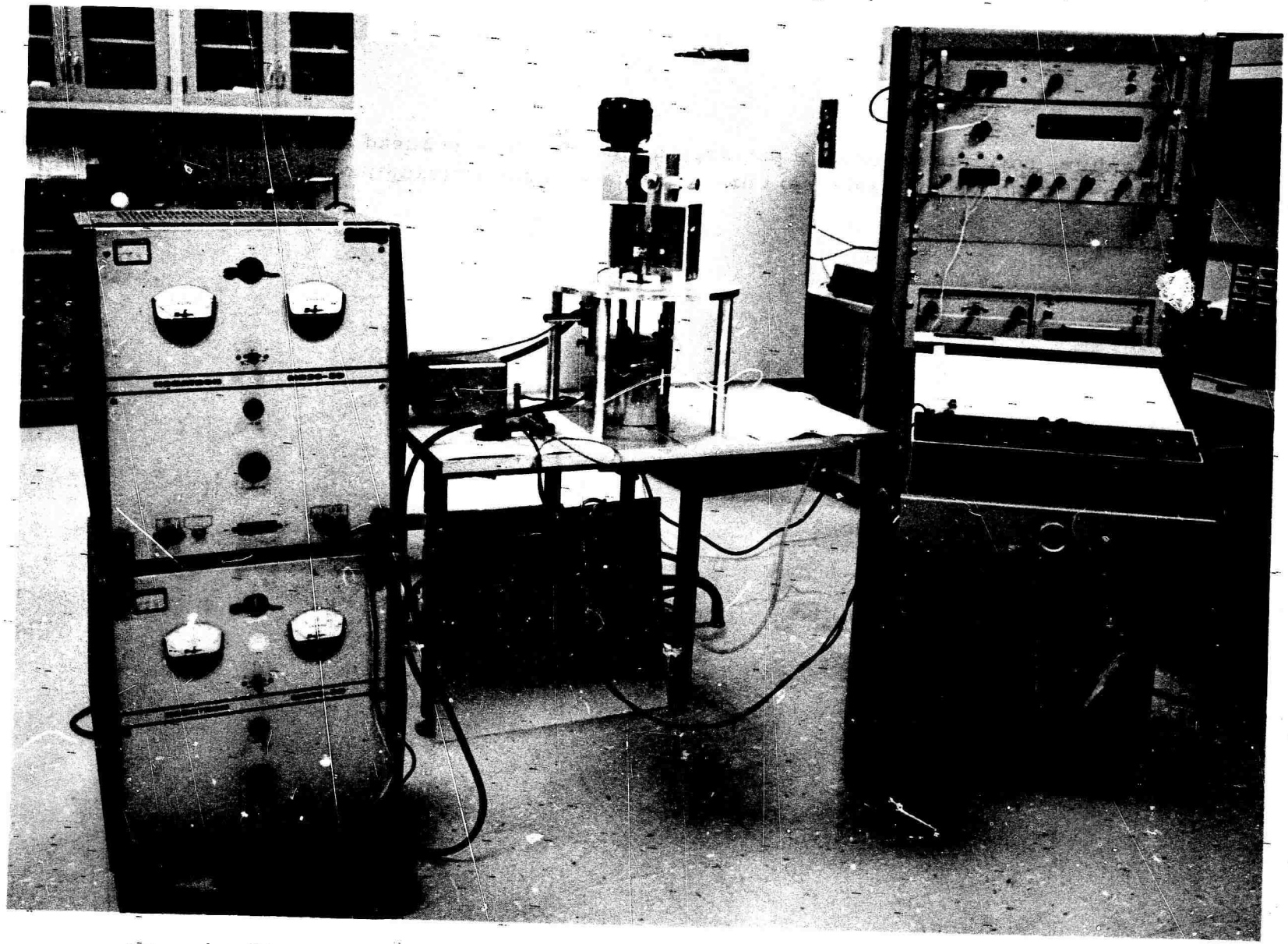

Figure 30. OSM setup for test and calibration with low-field solenoid magnet.

Mosley Model 7000 AM. The arrangement permits simultaneously the accurate reading of the magnetic moment from the digital display, and the convenient plotting of the magnetic moment as a function of either the magnetic field or the sample temperature on the x-y recorder.

The instrument functions basically in the following manner: the sample is magnetized vertically in the field produced by the solenoid or the superconducting magnet. It is moved slowly and in a periodic fashion up and down in the uniform field region of the magnet. This motion of the sample dipole induces a voltage in the pair of pickup coils which is proportional to the magnetic moment of the sample. The throw is adjusted such that the sample moves approximately between the centers of the two windings of the pickup coil. The coil is wound and positioned in such a manner that the signals induced in its two halves by the oscillating sample dipole add up, while any signal from a change of the magnetizing field cancels. Thus we get at the output of the pickup coil a voltage proportional to the sample moment which we desire to measure. This voltage is fed into the integrating digital voltmeter, is rectified there in the manner of a full wave rectifier and integrated over an integral number of cycles. At present, we typically use a gate time of 1 second and a sample motion frequency of 1 Hz, and consequently integrate over 1 full cycle. The signal, adjusted once every second, can be accurately read from the digital display or printed out on a paper strip. The digital-to-analog converter also permits the conversion of any three digits into a d. c. voltage that can be fed into

the y-axis of the recorder. Usually one will select the 3 most significant figures, but one could also resolve small changes of a large magnetic moment value by selecting the last 3 digits. The x-axis of the recorder can be driven either by the output voltage of a thermocouple in contact with the sample, if the objective is a measurement of the temperature dependence of the magnetization in a constant field or one can put the output of a Hall probe or a voltage derived from the solenoid current on the x-axis as a measure of the magnetizing field and plot magnetization curves of hysteresis loops by varying the magnetic field in a cyclic fashion. The record obtained is always a step curve, that is, the method is a point-by-point measurement with rapid automatic sampling. However, the sweep rate of the field or the temperature is usually so low that, for all practical purposes, the curves are continuous.

Figure 31 refers to the SCS-OSM version. It shows the magnetometer head in position on top of the dewar containing the superconducting solenoid. Figure 32 shows the entire system set up for operation. In the center of the picture we have again the superconducting solenoid dewar. The other small dewar attached contains liquid nitrogen for a cold trap and for the reference junction of the sample thermocouple. Behind the dewar is the superconducting-solenoid power supply and associated electronics. The tall instrument rack on the right of the dewar contains the temperature control system that can be used for maintaining or sweeping the temperature of the sample. This is accomplished by admitting helium gas from

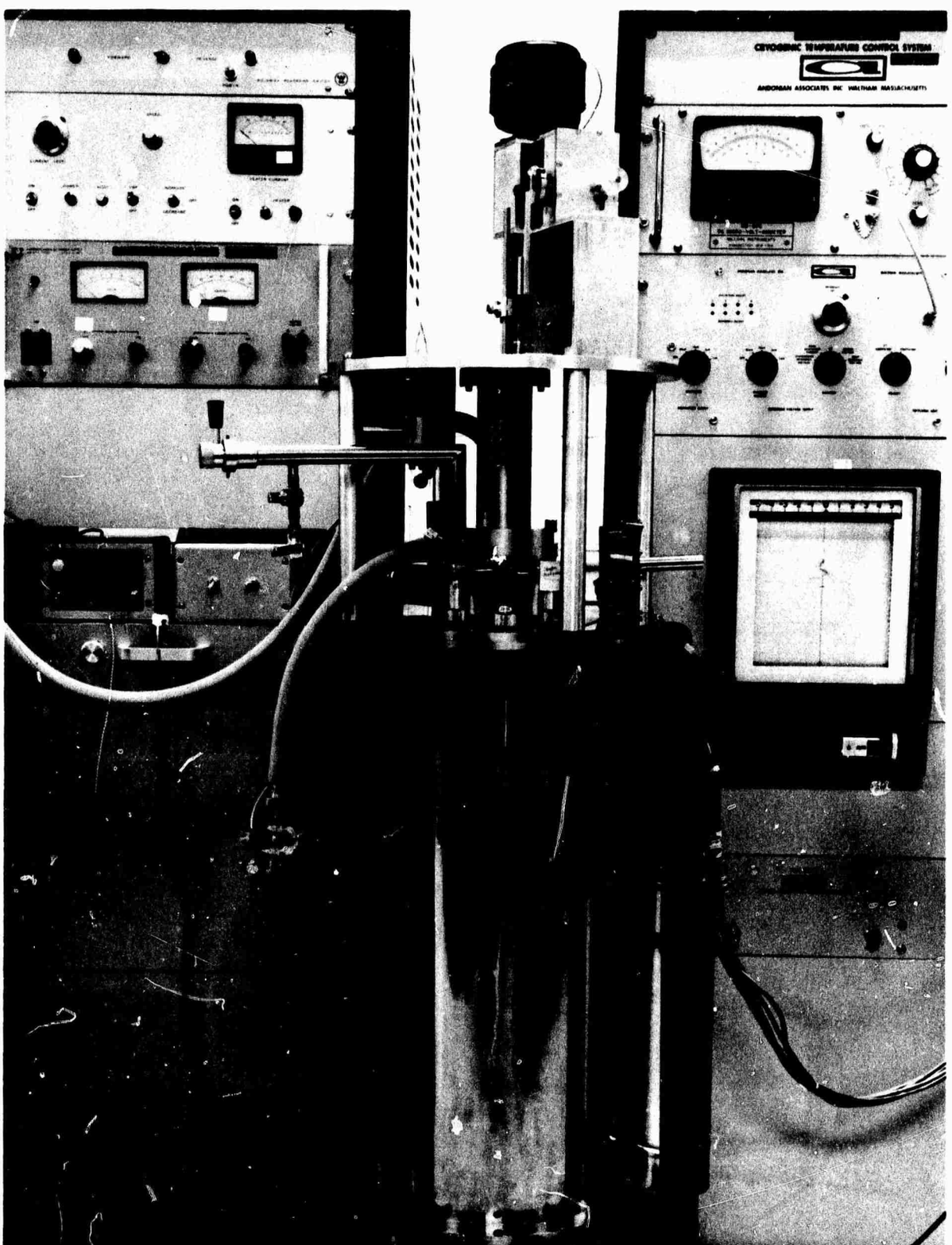

Figure 31. SCS-OSM: Magnetometer head set up on top of the superconducting-solenoid dewar vessel.

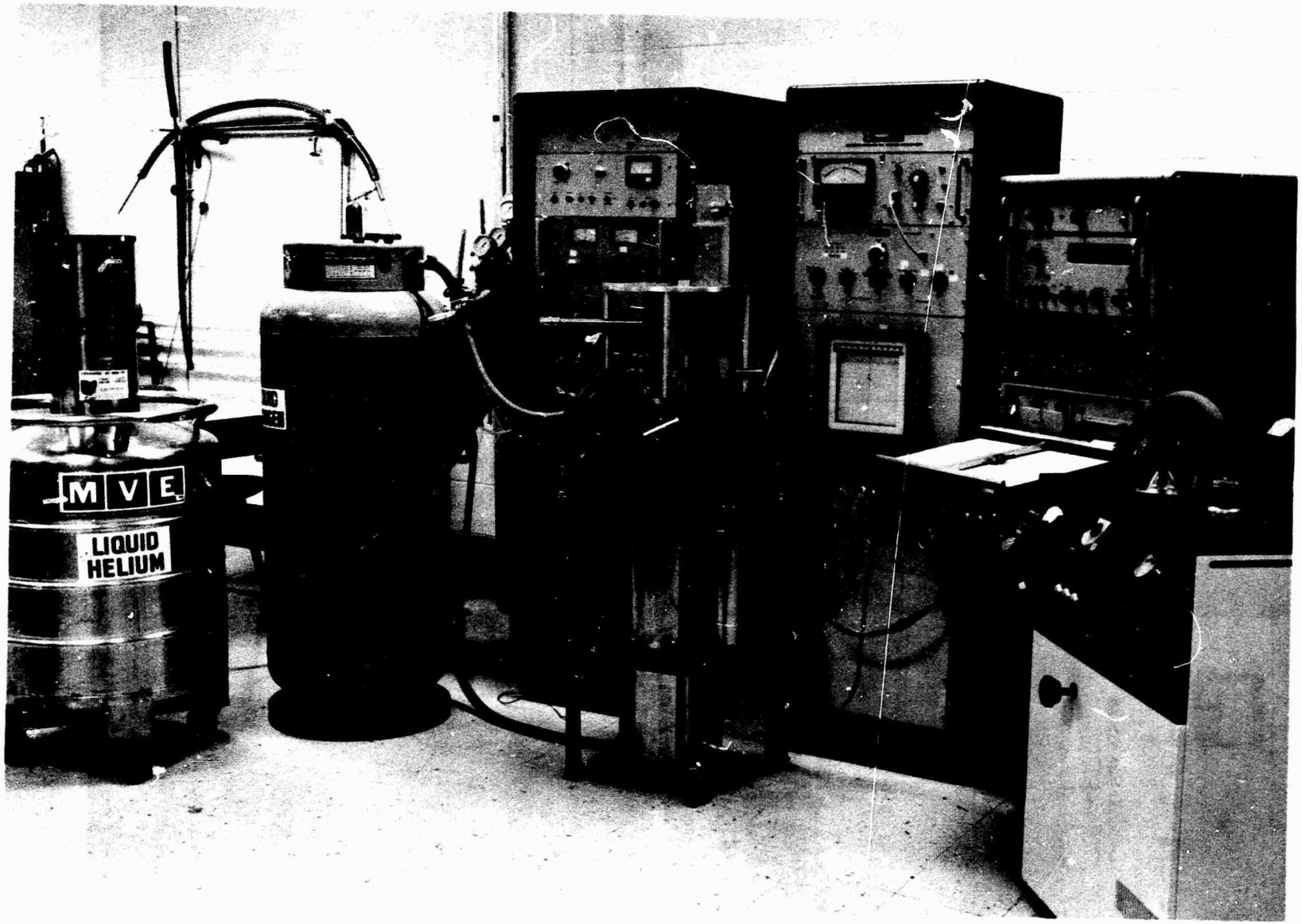

Figure 32. SCS-OSM: Complete magnetometer system showing the solenoid dewar with OSM head, associated electronics and cryogenic equipment.

the solenoid well into the center-access tube of the solenoid and electrically heating the gas column or the sample. Temperatures between 1.5°K and approximately 300°K can thus be achieved. The smaller instrument rack contains the electronic portion of the magnetometer discussed before. A vacuum system and leak detector, storage dewars for liquid helium and nitrogen, and helium transfer tubes (on the back wall) can also be seen in the picture. The FM-OSM version is shown in Figure 33. Here, the magnetometer head is in place on top of the Varian electromagnet and we can see the glass dewar which permits cooling of the sample down to the temperature of liquid helium. The magnetometer head and dewar are mounted on vertical columns that are fastened to the yoke of the electromagnet in such a way that the magnetometer can be withdrawn upward from the gap of the electromagnet so as to make room for other experiments. This arrangement was necessary because we use the same electromagnet in a number of operations, including the pressing of magnets, the plotting of hysteresis loops with a hysteresigraph, and the charging of permanent magnet samples.

At this point in time, unfortunately, neither of the two versions of the magnetometer is yet fully operational. Mechanical construction and electronic design have been completed for both. The version with sample motion and field direction parallel to each other has been calibrated and successfully operated at room temperature with a low-field coil as shown in Figure 30. In two attempts to operate it in conjunction with the superconducting solenoid, however, severe difficulties with the dewar

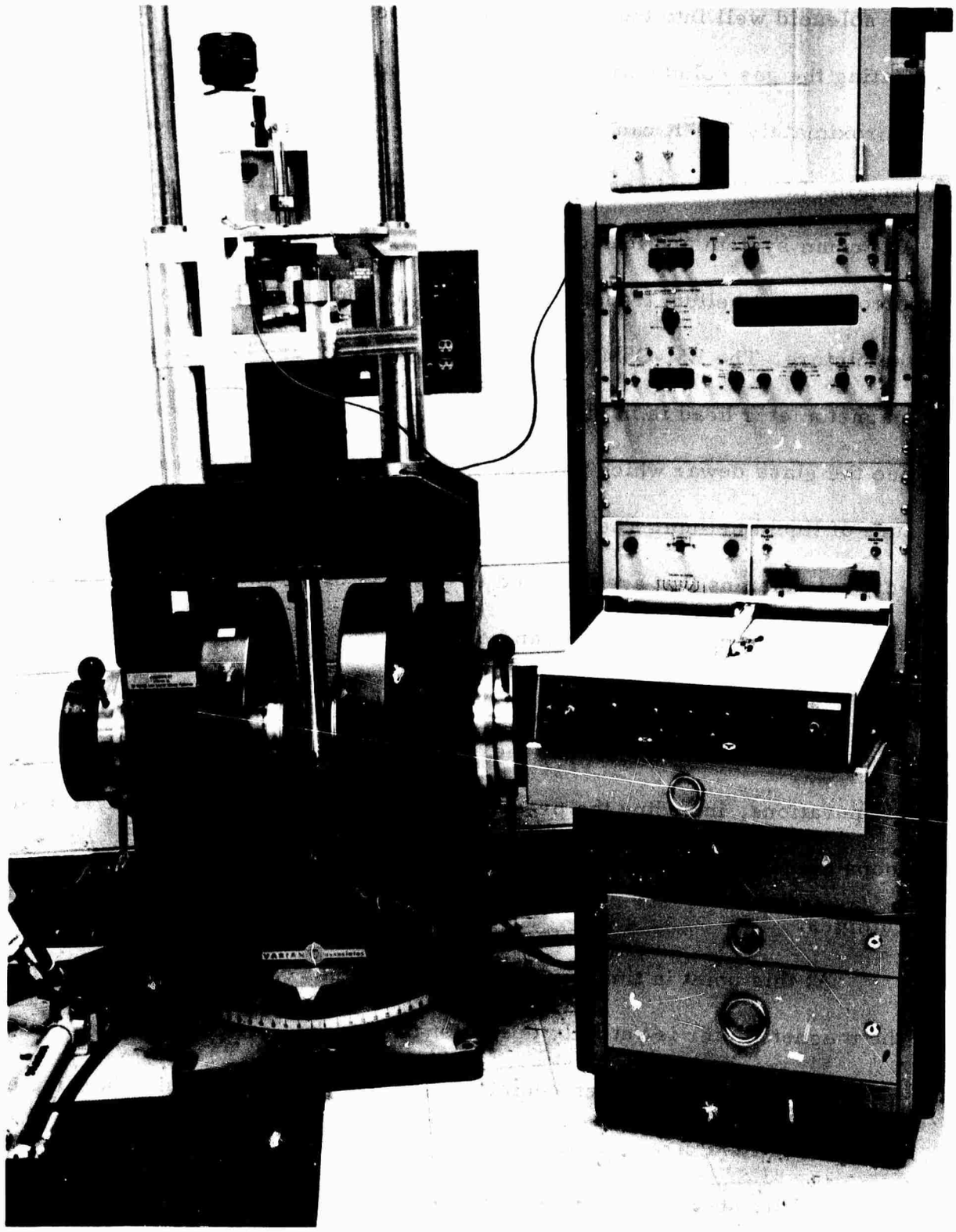

Figure 33. EM-OSM: Magnetometer head and sample dewar set up on Varian 9" electromagnet.

system of the SCS and with the helium transfer equipment were encountered which have not yet been overcome. The EM-OSM still lacks the appropriate pickup coil which is now under construction.

SECTION IV

SINTERING OF $NdCo_5$*

A. INTRODUCTION

$NdCo_5$ has the highest saturation magnetization among all the RCo_5 (R = rare earth) compounds. However, the anisotropic energy and thus the coercive force of $NdCo_5$ are low at room temperature. Thus $NdCo_5$ is not attractive as such for use in permanent magnets.

Our previous experience showed that coercive forces ($_MH_c$) of up to 24,500 Oe could be obtained by sintering $PrCo_5$ powders with a Sm-Co alloy sintering aid. These coercive forces far exceed those attainable with $PrCo_5$ alone. We have attributed the high coercive forces to a magnetically hard epitaxial shell being formed around the $PrCo_5$ particles. The purpose of this work is to learn if the coercive force of sintered $NdCo_5$ powders can also be improved by the formation of a hard magnetic shell around the individual $NdCo_5$ particles.

B. MATERIALS

The $NdCo_5$ employed was a portion of a 980 gm ingot obtained from the Bureau of Mines in Reno, Nevada in February, 1970. The ingot was prepared by the Bureau of Mines' electrowinning process and their analysis indicated the following (in weight percent):

---

* J. B. Y. Tsui

Nd	33.8	O	0.01	Ni	0.15
Co	65.7	Al	0.03	Si	0.10
C	0.09	Fe	0.12	Mg	0.002

At least three phases could be observed metallographically in the approximate ratio 50:40:10 in the polished area. Powder X-ray diffraction indicated $NdCo_5$ plus other phases present. Curie temperatures of 630°C ($NdCo_5$) and 880°C (Nd_2Co_{17}) were observed by thermomagnetic analysis. It was concluded that the primary phase in the as cast alloy was $NdCo_5$ with a significant amount of Nd_2Co_{17} and a lesser amount of a third phase, probably Nd_2Co_7 present.

The Pr-Co alloy used for the sintering aid was also obtained from the Bureau of Mines and prepared by the electrowinning process. The analysis accompanying the alloy indicated 69 wt.% Pr, 29 wt.% Co plus 2 wt.% other impurities.

The easy direction of magnetization of $NdCo_5$ shifts on cooling from the c-axis above room temperature through a cone to the basal plane at 0°C. To obtain an estimate of the degree of alignability of $NdCo_5$ at room temperature, the powder X-ray diffraction technique described in Section I. F was employed. It was observed that 37 to 44 μm $NdCo_5$ powders could be aligned reasonably well in a field of 5 kOe. A slight improvement was noted when the powders were warmed with hot air from a heat gun while in the aligning field.

The coercive forces, ${}_MH_c$, of dilute $NdCo_5$ powders of various size fractions ranging from 37 to 105 μm were all found to be less than 50 Oe.

Attritor milled $NdCo_5$ powder averaging 8-10 μm had a coercive force of 190 Oe.

For the sintering experiments, the $NdCo_5$ alloy was attritor milled for 5 minutes to an average particle size of 8-10μm. The 70 wt.% Pr 30 wt.% Co sintering aid was attritor milled for 60 minutes to an average particle size of 3-5μm. Four specimens were prepared; the $NdCo_5$ to Pr-Co alloy weight ratios were 80:20, 70:30, 60:40 and 50:50. The mixed powders were pressed under 125,000 psi into brick-shaped samples 1/4 x 1/4 x 3/4" while in an aligning field of 36 kOe along one of the short directions. The cold-pressed bricks were then sintered in vacuum at 1140°C for 30 minutes, and rapidly cooled to room temperature.

The results obtained from hysteresis loops and density measurements of the sintered magnets are shown in Table XIX. The highest coercive force observed was 4000 Oe for the sample with $NdCo_5$: Pr-Co weight ratio of 60:40.

C. CONCLUSIONS

These first sintering experiments with $NdCo_5$ show that the coercive force of $NdCo_5$ powders can be vastly improved by sintering with a Pr-Co alloy sintering aid and further support the view that a magnetically hard shell is an important source of the coercive force in sintered RCo_5 magnets. The maximum coercive force of 4000 Oe is not high when compared with values obtained with other sintered RCo_5 magnets. However, no attempt was made to optimize the sintering temperature.

TABLE XIX

Results of initial sintering experiments at 1140°C on $NdCo_5$ with a 70 wt.% Pr-30 wt.% Co sintering aid

Sample No.	$NdCo_5$:Pr-Co Ratio	Density g/cm^3	B_r G	$_MH_c$ Oe	M_r/M_p
M-596	80:20	7.95	3120	1000	.54
M-597	70:30	5.57	3640	2750	.63
M-598	60:40	7.62	2120	4000	.57
M-599	50:50	7.95	455	750	.21

Moreover, the $NdCo_5$ alloy employed was not annealed and any quantity of Nd_2Co_{17} remaining after sintering would have an adverse on the observed coercive force. Work on the sintering of $NdCo_5$ will be continued with new alloys annealed so that Nd_2Co_{17} is not present initially. Both Sm-Co and Pr-Co alloys will be evaluated as sintering aids for $NdCo_5$.

APPENDIX

LATTICE CONSTANTS FOR MIXED INTERMETALLIC PHASES OF THE TYPE $R_2(Co_{1-x}Fe_x)_{17}$

APPENDIX

LATTICE CONSTANTS FOR MIXED INTERMETALLIC PHASES OF THE TYPE $R_2(Co_{1-x}Fe_x)_{17}$*

1. Introduction

R_2Co_{17} and R_2Fe_{17} binary intermetallic phases of the rhombohedral Th_2Zn_{17}-type have been observed with R = Ce, Pr, Nd, Sm, Gd, Tb, and Y.[1, 2, 3, 4] The magnetic properties of these phases are discussed in several articles.[5, 6, 7, 8] The R_2Co_{17} phases are characterized by high saturation magnetizations and Curie temperatures between 800 and 950°C. The R_2Fe_{17} phases have still higher saturation magnetizations but Curie temperatures ranging from -200°C to +100°C. By replacing a portion of the Co with Fe in alloys of the type $R_2(Co_{1-x}Fe_x)_{17}$ we hope to increase the saturation magnetization without seriously lowering the Curie temperatures.

We have prepared a large number of essentially single phase $R_2(Co_{1-x}Fe_x)_{17}$ alloys with R = Ce, Pr, Nd, Sm, Y, and MM (Ce-rich mischmetal) and x ranging from 0 to 1. A detailed study of the magnetic properties of these alloys is in progress at the University of Dayton. The Curie temperatures and the melting data obtained by differential thermal analyses were reported previously.[9] The Curie temperatures are also given in Table I. In this paper we report on the lattice constants for these phases. The lattice constants of one series of alloys, $Y_2(Co_{1-x}Fe_x)_{17}$, were reported earlier by Lihl, et al.[10]

2. Experimental Procedure

The alloys were prepared by nonconsumable arc melting of the elemental components in an argon-helium atmosphere. Metallographic

* A. E. Ray and R. Harmer

TABLE I. Curie temperatures for $R_2(Co_{1-x}Fe_x)_{17}$ phases.[a]

x \ R	Ce	Pr	Nd	Sm	Y	MM
0.0	801	890	906	926	916	836
0.1	783	876	884	916	909	830
0.2	759	850	871	886	876	803
0.3	722	817	817	856	847	763
0.4	671	760	773	806	793	708
0.5	608	705	710	747	739	677
0.6	522	-	-	-	667[c]	-
0.7	433	-	-	-	577[c]	-
0.75	-[d]	466	475	-	-	534
0.8	303[d]	-	-	-	477[c]	-
0.9	130[d]	-	-	-	337[c]	-
1.0	-180[b]	10[b]	54[b]	126[b]	30[b]	(-75)[e]

a. Values obtained by DTA except as noted.
b. Strnat, Hoffer, and Ray.[5]
c. H. Kirchmayr, private communication, Ruhr-Universität Bochum, W. Germany, April 1970.
d. These values have low reliability.
e. Estimated value obtained by extrapolating from x = 0.75 to x = 1.0

inspection of the as-arc-melted buttons showed gross segregation developed during solidification in most of the Fe-containing alloys. Only the $Y_2(Co_{1-x}Fe_x)_{17}$ series of alloys, which melt and solidify congruently were not observed to segregate into layers during solidification. It is suspected that liquid miscibility gaps in the ternary alloys are the cause of the gross segregation. The bottom portions of the buttons containing thick dendritic crystals were ground away. The remaining portions with much finer dendritic microstructures were wrapped in tantalum foil and homogenized 6 to 72 hours in a vacuum of 1×10^{-6} Torr at temperatures approximately 100°C below the peritectic or melting temperatures of the alloys. Cross sections of the homogenized buttons were examined metallographically to determine that single phase alloys were prepared. A detailed description of the procedures employed for preparing the $R_2(Co_{1-x}Fe_x)_{17}$ alloys is given elsewhere.[11]

In addition to the peritectic and liquidus or melting temperatures of the homogenized $R_2(Co_{1-x}Fe_x)_{17}$ alloys, the Curie temperatures were determined by differential thermal analyses (DTA) and are given in Table I. The Curie temperature measurements for these phases have also been confirmed by thermomagnetic analyses (TMA). Both the DTA and TMA apparatus were described previously.[11]

The lattice constants of the $R_2(Co_{1-x}Fe_x)_{17}$ phases were determined from powder X-ray diffraction patterns. A G.E. XRD-6 diffractometer and Type 700 detector with V-filtered, CrK_α radiation was employed. Computer refinements of lattice constant data were obtained using the methods of Vogel and Kempter.[12] Zero degree 2θ errors were corrected through the use of Ni as an internal standard.

3. Results

Hexagonal lattice constants for the rhombohedral Th_2Zn_{17}-type phases, $R_2(Co_{1-x}Fe_x)_{17}$ with R = Ce, Pr, Nd, Sm, Y, and MM are given in Figure 1. The lattice constants for the a-axes of alloys with R = Sm and Y closely follow Vegard's law relationships and the alloys with R = Ce, Pr, Nd, and MM show only slightly positive deviations. On the other hand, the c-axis lattice constants for all phases show strongly positive deviations from linearity. For the series of alloys $Ce_2(Co_{1-x}Fe_x)_{17}$, the maximum deviation of 1.2% occurs between x = 0.7 and 0.8. Since only alloys with x = 0.75 have been prepared between x = 0.5 and x = 1.0 for R = Pr, Nd, Y, and MM it has not been determined whether or not x = 0.75 represents the point of maximum deviation of the c-axis for these alloys. The point at which the c-axis reaches a maximum for the $Sm_2(Co_{1-x}Fe_x)_{17}$ series of alloys is undetermined because of some difficulties encountered in preparing single phase alloys with x = 0.6 and 0.7.

4. Discussion

The rhombohedral R_2T_{17} crystal structure (where T = Co and/or Fe) is shown in Figure 2a. This structure is derived from the RT_5 structure by the substitution of one third of the R atoms by a pair of the smaller T atoms in each of the alternate planes according to the formula

$$3\,RT_5 - R + 2\,T = R_2T_{17}\,.$$

The two T atoms lie on either side of the planes containing the R atoms on lines aligned parallel to the c-axis. In the R_2Co_{17} and the R_2Fe_{17}

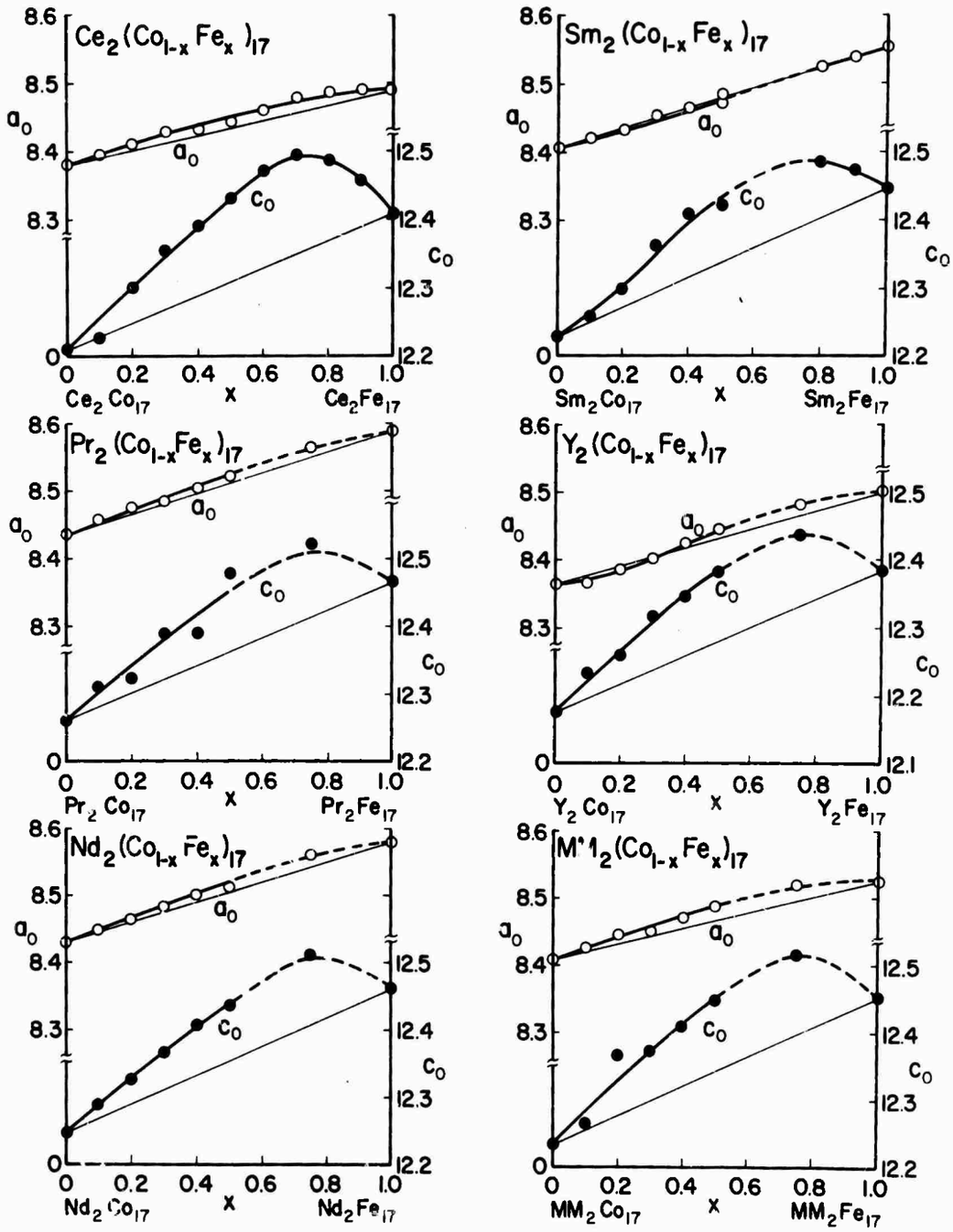

Figure 1. Hexagonal lattice parameters for the rhombohedral Th_2Zn_{17}-type phases $R_2(Co_{1-x}Fe_x)_{17}$.

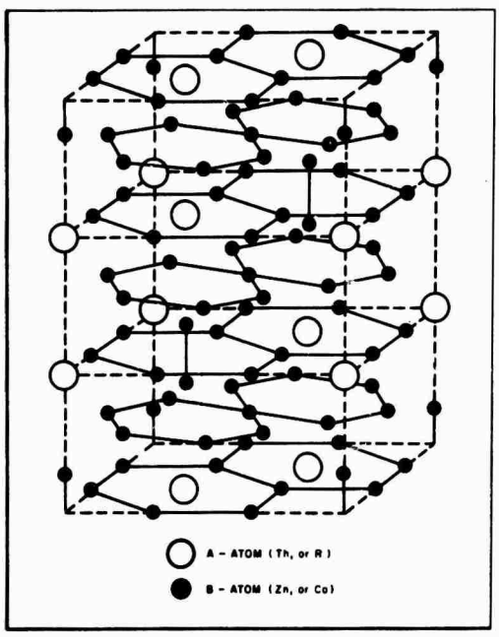

Figure 2a. The rhombohedral, Th_2Zn_{17}-type, R_2T_{17} structure. Pairs of T atoms aligned parallel to the c-axis occupy one-third of the R positions and the stacking repeats every third layer.

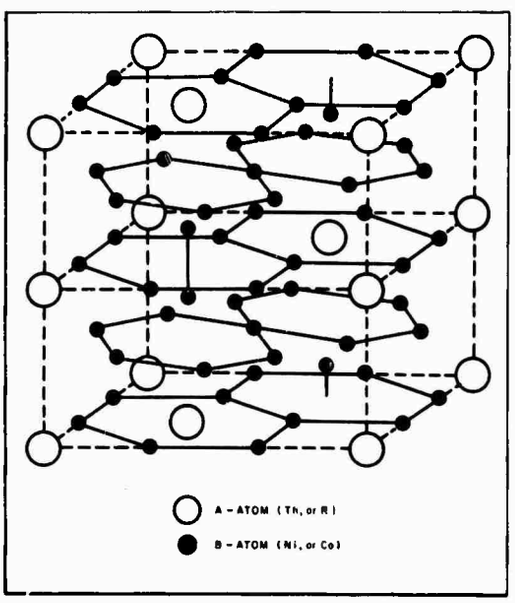

Figure 2b. The hexagonal, Th_2Ni_{17}-type, R_2T_{17} structure. Pairs of T atoms aligned parallel to the c-axis occupy one-third of the R positions and the stacking repeats every second layer.

structures, the Co-Co and Fe-Fe interatomic distances are nearly identical to those found in the pure metals except between the pair in the substituted positions where the distance is considerably shorter. (For example, the Fe-Fe distance is 2.393Å in the substituted positions vs 540Å overall in Pr_2Fe_{17}).[13] It is evidently the magnetic interactions between Fe-Co and Fe-Fe atoms in the substituted pairs that result in the abnormal expansion of the c-axis as Co atoms replace Fe atoms in the R_2Fe_{17} phases.

Givord, et al.[14] have observed large, negative thermal expansions of the c-axes of the hexagonal phases R_2Fe_{17} (with R = Y, Gd, and La) as these phases are cooled below their magnetic ordering temperatures. The crystal structures of the hexagonal R_2Fe_{17} phases, shown in Figure 2b, are similar to the rhombohedral R_2Fe_{17} phases except that in the former, the substituted pairs repeat in every other layer along the c-axis rather than every third layer. Givord, et al., interpret the negative thermal expansions of the c-axes of these phases as follows:

a. The magnetic exchange interactions in R-Fe interatomic compounds are determined primarily by the Fe-Fe interatomic distances and the coordination numbers of the Fe positions. For Co (and Ni) compounds, these factors play a secondary role.

b. Between the atoms of the substituted pairs, the short Fe-Fe interatomic distance gives rise to direct, negative exchange due to the overlap of the 3d wave functions which would tend to favor antiferromagnetic coupling.

c. Except for the substituted positions, the interatomic distances are almost identical to those in pure iron, which leads to direct, positive exchange and ferromagnetic behavior, even in the substitutional positions.

d. Because the magnetic moments of the paired Fe atoms in the substitution are forced to be parallel by their positive interactions with the other Fe moments, the magnetic energy involving the unsatisfied negative interactions is minimized by an expansion of the c-axis.

e. As the temperature decreases and the magnetization of the Fe increases, the c-axis must increase to minimize the stronger negative interaction between the paired Fe atoms.

The substitution of Co for Fe in the R_2Fe_{17} phases has essentially the same effect as cooling these phases far below their magnetic ordering temperatures. As shown in Table I, the initial substitution of 10% of the Fe by Co in Ce_2Fe_{17} and Y_2Fe_{17} raises the Curie temperatures of these phases by over 300°C. At room temperature the R_2Fe_{17} phases with R = Ce and MM are well above their magnetic ordering temperatures while those with R = Pr, Nd, Sm, and Y are at or only slightly below their Curie temperatures. On the other hand, the $R_2(Co_{1-x}Fe_x)_{17}$ phases with $x \leq 0.9$ are all well below their Curie temperatures and the magnetic interactions described in the previous paragraph become operative.

The significance of the observed maximum of the c-axis for $Ce_2(Co_{1-x}Fe_x)_{17}$ at x between 0.7 and 0.8 can probably be attributed to the fact that the Curie temperature rises rapidly with the initial substitution

of Co. This increases the spontaneous magnetization, thus the exchange energy, and consequently the c-parameter expansion demanded by the increased negative interactions of Fe atoms in the paired, substitutional positions. Beyond a certain amount of Co in the $R_2(Co_{1-x}Fe_x)_{17}$ phases, the increase in the Curie temperature will be compensated by fewer negative interactions, particularly of the Fe-Fe type. However, an increasing amount of strain will be associated with those Fe atoms occupying the paired, substitutional positions in the Co-rich alloys. Thus, rather than dropping off abruptly the c-parameter appears to shrink linearly with decreasing x. If the assumptions concerning the magnetic interactions of the Fe atoms in the substitutional zone are correct, one would expect the c-axes of the $R_2(Co_{1-x}Fe_x)_{17}$ phase to decrease when heated above their magnetic ordering temperatures. An investigation of this point is in progress.

The c/a ratio for $Ce_2(Co_{.3}Fe_{.7})_{17}$ is 1.473. To our knowledge, this is the largest c/a ratio ever reported for a Th_2Zn_{17}-type phase. Johnson, et al.[15] observed that the c/a ratios of forty-three then known Th_2Zn_{17}-type phases were remarkably constant, the smallest being 1.452 and the largest 1.468.

APPENDIX REFERENCES

1. A. E. Ray, Proc. 7th Rare Earth Research Conference, Coronado, California, Vol. II, (1968) 473.

2. A. E. Ray and G. I. Hoffer, Proc. 8th Rare Earth Research Conference, Reno, Nevada, Vol. II, (1970) 524.

3. W. Ostertag and K. J. Strnat, Acta. Cryst., 21 (1966) 560.

4. K. H. J. Buschow, J. Less-Common Metals, 11 (1966) 204.

5. K. Strnat, G. Hoffer, and A. E. Ray, IEEE Trans. Magnetics, Vol. MAG-2 (1966) 489.

6. K. Strnat, G. Hoffer, W. Ostertag, and J. C. Olson, J. Appl. Phys., 37 (1966) 1252.

7. R. Lemaire, Cobalt, 33 (1966) 201.

8. R. Lemaire, R. Pauthenet, and J. Schweizer, IEEE Trans. Magnetics, Vol. MAG-6 (1970) 153.

9. A. E. Ray, K. J. Strnat, and A. T. Biermann, "Curie Temperatures and Melting Data for Some Binary and Ternary $R_2(Co, Fe)_{17}$ Phases," Paper 22.5, 1971 Digest of the International Magnetics Conference, Denver, Colorado, April 1971.

10. F. Lihl, J. R. Ehold, H. R. Kirchmayr, and H. D. Wolf, Acta Physica Austriaca, 30 (1969) 164.

11. A. E. Ray and K. J. Strnat, Research and Development of Rare Earth-Transitional Metals as Permanent-Magnet Materials, ARPA Order No. 1617, AFML-TR-71-53, Wright-Patterson Air Force Base, Ohio, March 1970.

12. R. E. Vogel and C. P. Kempter, Acta Cryst., 14 (1961) 1130.

13. Q. Johnson, D. H. Wood, G. S. Smith, and A. E. Ray, Acta Cryst., B24 (1968) 274.

14. D. Givord, R. Lemaire, W. J. James, J. M. Morean, and J.S.Shah, "Magnetics Behavior of Rare Earth-Iron Rich Intermetallic Compounds," Paper 22.6, 1971 Digest of the International Magnetics Conference, Denver, Colorado, April 1971. To be published IEEE Trans. Magnetics, Vol. MAG-7, Sept. 1971.

15. Q. Johnson, G. S. Smith, and D. H. Wood, Acta Cryst., B25 (1969) 464.

REFERENCES

1. A. E. Ray and K. J. Strnat, "Research and Development of Rare Earth-Transition Metal Alloys as Permanent-Magnet Materials" Technical Report AFML-TR-71-53 March 1971.

2. R. E. Vogel and C. P. Kempter, Acta Cryst., 14 (1961) 1130.

3. J. Tsui and K. Strnat, "Sintering of $PrCo_5$ Magnets with Pr-Co Alloy Addition" Paper No. 7.2 Intl. Conf. on Magnetics, Denver, Colo., April 13-16, 1971. To be published in IEEE Trans. Magnetics Vol. MAG-7 (1971).

4. A. E. Ray and G. I. Hoffer, "Phase Diagrams for the Ce-Co, Pr-Co and Nd-Co Alloy Systems", Proc. 8th Rare Earth Res. Conf., Reno, Nevada, Vol. II, (1970) p. 524.

5. J. Schweizer, K. J. Strnat and J. B. Y. Tsui, "Coercivity of Heat Treated Pr-Co Powder Compacts," Paper No. 7.3 Intl. Conf. on Magnetics, Denver, Colo., April 13-16, 1971.

6. K. Gschneidner, "Rare Earth Alloys" D. Van Nostrand, Princeton N. J., (1961) p. 24.

7. K. H. J. Buschow and A. S. Van Der Goot, "The Crystal Structure of Rare Earth-Cobalt Compounds of the Type R_3Co", J. Less Common Metals, 18, (1969) p. 309.

8. J. W. Ross and J. Crangle, "Magnetization of Cubic Laves Phase Compounds of Rare Earths with Cobalt," Phys. Rev. 133, A 509 (1964).

9. R. Lemaire, "Magnetic Properties of the Intermetallic Compounds of Cobalt with the Rare Earth Metals and Yttrium," Cobalt, Nos. 32 and 33, (1966) pp 132 and 201.

10. L. R. Salmans, K. Strnat and G. I. Hoffer, "Magnetic Transition Temperatures of Intermetallic Compounds of Rare Earths with Cobalt and Iron," AFML-TR-68-159, USAF Materials Laboratory Technical Report, September, 1968.

11. K. Strnat, G. Hoffer, W. Ostertag and J. C. Olson, "Ferrimagnetism of the Rare Earth-Cobalt Intermetallic Compounds R_2Co_{17}," J. Appl. Phys. 37 (1966) 1252.

12. R. Lemaire, J. Schweizer and J. Yakinthos, Acta Cryst B25, (1969) 710.

13. F. H. Ellinger, C. C. Land, K. A. Johnson and V. O. Struebing Trans. Met. Soc. AIME, 236, (1966) 1577.

14. K. H. J. Buschow and W. A. J. J. Velge, J. Less-Common Met. 13, (1967) 11.

15. J. Tsui and K. Strnat, Appl. Physics Letters 18, (1970) 107.

16. K. Huml, Acta Cryst 22, (1967) 29.

17. K. Strnat, et al., "Ferrimagnetism of the Rare Earth-Cobalt Intermetallic Compounds R_2Co_{17}," J. Appl. Physics 37 (1966) 1252.

18. K. J. Strnat, G. I. Hoffer and A. E. Ray, "Magnetic Properties of Rare Earth-Iron Intermetallic Compounds," IEEE Transactions on Magnetics, Vol. MAG-2 (1966) 489.

19. M. Turner, AFML/LPE, Wright-Patterson Air Force Base, Ohio, oral communication.

20. R. M. Bozorth, Ferromagnetism, New York, D. Van Nostrand Co., (1955).

21. Soschin Chikazumi, Physics of Magnetism, New York, John Wiley and Sons, Inc., (1964).

22. J. E. Fredrickson and W. H. Redans, "Boron Nitride for Aerospace Applications," New York, Union Carbide Corporation, (1964).

23. K. Strnat, G. Hoffer and A. E. Ray, "Magnetic Properties of Rare Earth Iron Intermetallic Compounds." IEEE Transactions on Magnetics, Vol. MAG-2, No. 3 (Sept. 1966) 489-493.

24. K. Strnat, "Cobalt-Rare Earth Alloys as Promising New Permanent Magnet Materials." Cobalt No. 36 (Sept. 1967).

25. K. Strnat and L. Bartimay, "A Recording High-Field Oscillating Specimen Magnetometer," J. Appl. Physics 38 (1967) 1305.

26. D. Feldmann, Ph. D. Thesis, Technical University, Vienna, Austria (1966).

27. E. F. Bertaut, R. Lemaire, and J. Schweizer, Bull. Soc. Franc. Miner. Crist. (1965) 88, 580.